Marine and aeolian sediment transport at the Hondsbossche Dunes

Analysing and modelling the contribution of marine processes to beach and dune evolution

T. S. Pak

HKV LIJN IN WATER

TU Delft Delft University of Technology

Marine and aeolian sediment transport at the Hondsbossche Dunes

Analysing and modelling the contribution of marine processes to beach and dune evolution

by

T. S. Pak

in partial fulfillment of the requirements for the degree of

Master of Science
in Civil Engineering

at the Delft University of Technology,

to be defended publicly on Wednesday March 20, 2019 at 10:30 AM.

Student number:	4222237	
Project duration:	July 16, 2018 – March 20, 2019	
Thesis committee:	Prof. dr. ir. A. J. H. M. Reniers,	TU Delft
	Drs. C. Wegman,	HKV Lijn in Water
	Dr. ir. S. de Vries,	TU Delft
	Ir. J. Kroon,	TU Delft & Svašek Hydraulics

An electronic version of this thesis is available at `http://repository.tudelft.nl/`.

Cover image is obtained from `http://www.tkideltatechnologie.nl/`.

HKV LIJN IN WATER

TU Delft Delft University of Technology

Acknowledgements

This thesis finalises my MSc study Hydraulic Engineering at Delft University of Technology and is part of the specialisation Coastal Engineering. This research has been performed with the support of Delft University of Technology and HKV Lijn in Water.

I would like to thank all members of my graduation committee, Prof. dr. ir. A. J. H. M. Reniers, Drs. C. Wegman, Dr. ir. S. de Vries and Ir. J. Kroon, for their supervision and support during the project. I wish to express my appreciation to Ad Reniers, chair of the graduation committee, for his valuable input during all meetings. I would like to thank Carolien Wegman, my supervisor at HKV, for her permanent enthusiasm in the workplace and all feedback she provided on my interim reports. Sierd de Vries, my daily supervisor at TU Delft, never failed to enthuse me with his devotion to aeolian sediment transport and AeoLiS. I also recognise his critical view on the academic level of my report. Lastly, I would like to thank Anna Kroon, who assisted me with her large amount of practical knowledge on the Hondsbossche Dunes, and who reviewed all of my interim report.

I would like to express my appreciation to Petra Goessen from the Water Board Hollands Noorderkwartier for providing me with the AeoLiS models, and to Peter Brandenburg from Van Oord for providing the data set. I also want to thank them both for their substantive contribution to my study with their comprehensive knowledge on the Hondsbossche Dunes. My visits to Heerhugowaard and Rotterdam really helped me to keep a broad view.

I must express my gratitude to Laura, who supported and encouraged me throughout my entire study and through the process of writing this thesis. This accomplishment would not have been possible without her. Thank you.

Finally, I would like to thank HKV Lijn in water, for enabling me to graduate in this interesting topic and for facilitating my work environment for eight months. Thanks to all colleagues, who never refused a game of table tennis after the lunch break to clear my mind.

T. S. Pak
Delft, March 2019

Abstract

The Hondsbossche Dunes is a seven-kilometre-long dune, beach and shoreface nourishment that serves as a primary flood defence since 2015. In addition to its protective function, the Hondsbossche Dunes stimulate ecological habitat development in the coastal area, in line with Ecoshape's 'Building with Nature'-approach. After the nourishing works, the sediment on the beach is reshaped into five different profiles. Their morphologic development is monitored to simulate the morphological response to marine processes and aeolian sediment transport, and to determine the optimal profile for dune growth and nature development.

The monitoring program of Ecoshape (Bodde et al., 2019) studied the volume change of the beach and the dunes. The decrease of sediment volume on the beach is not equal to the increase of sediment volume on the dunes. The hypothesis is that the remaining sediment must stem from the intertidal zone and the shoreface. De Vries et al. (2014a) argue that the intertidal zone may be a dominant sediment source for aeolian transport on the beach, although it is affected by various marine processes. These processes may affect the supply of sediment and its size distribution. The research objective of this study is to investigate the contribution of sediment supply and marine processes in the intertidal zone to changes in morphology and bed composition in the beach and dune.

The data analysis using LiDAR and echo sounder measurements derives the sediment volume balance and net sediment transport rates for the Hondsbossche Dunes, distinguishing the offshore zone, shoreface, intertidal zone, beach and dunes as cross-shore zones. Volume changes of every cross-shore zone were calculated. A modelling study with AeoLiS aims to assess the effect of sediment supply and several marine processes to sediment transport, as well as the typical timescale of changes in morphology and bed composition. The conclusions of both studies are illustrated in Figure 1

The results of this data analysis show that sediment is transported from the intertidal zone to the shoreface in the north and south of the Hondsbossche Dunes (Profile 2 north, Profile 3 north and Profile 2 south). This behaviour is different from the middle of the domain (Profile 4 and Profile 3 south), where sediment is transported from the shoreface to the intertidal zone. The direction of cross-shore sediment transport between the shoreface and the intertidal zone may depend on the crest level of sandbars in the shoreface: The sandbars in the middle of the Hondsbossche Dunes break more short waves than those in the north and south, which causes 'freeing' of long waves and net landward sediment transport.

The modelling study suggests that wave runup and the presence of soil moisture reduce aeolian sediment transport from the intertidal zone to the beach, because grains in the intertidal zone are immobile when they are moist. This reduction results in increased erosion at the dry part of the beach, because the wind picks up sediment from the beach instead of the intertidal zone. The soil moisture content also significantly coarsens the bed composition in the intertidal zone, because the difference in threshold for aeolian transport between fine and coarse grains becomes larger. Hydraulic mixing does not contribute to significant morphological changes in the intertidal zone, but redistributes grains on the bed of the intertidal zone toward its initial distribution by stirring up the bed of the intertidal zone. These marine processes only affect dune growth if aeolian sediment transport is supply limited, which is mainly the case for Profile 2 north and Profile 4. Aeolian sediment transport in Profile 3 south is mainly transport limited, because the dune growth volume in most simulations is equal to the dune growth capacity following the formulation of Bagnold (1941). It seems that dune growth in this profile is less affected by marine processes. These results are likely to be related to the finer bed composition and wider beach at Profile 3 south.

The modelling study has also shown that the typical time scale for morphological changes in the dune is seasonal. Dune growth is roughly spread equally over the winter season, whilst the majority of sediment settled in the dune due to more severe wind conditions. The bed compositions show many short-term fluctuations, indicating that the typical time scale for changes in bed composition is in the order of hours, the scale of storm events.

A study on cross-shore sediment transport in the intertidal zone and its governing processes would give insight into prediction of morphodynamics in the intertidal zone and its timescale. This study should examine

the relative contributions of the undertow, wave skewness and long waves to cross-shore sediment transport between the shoreface and the intertidal zone. If cross-shore sediment transport between the shoreface and the intertidal zone is proven to depend on the crest level of sandbars in the shoreface, a further study on sandbar dynamics at the Hondsbossche Dunes could predict cross-shore sediment transport from the shoreface to the intertidal zone.

Additional features in AeoLiS are recommended to improve the quality of further studies. Implementation of the wind velocity threshold based on the bed slope enables AeoLiS to model the contribution of the sediment transport rate from the shoreface to the intertidal zone on aeolian sediment transport and dune growth. Implementation of the interaction between morphology and wind field enables AeoLiS to simulate the effect of dune geometry on aeolian sediment transport.

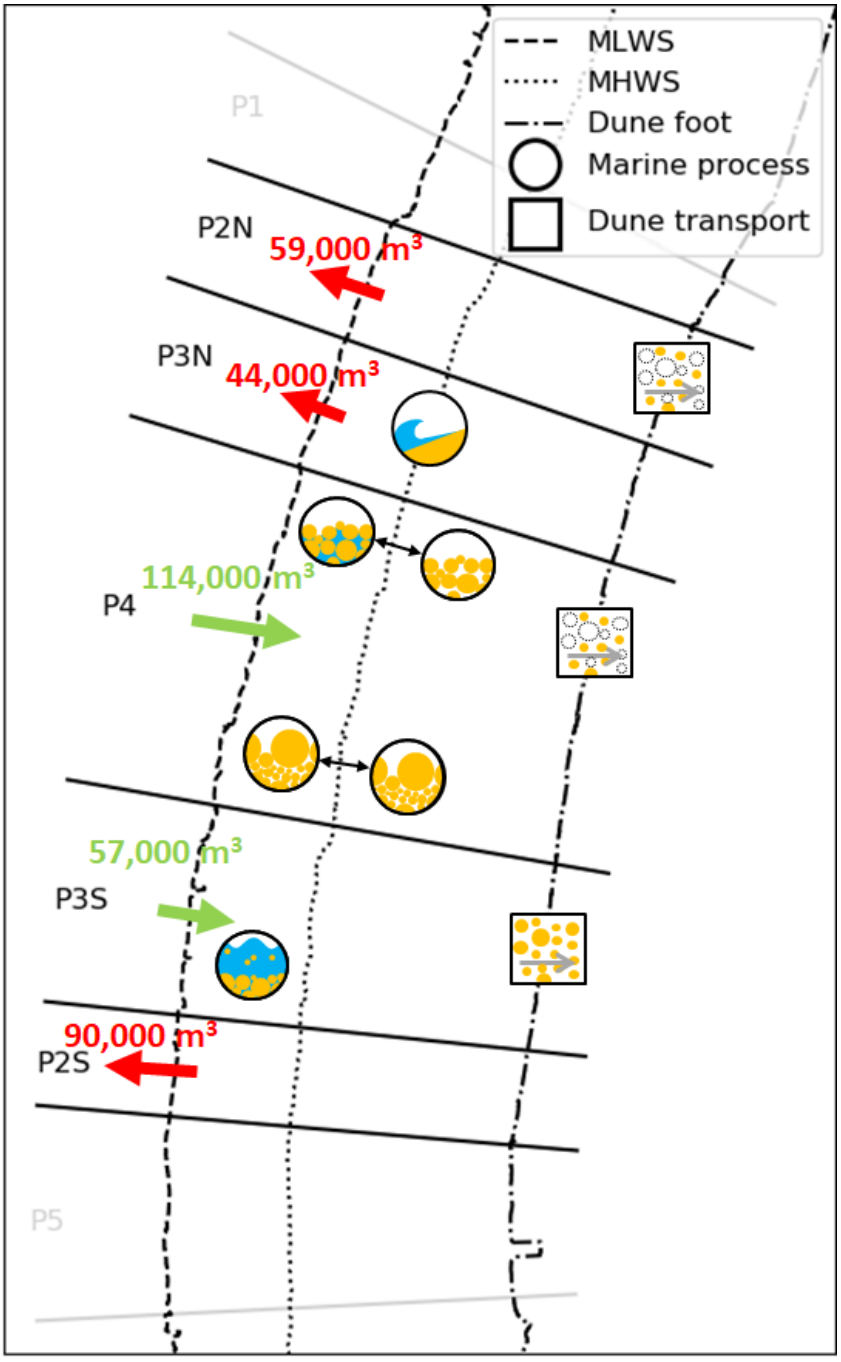

Figure 1: Schematic diagram of the Hondsbossche Dunes with net sediment transport rates from the shoreface to the intertidal zone between May 2015 and April 2018 (red and green arrows), marine processes (circles) and transport to the dunes (squares). Marine processes are wave runup (P3N), soil moisture content (P4 top), beach armouring (P4 bottom) and hydraulic mixing (P3S). Although these processes take place along the entire Hondsbossche Dunes, they are illustrated at a single location. Aeolian sediment transport to the dunes is supply limited in Profile 2 north and Profile 4, and transport limited in Profile 3 south.

Contents

List of Figures

List of Tables

Nomenclature

Acronyms

Acronym	Description
1DH	One-dimensional in the horizontal plane
2DH	Two-dimensional in the horizontal plane
2DV	Two-dimensional in the vertical plane
AeoLiS	Aeolian sediment transport with Limited Supply
BMI	Basic Model Interface
CERC	Coastal Engineering Research Center
HD	Hondsbossche Dunes ('Hondsbossche Duinen' in Dutch)
HPZ	Hondsbossche and Pettemer sea defence ('Hondsbossche en Pettemer Zeewering' in Dutch)
JARKUS	Yearly coastal measurements ('Jaarlijkse Kustmetingen' in Dutch)
LiDAR	Light Detection And Ranging
MHWS	Mean high water surface (NAP +0.84 m)
MLWS	Mean low water surface (NAP -0.76 m)
NAP	Amsterdam Ordnance Datum ('Normaal Amsterdams Peil' in Dutch)
P1	Profile type 1
P2N	Profile type 2 north
P2S	Profile type 2 south
P3N	Profile type 3 north
P3S	Profile type 3 south
P4	Profile type 4
P5	Profile type 5
RSP	Reference system of Rijkswaterstaat ('RijksStrandPaal' in Dutch)
RWS	Dutch Ministry of Infrastructure and Environment ('Rijkswaterstaat' in Dutch)

Variables

Symbol	Description	Unit
$\langle ... \rangle$	Time averaged	–
∂	Partial derivative	–
α	Conversion constant	–
β	Ratio between the drag coefficients of the roughness elements and the bed without roughness elements	–
γ	Breaker index	–
Δt	Time step	s
ΔV	Change in sediment volume	m^3
$\Delta V_{\text{per m}}$	Change in sediment volume per unit width	m^3/m
Δx	Cross-shore width of bed level grid cell	m
Δy	Alongshore width of the transect	m
Δz	Bed composition layer thickness	m
Δz_d	Depth of disturbance	m
Δ	Relative density	–
δ_e	Vapor pressure deficit	kPa
ε	Wave energy dissipation	W/m^3
ζ	Bed interaction parameter	–
η	Instantaneous water level	m + NAP
γ_v	Psychrometric constant	kPa/K
θ	Shields parameter	–
κ	Von Kármán constant	–
λ_v	Latent heat vaporization	MJ/kg

ρ	Density of the fluid	kg/m^3
ρ_a	Density of air	kg/m^3
ρ_s	Density of sediment	kg/m^3
ρ_w	Density of water	kg/m^3
σ	Ratio between the frontal area and the basal area of the roughness elements	–
τ	Shear stress	N/m^2
φ	Wave angle of incidence	°
A	Empirical coefficient	–
A	Sediment scale parameter	m$^{1/3}$
A_f	Sediment scale parameter of the fill sediment	m$^{1/3}$
A_n	Sediment scale parameter of the native sediment	m$^{1/3}$
C	Empirical coefficient related to the grain size distribution	–
c	Instantaneous sediment concentration	m^3/m^3 or kg/m^3
c_{br}	Wave celerity at the outer edge of the breaker zone	m/s
D	Deposition term	kg/m^2/s
D^+	Smallestmeasured grain size that is larger than D_P	µm
D^-	Largest measured grain size that is smaller than D_P	µm
D_n	Reference grain size	m
d_n	Nominal grain size	m
D_P	Grain size of percentile P	µm
D_{50}	Median grain size	m
E	Erosion term	kg/m^2/s
E_v	Evaporation rate	m/s
$f_{\Delta z_d}$	Empirical factor	–
g	Gravitational acceleration	m/s^2
H	Wave height	m
h	Water depth	m
h_*	Closure depth	m
H_s	Significant wave height	m
$H_{s,12h/y}$	Significant wave height that is exceeded 12 hours per year	m
K	Empirical coefficient	–
k	Lag	m
k_0	Index of the smallest non-erodible sediment fraction in current conditions	–
K_r	Refraction factor	–
K_{sh}	Shoaling factor	–
m	Factor to account for the difference between the mean and maximum shear stress	–
m_a	Available sediment in the bed	kg/m^2
m_v	Slope of the saturation vapor pressure curve	kPa/K
N	Number of samples	–
n	Exponentiality of the flow velocity to the sediment transport	–
n	Ratio between the group velocity and the higher phase velocity	–
n_k	Number of sediment fractions	–
P	Percentile	–
p	Porosity	–
p	Significance of the correlation	–
P^+	Percentile of D^+	–
P^-	Percentile of D^-	–
p_g	Mass percentage of water relative to dry sand	%
Q	Sink or source terms	m^3/s/m
q	Sediment flux	m^3/s/m^2 or kg/s/m^2
r^2	Correlation coefficient	–
r_k	Autocorrelation coefficient	–
R_n	Net radiance	MJ/m^2/day
S	Sediment transport rate	kg/s/m or m^3/s/m
s	Density ratio of sediment and water	–
$\hat{S}$	Effective sediment saturation of the air	–

S_b	Bed load transport	m^3/s or $m^3/s/m$
S_s	Suspended load transport	m^3/s or $m^3/s/m$
S_x	Sediment transport rate in x-direction	$kg/s/m$ or $m^3/s/m$
S_y	Sediment transport rate in y-direction	$kg/s/m$ or $m^3/s/m$
t	Time	s
t_1	The first moment in time	days
t_2	The second moment in time	days
T_a	Adaptation time scale	s
T_p	Peak wave period	s
T_{dry}	Drying time scale	s
$\overline{u}$	Time-mean velocity component	m/s
u, v	Horizontal flow velocities	m/s
u_2	Wind velocity at 2 m above the bed	m/s
u_z	Wind velocity	m/s
u_{hi}	Oscillatory motion at short wave scale	m/s
u_{lo}	Low frequency motion at wave group scale	m/s
V	Longshore current velocity	m/s
w	Unnormalised weighting factor	–
$\hat{w}$	Weighting factor	–
w^{air}	Weighting factor based on the grain size distribution in the air	–
w^{bed}	Weighting factor based on the grain size distribution on the bed	–
x, y	Horizontal coordinates	m
x_1	Cross-shore coordinate of the seaward boundary of the domain of interest	m
x_2	Cross-shore coordinate of the landward boundary of the domain of interest	m
Y	Measurement	m^3/m
$\overline{Y}$	Mean of the measurements	m^3/m
y_1	Alongshore coordinate of the left boundary of the domain of interest	m
y_2	Alongshore coordinate of the right boundary of the domain of interest	m
z	Vertical coordinate	m
z_0	Roughness length	m
z_a	Height where aeolian sediment is transported	m
z_b	Bed level	m + NAP

Subscripts

Symbol	Description
$(\,)_*$	Shear
$(\,)_0$	At deep water
$(\,)_c$	Critical
$(\,)_k$	For sediment fraction k
$(\,)_{eq}$	Equilibrium (or saturated)

1 Introduction

1.1. Hondsbossche Dunes

The Hondsbossche Dunes[1] is a sandy nourishment that serves as a primary flood defence since 2015. It is a dynamic system and very adaptive to changes in climatic forcing (like storm conditions and sea level rise). In addition to its protective function, the HD stimulates ecological habitat development in the coastal area, in line with Ecoshape's 'Building with Nature'-approach (Bodde et al., 2019).

Before construction of the HD, the Hondsbossche and Pettemer sea defence[2] acted as one of the primary sea defences along the Dutch coast for centuries. The HPZ in its latest form was built in 1981 and consisted of an artificial sea dyke with a crest at NAP +12 m, see Figure 1.1a. The legal safety standard for the Dutch coast was a storm surge flooding with an exceedance probability of 1/10,000 per year. In 2003, new insights into the loads on the coast due to climate change and sea level rise led to stricter wave boundary conditions (Karman et al., 2013) and a reassessment of the Dutch coastal protection system. The HPZ did not pass this safety assessment test (Ministerie van Verkeer en Waterstaat, 2006) and was reinforced with the HD. This seven-kilometre-long dune, beach and shoreface nourishment is placed in front of the HPZ, see Figure 1.1b.

(a) HPZ prior to construction (Archi, n.d.)

(b) HD and HPZ after construction (Hoogwaterbeschermingsprogramma, n.d.)

Figure 1.1: Overview of the study area. Both photos are taken from Camperduin

The total nourished volume is 35.6 million m^3, more than 1.5 times the volume of the Sand Engine (Bodde et al., 2019; De Schipper et al., 2016). Construction of the nourishment started in March 2014 at Camperduin, the southern end of the domain. It was finished 12 months later at Petten, in the north. The HD required 26.1

[1] 'Hondsbossche Duinen' in Dutch, hereafter referred to as HD

[2] 'Hondsbossche en Pettemer Zeewering' in Dutch, hereafter referred to as HPZ

million m^3 of sand for reinforcement and 9.5 million m^3 to cover settlements, and aeolian and marine losses. An aerial view of the study area, between Petten and Camperduin, is shown in Figure 1.2.

Figure 1.2: Map of the Dutch coast (Google Maps, 2018). The study area is marked in black.

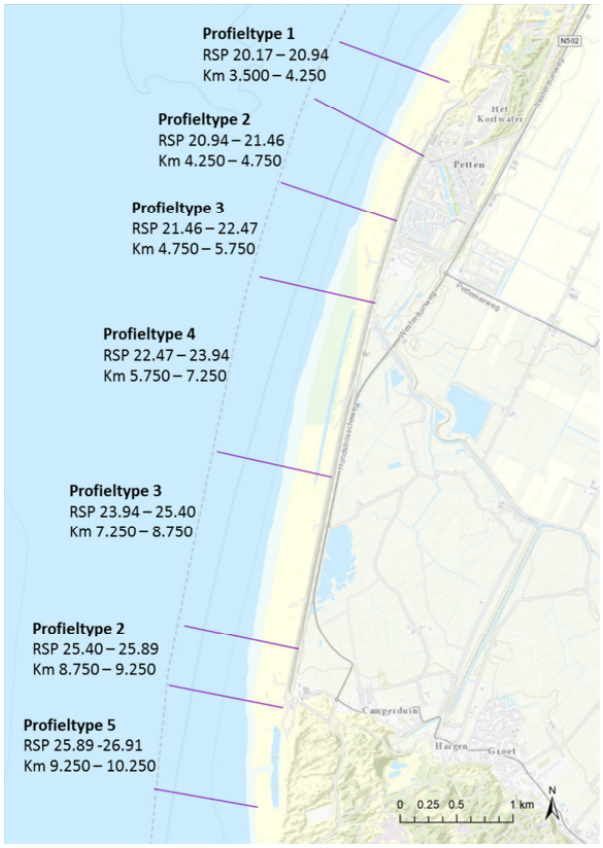

Figure 1.3: Study area with location of profile types (Leenders and Smit, 2016)

After the nourishing works, the sediment on the beach is reshaped into five different profiles, see Figure 1.3. The designs of the different profiles vary in crest height, dune slope, number of dunes and vegetation. The different profile types are briefly described in appendix A. The goal of the diversion of the HD into profile types is to assess the morphological development of the dunes as a result of marine processes and aeolian sediment transport for each profile, and to determine the optimal profile for dune growth and nature development.

To quantify profile developments, periodic measurements of the topography and bathymetry have been executed. The measurement frequency and domain of each measurement are briefly described in appendix A. This appendix also gives the measured initial grain size distributions. The finest grains are found in the south of the domain.

1.2. Problem description

In the monitoring program executed by Bodde et al. (2019), a study was conducted on the volume change of the beach and the dunes. For a closed system, the conservation of sediment mass applies. Though the longshore sediment transport is assumed to be constant and the loss of sediment behind the dunes is negligibly small, the decrease of sediment volume on the beach is not equal to the increase of sediment volume on the dunes (Bodde et al., 2019). When the intertidal zone is supplied with marine sediment from the shoreface during high tide, it is available for wind-driven transport during the subsequent low tide. The intertidal zone may be a dominant sediment source for aeolian transport on the beach (De Vries et al., 2014a). The hypothesis of Bodde et al. (2019) is that the remaining sediment must stem from the intertidal zone and the shoreface. This study elaborates on this hypothesis.

Aeolian sediment transport from the beach to the dune mainly consists of fine sediment from the top layer of the beach, because finer grains are easier transported by the wind. This results in coarsening of the sediment on the beach and a decrease of aeolian sediment transport. Waves and tides stir up the bed layer of the intertidal zone, redistributing the composition of (fine) grains on the bed. During the subsequent low tide, the wind is able to transport these fine grains to the beach and the dune, which makes the intertidal zone a very effective sediment source for aeolian transport. Aeolian sediment transport is also limited when the sediment is moist, for example when the sea wets the intertidal zone. Although several numerical models have implemented these marine processes in their calculations, current modelling studies on the HD have not included them.

The timescale of changes in sediment transport and grain size distribution could be in the order of hours to months. Changes in wave and wind conditions within a year develop a summer-winter profile cycle, where large quantities of sediment are repeatedly transported offshore and onshore. On a shorter timescale, extreme storm events transport and redistribute sediment over the entire coastal area within a few hours. Also, hydraulic mixing redistributes the sediment composition over a tidal period. The relative contributions of these processes to the development of the HD are currently unknown.

1.3. Research objective

The research objective of this study is to investigate the contribution of sediment supply and marine processes in the intertidal zone to changes in morphology and bed composition in the beach and dune. These processes may affect the supply of sediment and its grain size distribution. The typical timescale of these changes must also be assessed.

The following main research question is formulated to meet the research objective:

What is the causal relationship between marine processes and beach and dune evolution at the Hondsbossche Dunes?

The following sub-questions relate to the main research question:

1. What are the cross-shore and alongshore net sediment transport rates and which processes govern these transports?
2. How do the net sediment transport rate from the shoreface to the intertidal zone and marine processes influence dune growth?

3. How are changes in morphology and bed composition caused by marine processes in the intertidal zone?
4. What is the typical timescale of changes in morphology and bed compositions in the coastal area?

1.4. Thesis outline

The first phase of this study, which consists of a literature study on marine and aeolian sediment transport and sediment supply-limiting factors, is presented in chapter 2. Chapter 3 describes the methods used to derive the results of this study. These results are obtained through a data analysis with LiDAR, echo sounder and JARKUS measurements, and a modelling study with three 1DH AeoLiS models. The results of the data analysis and the modelling study are presented in chapters 4 and 5 respectively. Chapter 6 discusses the significance of the results, as well as the limitations and assumptions that were required or made in both studies. The main conclusions and recommendations are summarised in chapter 7.

2

Literature review

This chapter aims to give insight into the relevant theoretical background of aeolian and marine sediment transport, morphology of the intertidal zone, and nourishments. The definitions of terms for coastal features stem from the Shoreline Management Guidelines by Mangor et al. (2017).

2.1. Sediment transport

2.1.1. Physics of sediment transport

Sediment transport can be defined as the movement of sediment particles over a certain period of time through a well-defined plane (Bosboom and Stive, 2012). Changes in morphology depend on spatial and temporal fluctuations in sediment transport rates. For porous materials, this can be expressed as a continuity or mass balance:

$$(1-p)\frac{\partial z_b}{\partial t} + \frac{\partial S_x}{\partial x} + \frac{\partial S_y}{\partial y} = Q \tag{2.1}$$

where:

p	Porosity
z_b	Bed level
t	Time
S_x	Sediment transport rate in x-direction
S_y	Sediment transport rate in y-direction
x, y	Horizontal coordinates
Q	Sink and source terms

Sediment transport, both aeolian and marine, generally consists of three phases:

1. Initiation of sediment motion
2. Transport of sediment
3. Deposition of sediment

Transport of sediment is initiated when the fluid (air or water) exerts a high enough shear stress τ on the grain. This shear stress is given by:

$$\tau = \rho u_*^2 \tag{2.2}$$

where:

τ	Shear stress
ρ	Density of the fluid
u	Velocity of the fluid
$(\,)_*$	Shear

Figure 2.1 show the different forces that act on a single grain, both for grains in the air and in water. All forces, including the lift force, are based on the shear stress multiplied by a cross-sectional area of the grain. The grain can either roll over another grain or be lifted completely from the bed. These transport mechanisms are explained in more detail in the subsections 2.1.2 and 2.1.3.

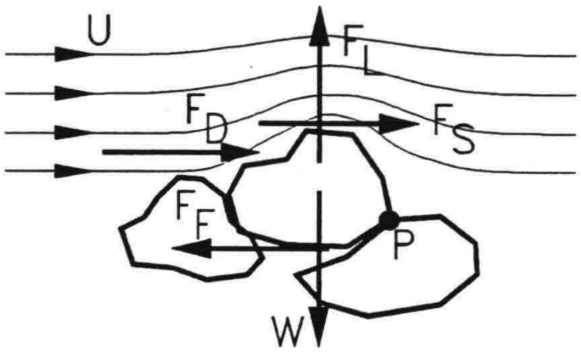

Figure 2.1: Forces on a grain in flow (Schiereck, 1993)

The sediment concentration is the dry weight of sediment per unit volume of the fluid. Sediment particles are transported by the movement of the fluid, with the same velocity u.

Given that at any height sediment particles flow through a vertical plane with the horizontal velocity, the sediment flux can be calculated from the vertical distribution of the sediment concentration and the flow velocity (Bosboom and Stive, 2012). Figure 2.2 presents these distributions for the marine transport. To a moderate extent, the distributions are similar for aeolian sediment transport.

$$q(z,t) = c(z,t)u(z,t) \tag{2.3}$$

where:

c	Instantaneous sediment concentration
q	Sediment flux
z	Vertical coordinate

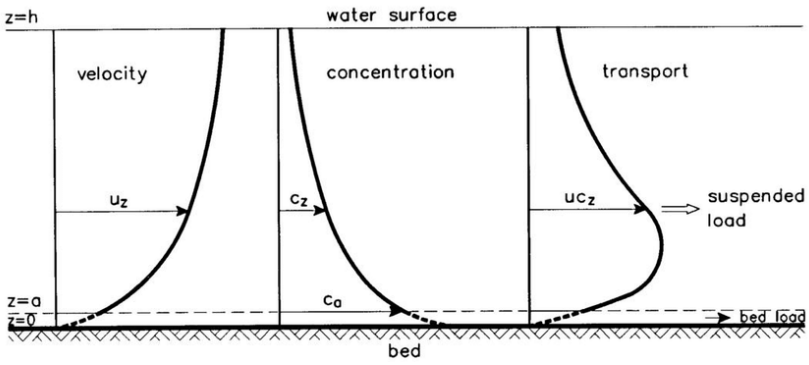

Figure 2.2: Vertical distribution of the flow velocity, sediment concentration and sediment flux (Van Rijn et al., 1993)

The sediment transport rate follows by integrating the sediment flux from a given lower to upper boundary:

$$S(t) = \int_{z=a}^{b} c(z,t)u(z,t)dz \tag{2.4}$$

where:

S	Sediment transport rate

The concentration c depends on the flow velocity u to a certain power (i.e. $c \propto u^{n-1}$). n relates the flow velocity to the sediment transport rate, i.e.:

$$S \propto u^n \tag{2.5}$$

where:

n	Exponentiality of the flow velocity to the sediment transport

Numeric values for n differ between aeolian and marine transport, and for different transport mechanisms. Typical values for n lie between 3 and 5 (Bagnold, 1937; Bosboom and Stive, 2012). Generally, marine sediment transport rates are much larger than aeolian sediment transport rates, because the density of the transporting fluid is three orders of magnitude higher (e.g. Bagnold, 1937). The different transport mechanisms are described below.

2.1.2. Aeolian sediment transport

Bagnold (1937) laid the foundations of transport of sand by wind, based on physics and laboratory experiments. Using Prandtl-Von Kármán's Law of the Wall, the wind velocity u_z at any height z can be described as a function of the shear velocity u_* (from equation 2.2) according to:

$$u_z = \frac{u_*}{\kappa} \ln\left(\frac{z}{z_0}\right) \tag{2.6}$$

where:

u_z	Wind velocity
κ	Von Kármán's constant ($\kappa = 0.4$)
z_0	Roughness length

For cohesionless beds composed of sedimentary particles like sand, individual grains begin motion when the shear stress exceeds a threshold value (Sherman and Hotta, 1990). A sand grain is lifted from the bed due to a lift force that arises due to an uneven wind velocity distribution, see Figure 2.1. This critical shear velocity u_{*c} is described by Bagnold (1941) in the following expression:

$$u_{*c} = A\sqrt{\frac{\rho_s - \rho_a}{\rho_a} g d_n} \tag{2.7}$$

where:

A	Empirical coefficient ($A \approx 0.1$)
ρ_s	Density of sediment
ρ_a	Density of air
g	Gravitational acceleration ($g = 9.81$)
d_n	Nominal grain size
$(\,)_c$	Critical

This expression describes a so-called dynamic threshold. When the wind velocity exceeds this threshold, an initial movement of sand grains on the surface will give rise to sufficient new flying grains to continue the process of sand movement down-wind.

When the wind velocity exceeds the threshold wind velocity described in equation 2.7, the wind forces particles into suspension, saltation or creep, depending on the grain size. Figure 2.3 presents the different particle transportation types. Grains are in suspension when they are lifted and carried by the wind, without touching the bed. However, this only covers a small fraction of the total transport. Grains in saltation fly through the air before they strike the surface at a relatively flat angle. A portion of the energy they have acquired from the

wind is passed on to the grains that are ejected upwards to continue the saltation (Bagnold, 1941). Creep is the process when individual grains are pushed over the bed surface by a push of wind. This transport mechanism is initiated when a grain topples over another grain, see point P from Figure 2.1. Though saltation is the predominant transport type, creep accounts for a significant fraction of the total aeolian transport (Bagnold, 1941). Grains in creep can also receive their momentum by impact from a grain in saltation.

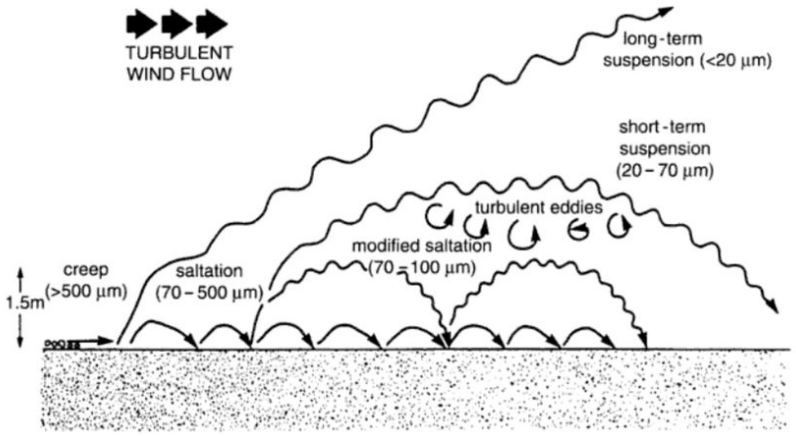

Figure 2.3: Aeolian sediment transport types (Pye, 1987)

Bagnold (1941) describes the equilibrium or saturated sand flow S_{eq} (in kg/s/m) as a function of the wind velocity with the following equation:

$$S_{eq} = \alpha C \frac{\rho_a}{g} \sqrt{\frac{d_n}{D_n}} (u_z - u_c)^3 \tag{2.8}$$

where:

α	Conversion constant
C	Empirical coefficient related to the grain size distribution ($C = 1.5 - 2.8$)
D_n	Reference grain size ($D_n = 250$ μm)
$(\,)_{eq}$	Equilibrium (or saturated)

Bagnold (1941) assigned typical values for C, ranging from 1.5 for nearly uniform sand, 1.8 for typical dune sands, and 2.8 for sand with a wide range in grain size. α is a constant to account for the conversion of the measured wind velocity to the near-bed shear velocity. Its expression stems from equation 2.6 and is given by:

$$\alpha = \left(\frac{\kappa}{\ln(z/z_0)} \right)^3 \tag{2.9}$$

Many studies have followed that of Bagnold (1937) with different parameterisations or velocity thresholds, but the structure and application of those studies stayed essentially the same (Hoonhout and De Vries, 2016). Equation 2.8 requires steady flow conditions and sufficient availability of sand. In that case, sediment transport is transport limited. In coastal areas, this is often not the case. Parameters like sediment sorting, soil moisture content, beach slope, fetch length, and the presence of vegetation limit the sand availability for transport (Muller et al., 2012; Hoonhout et al., 2013; De Vries et al., 2014b) and sediment transport is supply limited. These parameters are highly dependent on meteorological and morphological conditions (De Vries et al., 2012). Section 2.2 focuses on the impact of sediment sorting and moisture content on sediment transport.

The slope of the beach increases the threshold of motion for grains in creep, as the grains do not only need to move down-wind but also upward. Also, the suspension time for grains is shorter. The fetch length depends

on the orientation of the wind and the tidal amplitude. As the wind direction, wind magnitude, and tidal level vary on an hourly to daily basis, the fetch, and therefore the transport capacity, is highly influenced. Dense vegetation in dune areas acts as a catchment for grains in saltation (Hoonhout et al., 2013).

Many studies on the impacts of these parameters on aeolian sediment transport have been executed. These studies have often resulted in modified critical wind velocities (Hoonhout and De Vries, 2016).

2.1.3. Marine sediment transport

Marine sediment transport is the movement of grains through water. Similar to aeolian sediment transport, marine sediment transport is initiated when a certain critical shear stress on the grain is exceeded. The fluid excites a lift force, which results from a variation in the flow velocity profile, that moves a grain upward and streamwise. Marine sediment transport also consists of several transport mechanisms. It can be divided into suspended load transport and bed load transport. Grains in suspension are lifted from the seabed and are carried by the fluid through turbulence, and grains on the bed roll over other grains while staying within the boundary layer. See Figure 2.4.

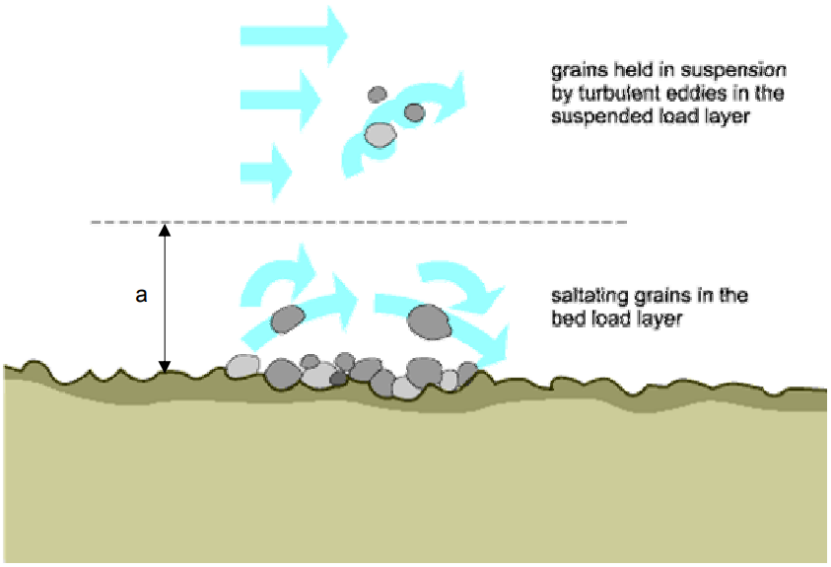

Figure 2.4: Marine sediment transport types (Sorgedrager, 2002)

Shields (1936) compared the lift force and gravity force acting on a single grain (see Figure 2.1), and found the following relation for the critical shear velocity for bed load transport due to currents:

$$u_{*c} = \sqrt{\Delta g D_{50} \theta_c} \tag{2.10}$$

where:

Δ	Relative density ($\Delta = (\rho_s - \rho_w)/\rho_w = 1.65$)
ρ_w	Density of water
D_{50}	Median grain size
θ	Shields parameter

For turbulent flow, an approximation for the critical Shields parameter is given: $\theta \approx 0.055$. This equation shows a high similarity with equation 2.7, as the critical flow velocity for both aeolian and marine sediment transport equals $\sqrt{\Delta g D}$, multiplied by a certain factor. Note that the relative density Δ for aeolian transport depends on the density of air ρ_a, while the density of water ρ_w determines the relative density for marine sediment transport.

The velocity threshold for suspended load transport is the same as for bed load transport (Bosboom and Stive, 2012). When a grain is lifted beyond a certain level, the turbulent upward forces force a grain into suspension.

Due to the large number of hydraulic processes, there is no clear nearshore velocity profile (like equation 2.6 for aeolian sediment transport), but it shows temporal and spatial variations. Calculating bed profile dynamics is generally done through process-based models, which in most cases solve the shallow water equations for the flow velocity and an advection-diffusion equation for the sediment concentration.

Although morphological changes in the coastal area are three-dimensional, it is customary to consider cross-shore and longshore evolution separately (Dean, 2002). Cross-shore sediment transport tends to move sediment onshore or offshore, and results in development of the profile. Longshore sediment transport contributes to shaping the coastline by moving grains along the coast.

Cross-shore sediment transport
Cross-shore hydrodynamics, sediment transport dynamics and resulting bed profile dynamics are very complex (Bosboom and Stive, 2012). It is a combination of bed and suspended load due to undertow, short wave skewness, and bound and free long waves.

There are many differences in the notation of the sediment transport formulations listed above, making the uncertainty in computations large. However, a common attribute in all formulations is that the sediment transport rate depends on the flow velocity to a certain power. The contribution of the flow velocity to the cross-shore sediment transport is elaborated upon below, to understand better the hydraulic processes what result in sediment transport.

At any point in space and time, the flow velocity consists of the sum of the velocity components of the three processes mentioned above:

$$u = \overline{u} + u_{lo} + u_{hi} \tag{2.11}$$

where:

$\overline{u}$	Time-mean velocity component
u_{lo}	Low frequency motion at wave group scale
u_{hi}	Oscillatory motion at short wave scale

Based on the energetics approach and equation 2.5, Bosboom and Stive (2012) found a relation between the flow velocity and sediment transport for bed load and suspended load transport:

$$\langle S_b \rangle \propto \langle u|u|^2 \rangle \tag{2.12}$$

$$\langle S_s \rangle \propto \langle u|u|^3 \rangle \tag{2.13}$$

where:

S_b	Bed load transport
S_s	Suspended load transport
$\langle ... \rangle$	time-averaged

Again, the exponentiality n is purely empirical and differs between several sediment transport formulations. However, most formulations agree that the exponentiality of the flow velocity to the suspended load transport is approximately one point higher than to the bed load transport.

Substituting the terms from equation 2.11 into the bed load equation results in a better understanding of the physical interpretation of transport:

$$\langle u|u|^2 \rangle = 3\langle \overline{u}|u_{hi}|^2 \rangle + \langle u_{hi}|u_{hi}|^2 \rangle + 3\langle u_{lo}|u_{hi}|^2 \rangle + ... \tag{2.14}$$

Only the three most important terms are depicted here. The term $|u_{hi}|^2$ can be interpreted as stirring up of sediment load by short waves. Subsequently, the sediment load is transported either by the wave-induced near bed streaming or the undertow ($\overline{u}$), skewed short waves (u_{hi}), or bound or free long waves (u_{lo}). Decomposition of suspended load transport shows similar results, except that the stirring components are related to the third power of the flow velocity.

Roelvink and Stive (1988) analysed the decomposition of the third and fourth power velocity moments using laboratory measurements in a large-scale wave flume, see Figure 2.5. Wave skewness results in a net onshore

directed sediment transport. The undertow transports sediment offshore. The contribution of bound long waves is seaward directed in deeper water, because the trough of the bound long wave, where the horizontal velocity is offshore directed (u_{lo} is negative), coincides with the highest short waves of the wave group ($|u_{hi}|^2$ is highest). When approaching shallower water, the highest short waves in the wave group break, releasing their turbulent energy and 'freeing' the bound long wave. The result is a change of direction of sediment transport, as only the crest of the long wave can transport sediment.

Because sediment transport through long waves is the only transport mechanism that changes its cross-shore direction when approaching the coast, the direction of the net sediment transport between the shoreface and the intertidal zone may depend on this transport mechanism. Based on physical and numerical modelling, Broekema et al. (2016) showed that short-wave grouping and long wave effects contribute to the cross-shore profile development.

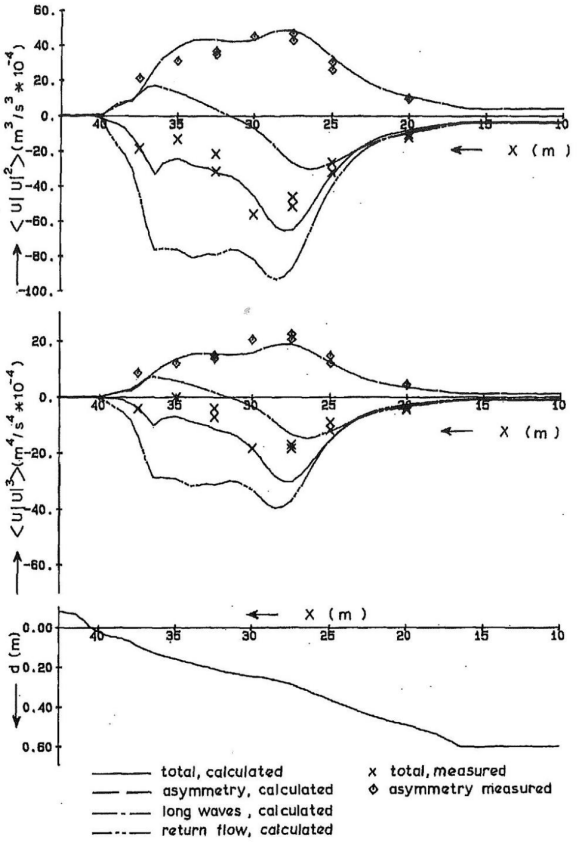

Figure 2.5: Bed load and suspended load transport for waves approaching the coastline (Roelvink and Stive, 1988)

Longshore sediment transport

Spatial gradients in longshore sediment transport, sources, and sinks are responsible for changes in the shape of the coast (Bosboom and Stive, 2012). The main transport mechanism is the wave-driven longshore transport. When waves reach the coast under an angle, the longshore component of the flow velocity contributes to a uniform longshore transport of grains. Spatial gradients in longshore sediment transport stem from variations in orientation of the coastline or the presence of hard structures like breakwaters.

The longshore sediment transport can be approximated with equation 2.5, where n is 3. Sediment is stirred up by either the short wave orbital motion or the longshore current, and consequently transported by the longshore current. The time-averaged longshore sediment transport can be calculated with:

$$\langle S_y \rangle \propto \langle u_{hi}^2 + V^2 \rangle V \tag{2.15}$$

where:

V	Longshore current velocity

Since $u_{hi} >> V$, equation 2.15 can be simplified to $S_y \propto u_{hi}^2 V$.

Coastal Engineering Research Center (2008)[1] provided an expression for the total longshore sediment transport due to waves approaching the coast under an angle. It is given by:

$$S = \frac{K}{32(s-1)(1-p)} c_{br} \sin\left(2\varphi_0\right) H_0^2 \tag{2.16}$$

where:

K	Empirical coefficient
s	Density ratio of sediment and water ($s = \rho_s / \rho_w = 2.65$)
c_{br}	Wave celerity at the outer edge of the breaker zone
φ	Wave angle of incidence
H	Wave height
$(\,)_0$	At deep water

This notation uses deep water wave conditions, which is convenient because the deep water wave height and angle of incidence are not yet influenced by shoaling or refraction, see Figure 2.6a. Shoaling and refraction change the offshore wave height according to:

$$H = K_{sh} K_r H_0 = \sqrt{\frac{1}{\tanh kh} \frac{1}{2n}} \sqrt{\frac{\cos\varphi_0}{\cos\varphi}} H_0 \tag{2.17}$$

where:

K_{sh}	Shoaling factor
K_r	Refraction factor
n	Ratio between the group velocity and the higher phase velocity

Equation 2.16 shows the longshore sediment transport is largest when the wave angle of incidence $\varphi = 45°$, see also Figure 2.6b. Figure 2.6c and 2.6d show the influence of the wave angle of incidence on the longshore sediment transport on a non-uniform coast. For a small angle of incidence ($\varphi < 45°$), the longshore sediment transport increases for an increasing angle. The result is flattening of the shape, see Figure 2.6c. For $\varphi > 45°$, the longshore sediment transport decreases for an increasing angle and the crest of the coastal shape silts up, see Figure 2.6d.

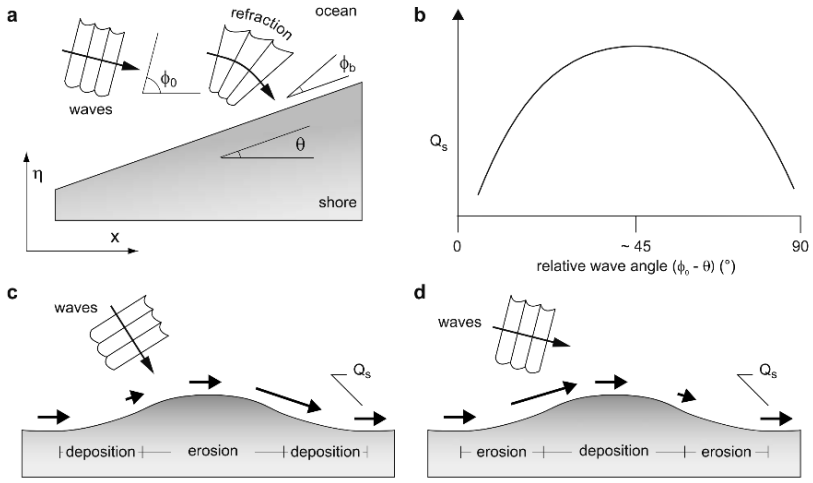

Figure 2.6: Longshore sediment transport depending on the wave angle of incidence (Ashton and Murray, 2006). (a) Definition of terms and axes. (b) Relation between longshore sediment transport and the wave angle of incidence, based on the CERC formula. (c) Longshore sediment transport at a non-uniform coast for $\varphi < 45°$. (d) Longshore sediment transport at a non-uniform coast for $\varphi > 45°$.

[1] hereafter referred to as CERC (2008)

Longshore sediment transport generally takes place up to the closure depth. The closure depth is defined as the depth beyond which no significant seabed changes take place due to littoral transport processes (Mangor et al., 2017). According to Hallermeier (1981), it is a function of the wave height and the wave period according to:

$$h_* = 2.28 H_{s,12h/y} - 68.5 \frac{H^2_{s,12h/y}}{g T_p^2} \tag{2.18}$$

where:

h_*	Closure depth relative to mean low water level
$H_{s,12h/y}$	Significant wave height that is exceeded 12 hours per year
T_p	Peak wave period

Morphological development beyond the closure depth can occur. Van de Rest (2004) proved that sediment is transported even beyond the NAP -20 m depth contour along the entire Dutch coast. This development can have the following causes:

- The closure depth is defined as the depth beyond which no significant seabed changes take place due to littoral transport processes (i.e. longshore transport) (Mangor et al., 2017). This does not exclude cross-shore sediment transport processes. According to Van Rijn (1997), Longuet-Higgins streaming, asymmetry in wave velocity and density gradients cause landward cross-shore sediment transport in deep water, while bound long waves and the undertow result in seaward transport. The presence of finer grains may result in relatively large offshore-directed transport, while coarser grains tend to move in onshore direction.
- Flow contraction may lead to gradients in longshore sediment transport in the offshore zone, as the flow velocity is higher at the tip of the nourishment. This effect has been observed at the Sand Engine (Radermacher et al., 2017).
- Extreme storm surge and extreme storm wave events can result in a permanent offshore loss of sediment (Mangor et al., 2017).

2.2. Morphology of the intertidal zone

The intertidal zone is a complex area, as it is influenced by wave dissipation, wave breaking, spatial and temporal variations in grain size distributions, groundwater dynamics, and change in the mean water level by tides and other processes (Cohn et al., 2017). Sediment transport consists of both aeolian and marine transport, depending on the instantaneous water level. At high tide, hydraulic processes like skewed waves and free long waves can transport sediment onshore and deposit it on the bed in the intertidal zone. During the subsequent low tide, this sediment is available for aeolian transport. The intertidal zone is thought by De Vries et al. (2014a) to be the primary source of aeolian sediment transport.

2.2.1. Sandbars

During mild wave conditions, sandbars at the foreshore migrate onshore, because short waves release their transport capacity when they break above the sandbar and deposit sediment on the landward side of the bar. Meanwhile, sediment is eroded from the seaside of the bar. The bar eventually emerges from the water and forms an intertidal sandbar. This intertidal sandbar provides a new sediment source for aeolian transport in the intertidal zone. A study by Cohn et al. (2017) showed that the beach width could increase up to 20 m over a six-week-period due to the emergence of intertidal sandbars.

Measurements by Cohn et al. (2018) showed that marine processes account for 9% to 36% of the annual dune growth. While intertidal sandbar migration drives beach widening in the summer, the most substantial dune growth occurred during the winter, when the wind velocity was highest. This result shows that aeolian sediment transport at beaches can be transport limited, rather than supply limited, and that the relative contribution of different processes to seasonal variation in sediment transport is highly uncertain.

In environments where the wave height has an annual cycle of change (e.g. high storm waves in winter and low swell in summer, which is the case for the Holland coast), a beach state can vary from a dissipative 'winter' profile to a reflective 'summer' profile, see Figure 2.7. High energy storm events can cause a shift of beach state from reflective or intermediate to dissipative in a matter of days, because the energy is high. The return to reflective conditions under low energy can require weeks or months or longer (Wright and Short, 1984). The profiles in Figure 2.7 can also represent the beach profile before and after a storm.

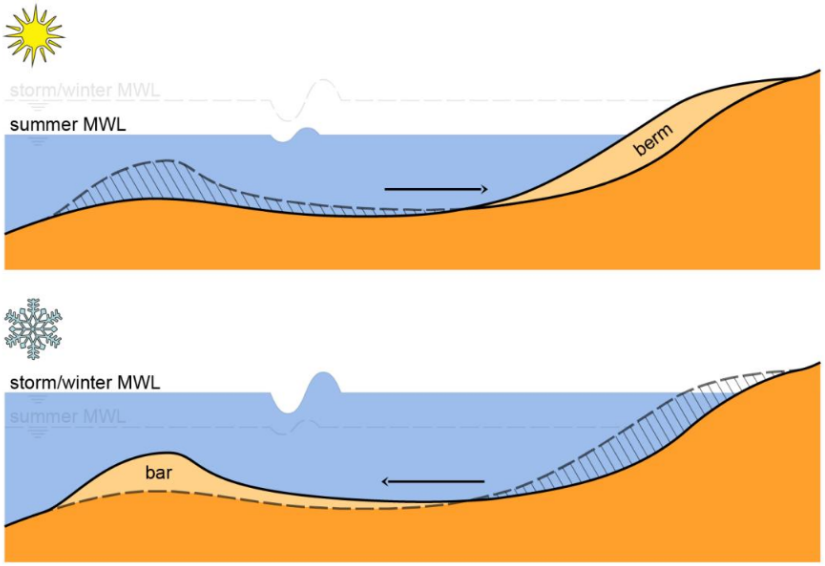

Figure 2.7: Summer and winter equilibrium profile (Bosboom and Stive, 2012)

2.2.2. Sediment sorting and hydraulic mixing

Sediment transport, both aeolian and marine, depends on the grain size on the bed. Bagnold (1941) showed that the threshold of motion for aeolian sediment transport is positively related to the grain size. Also, Van Rijn (2007a,b) showed that suspended load transport is inversely related to the median grain size D_{50}. Bed load transport may increase weakly with increasing grain size. When fine grains are easier transported than coarse grains, the grain size distribution of the top layer of the bed will change. Erodible elements (fine grains) may be deposited on top of non-erodible elements (coarse grains) or, reversely, erodible elements may be eroded from the bed surface leaving non-erodible elements to reside on top of the original, mixed sediment. The latter is called winnowing. These non-erodible elements may shelter the erodible bed from wind erosion, resulting in a reduced sediment availability (Hoonhout, 2018). Holland and Elmore (2008) revealed that sediment heterogeneity is significant regarding its impact on coastal processes.

As winnowing can lead to armouring of a beach surface, mixing of the beach surface or erosion of course material may undo the effects of armouring (Hoonhout and De Vries, 2016). In the presence of tides, the intertidal beach is flooded periodically. Hydraulic processes like wave breaking mix the bed surface layer of the intertidal beach, break the beach armouring and thereby influence the availability of sediment. De Vries et al. (2014a) discovered a relatively large sediment supply in the intertidal zone (when exposed) and a small supply on the upper beach due to sorting processes. The bed composition is also strongly influenced by long waves (Broekema et al., 2016).

Prodger et al. (2016) observed seasonal variability in grain size distributions in the intertidal zone, based on observations. Relatively fine grain sizes were found in June to September, when low-steepness swell waves dominated the wave climate. Coarser sediments were found from January to February, when high-steepness storm waves attacked the coast. It became clear that fine sediment fractions increased in relative abundance during prolonged periods of low wave energy. The same holds for coarse sediment fractions and periods of high wave energy. This relation holds because high-steepness waves (small wave period, high wave height) tend to move sediment offshore, while low-steepness waves transport sediment onshore. Because fine sediment is easier transported than coarse sediment, it is predominantly the fine sediment that is transported onshore and offshore during the winter-summer cycle, see Figure 2.7.

2.2.3. Soil moisture content

The threshold for motion of moist sand is generally higher than for dry sand, because of the cohesive effects. Also, the transition of momentum from grains in saltation to grains on the bed is less effective (Hoonhout et al., 2013). The soil moisture content depends on the tide, wave runup, storm surges, rain showers, solar radiation and wind. Many studies on the influence of the moisture content on the threshold velocity have been conducted, which resulted in different shear threshold velocities (e.g. Belly (1962): equation 2.19).

$$u_{*c} = A\left(1.8 + 0.6 \cdot \log_{10} p_g\right) \sqrt{\frac{\rho_s - \rho_a}{\rho_a} g d_n} \tag{2.19}$$

where:

p_g Mass percentage of water relative to dry sand

Hydraulic processes like tides and waves periodically wet the intertidal beach, temporally increasing the shear velocity threshold. Hydrology model runs show that the increase of the water content to saturation is almost instantaneous with rising tide (Simunek et al., 2005). Infiltration and evaporation subsequently dry the beach. Infiltration shows an exponential decay, while the evaporation rate is an adapted version of the Penman equation (Maidment et al., 1993). De Vries et al. (2014a) found a correlation between the aeolian sediment transport rate and the tidal water level. Although the wind velocity and direction were more or less constant ($u_z \approx 10$ m/s and $\varphi \approx 310°$), approximately 90% of the total transport occurred during low tide, when the moisture content of sediment in the intertidal zone is lowest, see Figure 2.8.

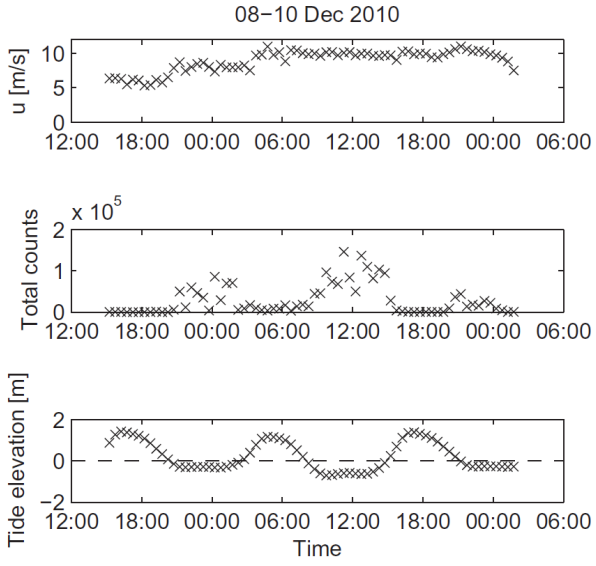

Figure 2.8: Measured wind velocity, transported grain count, and tidal water level (De Vries et al., 2014a)

2.3. Morphology of nourishments

Nourishments comprise the placement of sand in the coastal zone to advance the coastline and to counteract erosion (Dean, 2002). They are a widely applied technique aimed to increase recreation and coastal safety (Verhagen, 1992; De Schipper et al., 2016). Unlike 'hard' measures like breakwaters or groynes, this 'soft' measure does not disturb the natural sediment transport, but enhances it as it brings sediment into the coastal system and widens the beach, see Figure 2.9.

After the nourishment is constructed, the cross-shore profile evolves towards an equilibrium shape, which depends on the grain size of the nourishment. Bruun (1954) described this shape, see equation 2.20:

$$h(x) = Ax^{\frac{2}{3}} \tag{2.20}$$

where:

h	Water depth
A	Sediment scale parameter
x	Horizontal distance from the shoreline

Dean (1991) derived an expression for A, based on the shallow water wave theory:

$$A = \left(\frac{24 \varepsilon D_{50}}{5 \rho_w g^{3/2} \gamma^2} \right)^{2/3} \tag{2.21}$$

where:

ε	Wave energy dissipation
γ	Breaker index

The seaward boundary of equation 2.20 is the closure depth, which is defined in equation 2.18. If the sediments of the nourishment are the same as the sediments of the native beach, the new beach shape is the same as the shape before the nourishment, see Figure 2.9. If the coastline must advance with a distance Δx, the required quantity of sediment is $h_* \Delta x$.

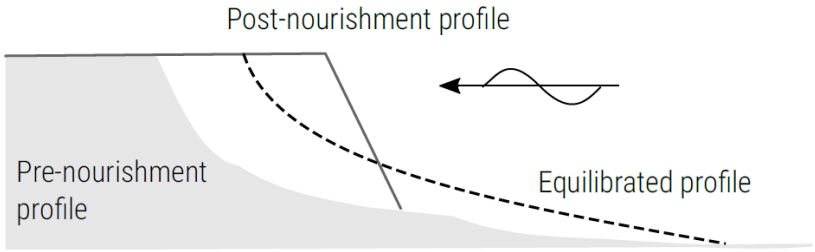

Figure 2.9: Profile equilibration after a nourishment through cross-shore transport (Elko and Wang, 2007, as cited in De Jongh, 2017)

The expression of Bruun (1954) is very simplified. It does not take into account the occurrence of sand bars or temporal variation in the beach profile (for example Figure 2.7).

Also, the shoreline planform adjusts via alongshore spreading of the nourished sediment (CERC, 2008; Wang et al., 2009), see Figure 2.10. Section 2.1.3 stated that the shape of a nourishment flattens out for a small wave angle of incidence, see also Figure 2.6c. Longshore spreading eventually results in loss of sediment, see the left and right side of Figure 2.10. Verhagen (1992) estimated the loss of sediment volume in the first period after completion of nourishments to be 40%. The volumetric sediment loss of the Sand Engine was calculated to be 72% (De Schipper et al., 2016). A year after construction of the HD, 2.5% of the nourished sediment is lost, especially due to alongshore spreading (De Jongh, 2017). This process is mainly the result of individual events: Large morphological changes coincide with months with energetic waves.

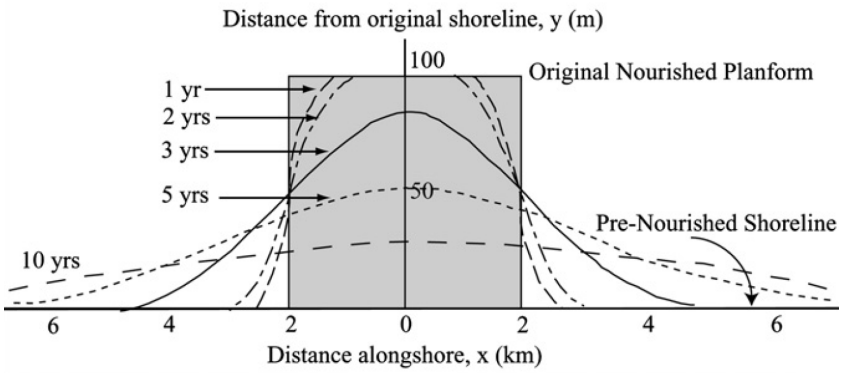

Figure 2.10: Planform nourishment adjustment via longshore transport (Elko and Wang, 2007)

Depending on the relation of the sediment scale parameter of the native sediment A_n and the fill sediment A_f, the beach profiles are either intersecting, non-intersecting or submerged (Dean, 1991). Intersecting profiles require that the sediment of the nourishment is coarser than the native sediment, although this condition does not guarantee an intersecting profile. Non-intersecting and submerged profile always occur when the fill sediment is the same as the native sediment, or when the fill sediment is finer. A submerged profile can only occur when the fill sediment is finer than the native sediment.

Figure 2.11 presents the equilibrium beach profile for different nourishment grain sizes. In every panel, the native grain size is 0.20 mm and the nourished volume of sediment is 340 m^3/m. The closure depth h_* is set to 6 m. The top panel shows an intersecting profile with a fill grain size of 0.40 mm. The beach has accreted by 92.4 m. The second panel shows a non-intersecting profile, where the fill sediment is the same as the native sediment. This panel shows a similar shape as Figure 2.9. The coastline has advanced by 45.3 m. The third panel shows a non-intersecting profile where the fill sediment is finer than the native sediment: 0.17 mm. The coastline has advanced by only 15.9 m. The bottom panel shows a submerged profile with a fill grain size of 0.15 mm. No dry beach is yielded since all added sediment is used to satisfy the underwater requirements. This figure shows that the nourished grain size greatly influences the equilibrium beach profile and beach width.

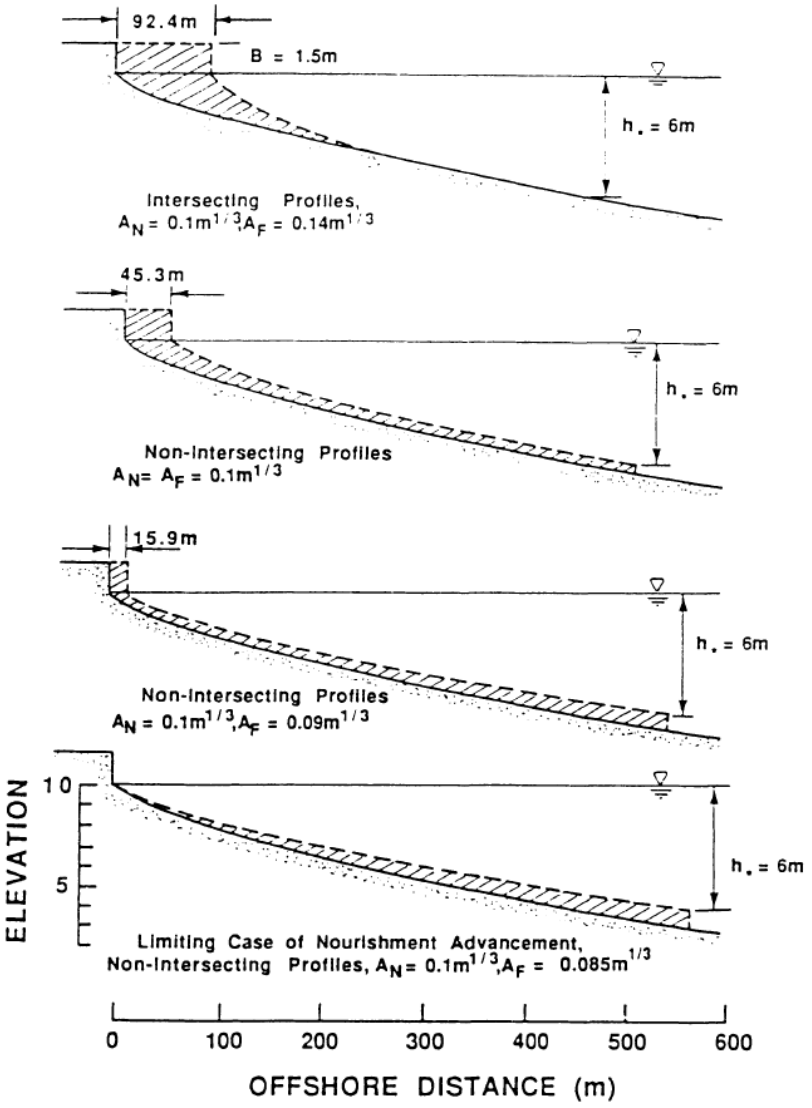

Figure 2.11: Effect of nourishment grain sizes on the beach profile (Dean, 1991)

2.4. Conclusions

As mentioned in this literature review, sediment transport in the intertidal zone is very complex, because it consists of both marine and aeolian sediment transport and is affected by many marine and aeolian processes. These processes can change the morphology and bed composition of the intertidal zone.

Equation 2.8 defines the aeolian sediment transport capacity following Bagnold (1941), which requires steady flow conditions and a sufficient quantity of sand. However, this may not be the case in coastal areas, because sediment transport is limited by sorting, soil moisture through tides and waves, fetch length and the presence of vegetation. Therefore, it is uncertain whether the wind reaches its sediment transport capacity when it approaches the dunes. The modelling study elaborates on the effect of marine processes on aeolian sediment transport and dune growth, see chapter 3.

Sediment transport through long waves is the only transport mechanism that is able to transport sediment both onshore and offshore, see Figure 2.5. When bound long waves approach the coast, they transport sediment net offshore. When the highest short waves of their corresponding wave group break, the 'freed' long waves transport sediment net onshore. Therefore, the direction of the net sediment transport between the shoreface and the intertidal zone may depend on this transport mechanism.

Breaking of short waves depends on the wave height and the water depth. Subsection 2.2.1 explains that short waves are likely to break on top of sandbars. The number of waves that break on top of a sandbar depends on the crest level of this sandbar. If the crest of the sandbar is deep (relative to the still water level), only the highest waves will break on top of it. If it is shallow, many low waves are likely to break as well. Based on this statement and the physics of sediment transport through long waves, it may be possible that the direction of sediment transport between the shoreface and the intertidal zone, through long waves, depends on the crest level of sandbars in the shoreface. The data analysis elaborates, among others, on this hypothesis, see chapter 3.

3

Methodology

This chapter describes the research steps and methods of this study, as well as the assumptions required to obtain the results. The study consists of two parts: A data analysis and numerical modelling. These two parts aim to answer the four sub-questions defined in section 1.3:

- Data analysis
    1. What are the cross-shore and alongshore net sediment transport rates and which processes govern these transports?
- Numerical modelling
    2. How do the net sediment transport rate from the shoreface to the intertidal zone and marine processes influence dune growth?
    3. How are changes in morphology and bed composition caused by marine processes in the intertidal zone?
    4. What is the typical timescale of changes in morphology and bed compositions in the coastal area?

3.1. Data analysis

The study of Bodde et al. (2019) used the LiDAR-measurements[1] to realise the sediment volume balance of the beach and the dunes of the HD. With the inclusion of marine data (echo sounder and JARKUS), this domain can be extended with the offshore zone, shoreface and intertidal zone. As a result, marine morphological development can directly be linked to dune and beach evolution.

Description of the study area
The cross-sectional domain can be divided into five cross-shore zones: The dunes, the beach, the intertidal zone, the shoreface, and the offshore zone. The boundaries of these zones depend on the bed level relative to NAP, see Table 3.1. The definitions of the cross-shore zones are also presented in Figure 3.1.

Table 3.1: Definition of different cross-shore zones at the HD (Bodde et al., 2019)

Profile zone	Seaward boundary	Landward boundary
Dune	NAP +3 m	Connection to the HPZ
Beach	NAP +0.84 m	NAP +3 m
Intertidal zone	NAP -0.76 m	NAP +0.84 m
Shoreface	NAP -10.9 m	NAP -0.76 m
Offshore zone	NAP -14 m	NAP -10.9 m

[1] Light Detection And Ranging

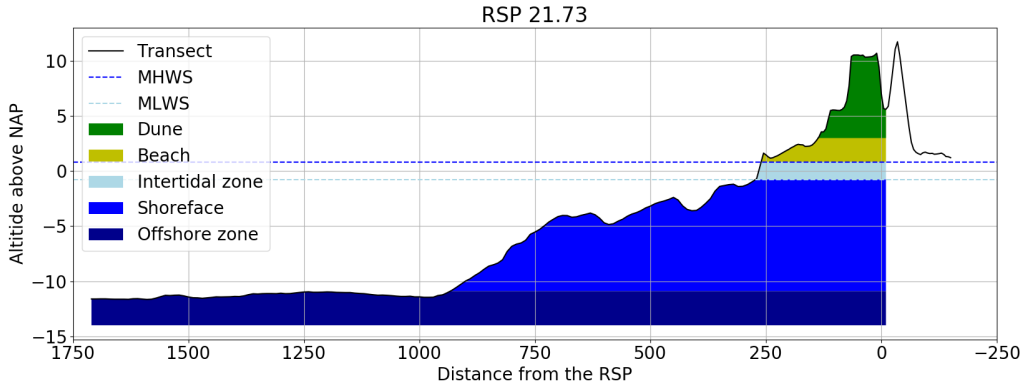

Figure 3.1: Definition of cross-shore zones

The boundary between the shoreface and the offshore zone is the closure depth, which is defined at NAP -10.9 m, based on wave data from Rijkswaterstaat[2] and equation 2.18. In case of multiple dune rows separated by dune valley which lies below NAP +3 m (see for example Figure A.4), the most seaward dune is normative for the seaward boundary of the dunes.

Distinctions are made between the different profiles. Profile type 1 and 5 (P1 and P5, see Figures A.1 and A.5) are excluded in this analysis because they are constructed for touristic purposes instead of coastal safety or ecological development. P1 near Petten consists of a high, sandy lookout tower, while P5 near Camperduin contains a large lagoon which is connected to the sea. Both profiles show atypical morphologic behaviour (Bodde et al., 2019). Figure 3.2 is a satellite image, showing the boundaries and profiles fully to scale.

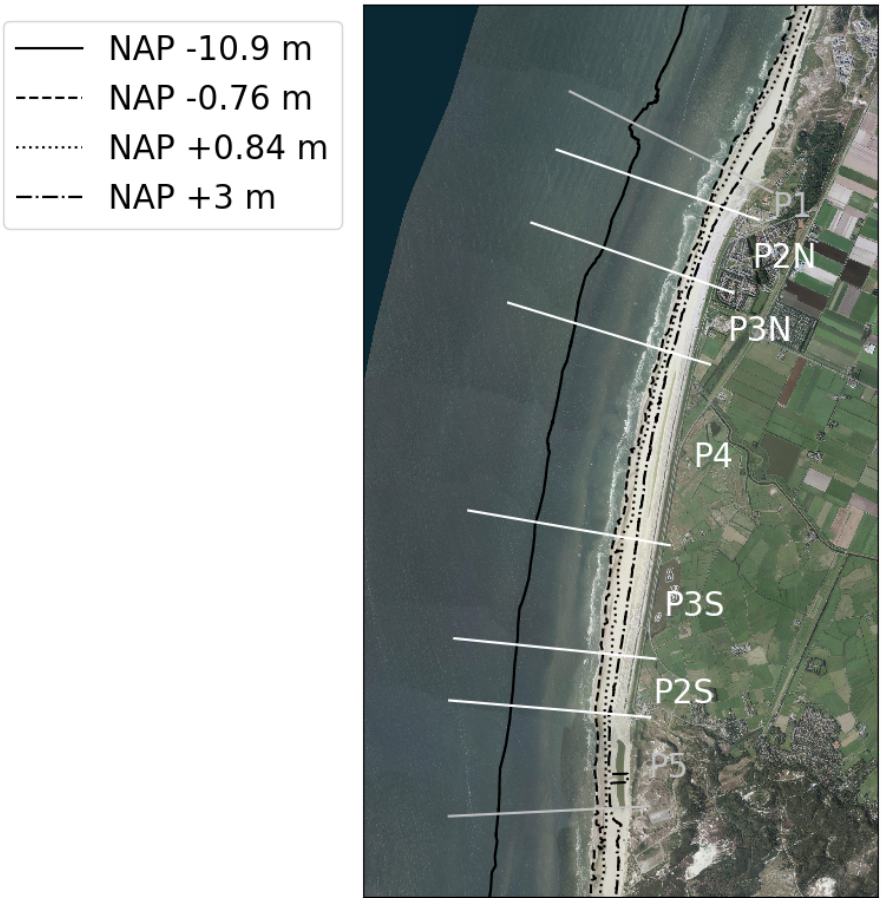

Figure 3.2: Satellite image of the HD showing the boundaries between cross-shore zones and profile types

[2] the Dutch Ministry of Infrastructure and Environment, hereafter referred to as RWS

Volume changes and net sediment transport rates
The sediment volume balance of the dunes, beach, intertidal zone, shoreface and offshore zone is shown in Figure 3.3. Sediment transport rates follow from changes in sediment volume. Figure 3.3 distinguishes the different profile types, but excludes P1 and P5. The satellite image in Figure 3.2 shows the cross-shore and longshore boundaries fully to scale.

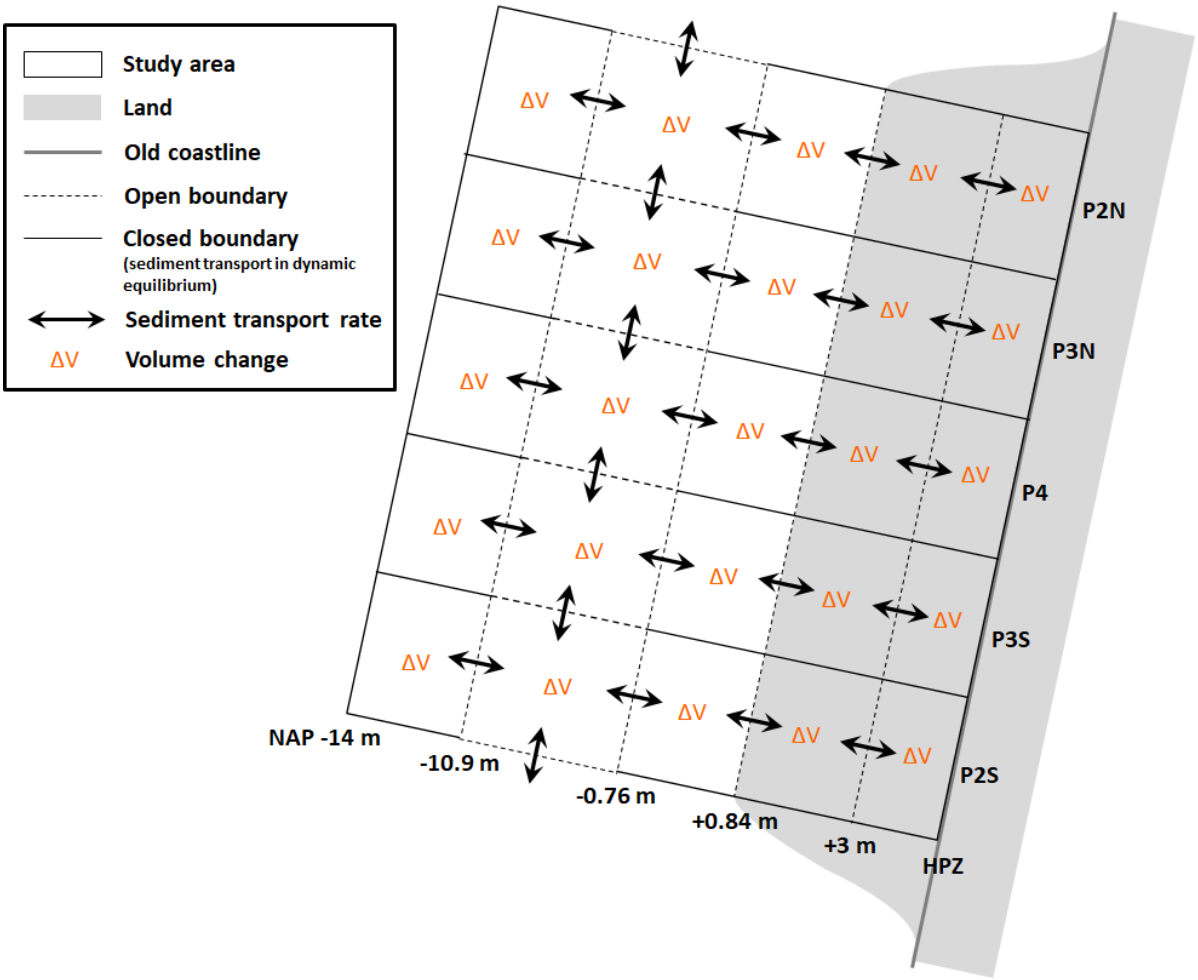

Figure 3.3: Sediment volume balance of the dunes, beach, intertidal zone, shoreface and offshore zone of the HD, with volume changes (orange numbers) and net sediment transport rates (black arrows)

The main assumption in this balance is that gradients in longshore sediment transport only occur in the shoreface. This longshore sediment transport is the result of breaking waves and tidal asymmetry. This assumption creates a closed system, which is necessary to be able to calculate all transport rates. Sediment transport through a closed boundary can take place, but it is assumed to be in dynamic equilibrium and does not result in volume changes. In the offshore zone, which lies below the closure depth, there is little longshore sediment transport due to the absence of breaking waves. Sediment transport rates in the dunes, beach and intertidal zone mainly consist of aeolian transport, where sediment is only transported in the direction of the wind. These assumptions imply that sediment transport in these cross-shore zones is in dynamic equilibrium and suggest little transport gradients in alongshore direction. Also, aeolian sediment transport from the HD to the HPZ is negligibly small for all profile types (Bodde et al., 2019).

Apart from these gradients in sediment transport, a settlement of the subsoil must be taken into account. The volume loss over the entire nourishment during the first year is approximately 200,000 m^3, or 35 m^3 per unit width, based on measurements (De Jongh, 2017).

Volume changes within a given domain of interest can be calculated from the bed level data by subtracting

the new bed level from the old bed level, and multiplying the sum of the bed level changes by the horizontal accuracy of measurements, both in cross-shore and alongshore direction. For a spatial and temporal varying horizontal accuracy, the volume change can be calculated according to:

$$\Delta V = \sum_{n=y_1}^{y_2} \left(\sum_{m=x_1}^{x_2} \left(z_{t_2,m,n} \cdot \Delta x_{t_2,m,n} \right) - \sum_{m=x_1}^{x_2} \left(z_{t_1,m,n} \cdot \Delta x_{t_1,m,n} \right) \right) \Delta y_n \tag{3.1}$$

where:

ΔV	Change in sediment volume
z	Bed level
Δx	Cross-shore width of bed level grid cell
Δy	Alongshore width of the transect
t_1	The first moment in time
t_2	The second moment in time
y_1	Alongshore coordinate of the left boundary of the domain of interest
y_2	Alongshore coordinate of the right boundary of the domain of interest
x_1	Cross-shore coordinate of the seaward boundary of the domain of interest
x_2	Cross-shore coordinate of the landward boundary of the domain of interest

When constructing the volume balance from Figure 3.3, the left and right boundaries (y_1 and y_2) are set to the boundaries between two profile types (see Figure 1.3) and the seaward and landward boundaries (x_1 and x_2) are set according to Table 3.1.

The sediment transport rates follow directly from the volume differences. The net sediment transport from the beach to the dunes equals the volume change in the dunes, assuming closed boundaries beyond the HD and perpendicular to the coastline. The transport rate from the intertidal zone to the beach equals the sum of transport rate from the beach to the dunes and the volume difference on the beach. This method produces all cross-shore transport rates. Finally, the difference between the volume change in the shoreface and the transport rates from the shoreface gives the gradient in longshore sediment transport.

Volume changes and net sediment transport rates per unit width
To precisely determine the locations of sedimentation or erosion, the change in sediment volume can be expressed per unit width in alongshore direction (in m^3/m), see equation 3.2.

$$\Delta V_{\text{per m}} = \sum_{m=x_1}^{x_2} \left(z_{t_2,m} \cdot \Delta x_{t_2,m} \right) - \sum_{m=x_1}^{x_2} \left(z_{t_1,m} \cdot \Delta x_{t_1,m} \right) \tag{3.2}$$

When calculating the volume change per unit width of one of the cross-shore zones from Figure 3.1, the seaward and landward boundaries (x_1 and x_2) are set according to Table 3.1. The representation of volume changes per unit width in chapter 4 is similar to that of Wittebrood (2017) and Bodde et al. (2019).

To assess the volume changes and net sediment transport rates of the entire North-Holland coast, equation 3.2 can be applied to the JARKUS measurements of the North-Holland region (from Den Helder to IJmuiden). These results will give insight into morphological developments the HD compared to the those of the rest of the North-Holland coast.

Sediment transport in relation to processes
To determine whether a given process governs a net cross-shore or longshore sediment transport rate, these two variables are plotted in a scatter plot. The relation between two variables is assessed through the correlation coefficient (expressed as r^2) and the significance of the results (expressed as the p-value). A correlation is assumed significant when $p < 0.05$ and the data points are statistically independent. Because the correlation coefficient requires independently sampled data points, the p-value and r^2 are calculated for every 100 longshore meters to prevent distortion of the results when using BIP data: This data has been interpolated from transects with a lower resolution. However, this does not guarantee statistically independent variables, because bed levels that follow from two independent measurements could still be autocorrelated. The autocorrelation coefficient is defined by Box et al. (2015) as follows:

$$r_k = \frac{\sum_{i=1}^{N-k} \left(Y_i - \overline{Y}\right)\left(Y_{i+k} - \overline{Y}\right)}{\sum_{i=1}^{N} \left(Y_i - \overline{Y}\right)^2} \tag{3.3}$$

where:

r_k	Autocorrelation coefficient
N	Number of samples
k	Lag
Y	Measurement
$\overline{Y}$	Mean of the measurements

When $r_k \approx 0$ for a given lag k, this lag indicates the smallest sample resolution that is required to obtain statistically independent variables.

Figure 3.4 presents the spatial autocorrelation coefficient of the dune growth. This figure shows that a sample resolution of at least 1,500 m is required to obtain statistically independent data points, and statistically valid values for r^2 and p. However, because the longshore width of the domain of interest is approximately 5,500 m, sampling with a resolution of 1,500 m would only give four data points, which is insufficient to draw statistically valid conclusions on significance. Therefore, the sample resolution of the data is unchanged, but the significance of the results is statistically not completely valid.

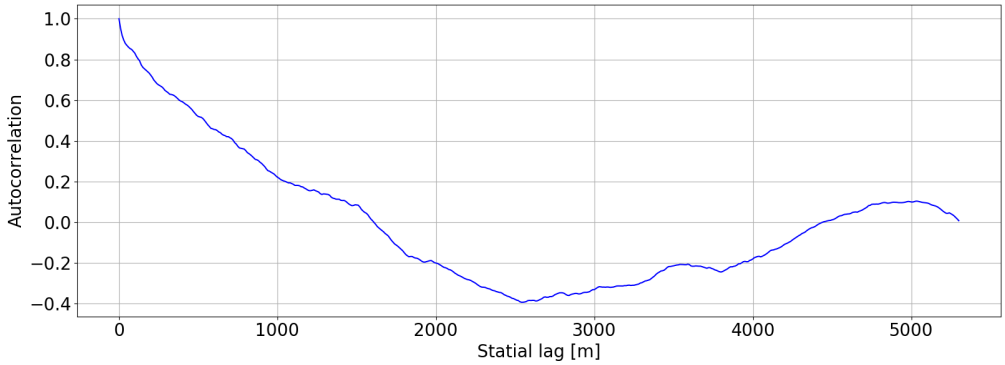

Figure 3.4: Spatial autocorrelation of dune growth

Dune growth may is expected to depend on the wind angle of incidence, because the formulation of Bagnold (1941) (equation 2.8) defines the saturated sand flow in direction of the wind. The weighted wind angle used in Figure 4.2, which gives the representative aeolian sediment transport according to the relation of Bagnold (1941), is 224°, based on data from KNMI between May 25, 2015 and March 19, 2018 (see Figure 3.9a).

Similarly, the net longshore sediment transport rate may be related to the wave angle of incidence, according to the formulation of CERC (2008) (equation 2.16). The weighted wave direction that gives the representative longshore sediment transport according to CERC (2008) is 268°, based on data from RWS between May 25, 2015 and March 19, 2018 (see Figure 3.9b).

As discussed in the literature review, the net cross-shore sediment transport between the shoreface and the intertidal zone may depend on the presence of long waves, see the third term on the right-hand side of equation 2.14. Sediment transport through long waves is the only transport mechanism that changes its cross-shore direction when approaching the coast, see Figure 2.5. Bound long waves in deep water cause offshore sediment transport. When the highest short waves of the wave group break and release their energy while approaching the coast, the 'free' long wave can only transport sediment in onshore direction.

The shoreface of the HD contains shallow sandbars (between NAP -4 m and NAP -3 m), see Figure 3.5. Although sandbars progress in a net offshore direction, they do not cause a net offshore directed sediment

transport. They only redistribute sediment within the shoreface (Wijnberg, 1997). However, these sandbars may play an important role in the process of freeing of long waves, because short waves are likely to break on top of them. The number of short waves that break depends on the water depth (γ = H/h ≈ 0.78). If the majority of the waves break on a relatively shallow sandbar, the free long waves can transport relatively much sediment onshore. When the sandbar is deeper, short waves at the long wave trough do not break and are still able to transport sediment offshore when approaching the intertidal zone. Therefore, sediment transport from the shoreface to the intertidal zone may depend on the crest level of sandbars in the shoreface.

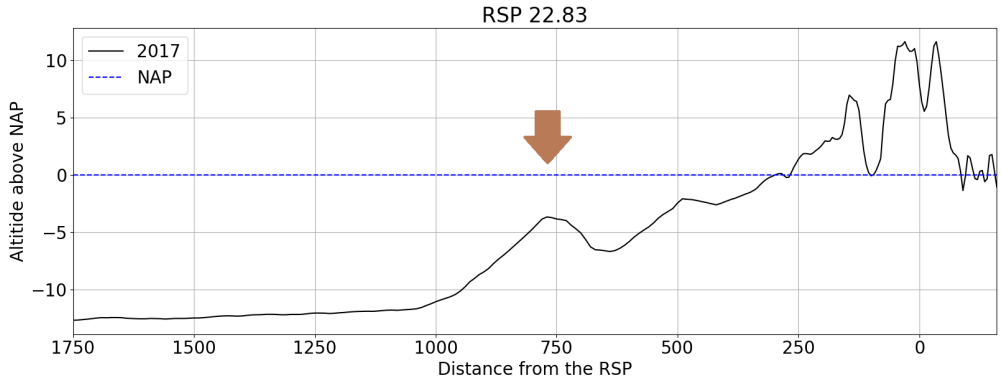

Figure 3.5: A sandbar in the shoreface of RSP 22.83, between NAP -4 m and NAP -3 m

Because sediment transport through long waves depends on the breaking of short waves, the crest level of the sandbar is used to calculate the wave height of the smallest wave that will break on top of the sandbar. If this wave height is small, the majority of short waves is expected to break on top of the sandbar, resulting in onshore sediment transport. If this wave height is large, sediment transport from the shoreface to the intertidal zone is expected to be offshore directed. To account for shoaling and refraction (see equation 2.17), the offshore wave height H_0 is used. This wave height is calculated according to:

$$H_0 = \frac{\gamma h}{K_{sh} K_r} \tag{3.4}$$

where h is the crest level of the sandbar. Shoaling and refraction depend on the wave direction. The weighted wave direction that gives the representative cross-shore sediment transport according to equation 2.12 is 273°, based on data from RWS between May 25, 2015 and March 19, 2018 (see Figure 3.9b).

Aeolian sediment transport in coastal areas can be supply limited or transport limited, as discussed in subsections 2.1.2 and 2.2. Transport limited sediment transport is proven by Bagnold (1941) to depend on the third power of the wind velocity. On the other hand, supply limited transport is limited, among other parameters, by the fetch length (De Vries et al., 2014b). The extent to which aeolian sediment transport in the HD is supply limited and transport limited is quantified by relating dune growth to the beach width and the third power of the wind velocity for every LiDAR measurement interval.

3.2. Numerical modelling

This section describes the model setup for this modelling study, as well as the methods used to determine the dune growth volume, profile developments and typical timescale. The modelling study qualifies the effect of multiple marine processes (hydraulic mixing, wave runup, soil moisture content in the intertidal zone, beach armouring and marine sediment supply) on morphology and bed compositions. Although beach armouring itself is not a marine process, it is accounted for because it affects the operation of hydraulic mixing.

A numerical description of AeoLiS is given in appendix E.

3.2.1. AeoLiS model setup

Model configuration

For this study a set of 2DH AeoLiS models, created by the Water Board Hollands Noorderkwartier[3] (Wittebrood, 2017), was adapted to three 1DH models, corresponding to three different profile types (P2N, P4 and P3S). The location of these models within the HD is shown in Figure 3.6.

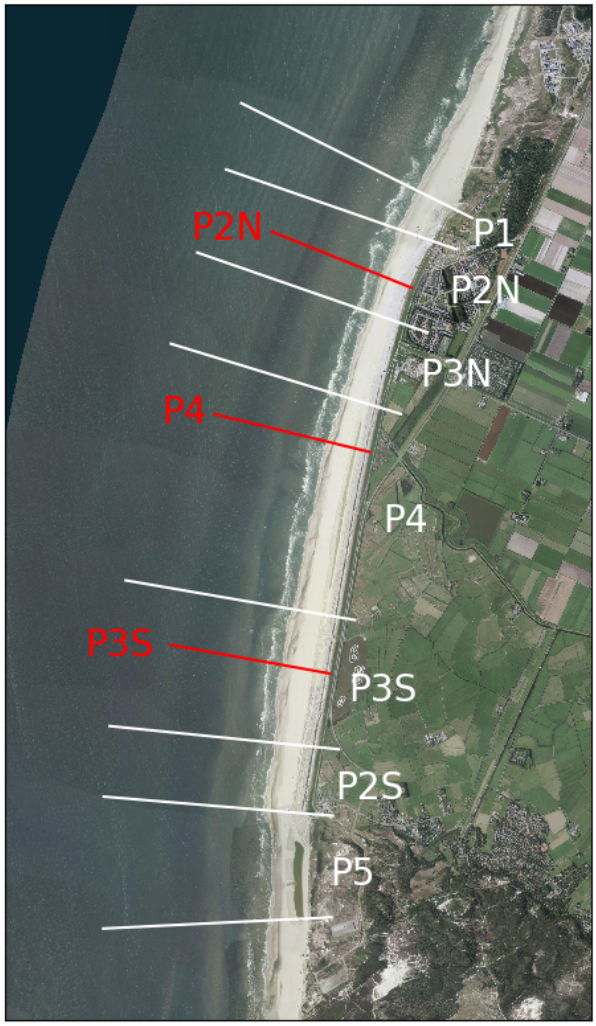

Figure 3.6: Location of the three 1DH AeoLiS models (shown in red) and profile boundaries (shown in white)

The most important limitations of the original 2DH AeoLiS models were:

1. No marine sediment transport was modelled.
2. A constant vegetation cover in time and space was imposed on the dune area.
3. A single, representative grain size distribution was imposed on the entire domain of each 2DH model.
4. Soil moisture content at the beach was not taken into account.

This study assesses the effect of the first, third and fourth limitation of the original models.

The initial beach and dune profiles of the 1DH models correspond to the first monthly echo sounder measurement of April 2015, see Figure 3.7. For clarification, the dune foot and intertidal zone are marked in each profile. Note that the wet part of the dune valley at P4 (between the two dune rows) is not measured. The

[3]'Hoogheemraadschap Hollands Noorderkwartier' in Dutch

grid has a horizontal accuracy of 1 m, which is equal to the resolution of the monthly echo sounder measurements that were executed in the first year after construction. The models use a time step of 600 s and the model duration is 302 days, which corresponds to the last monthly echo sounder measurement of the dunes. Model runs with multiple sediment fractions use a bed interaction parameter of 0.05.

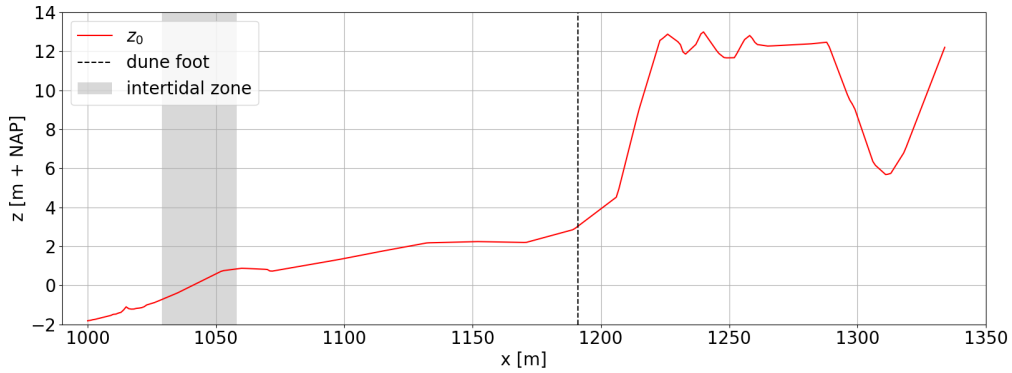

(a) P2N

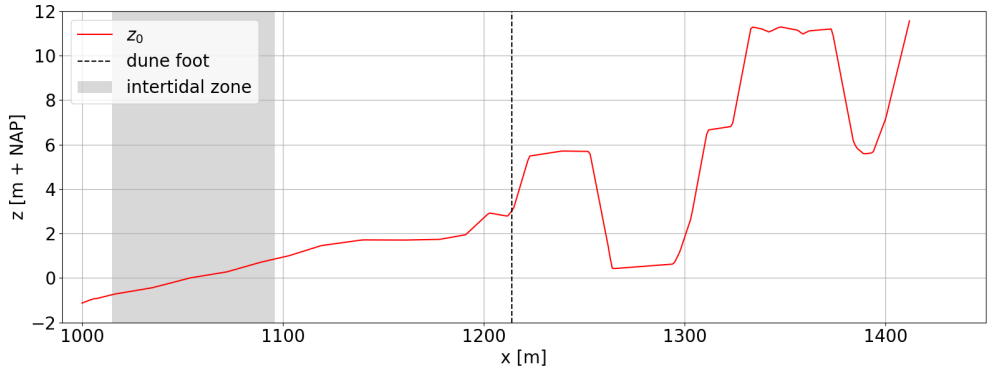

(b) P4

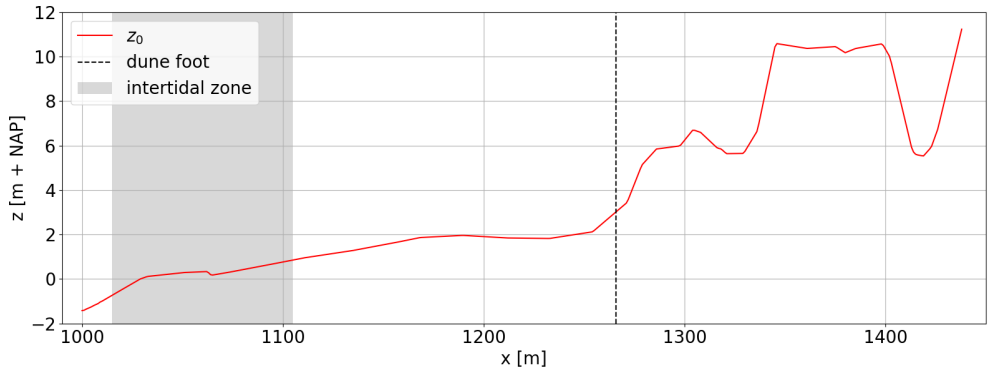

(c) P3S

Figure 3.7: Initial profiles. The intertidal zone (grey area) and dune foot (dashed black line) are marked in each profile.

The seaward and landward boundaries are located far away from the domain of interest: The seaward end of the model is located beyond the mean low water line (NAP -0.84 m) and the landward end is located at the HPZ.

The velocity threshold for aeolian transport based on the bed slope is not yet implemented in AeoLiS. Therefore, a vegetation mask artificially increases the velocity threshold in the dunes. The threshold in this mask is increased by 1.5 m/s, as was done in the 2DH AeoLiS models of Wittebrood (2017). The threshold velocity at the HPZ is set to infinity to prevent any sediment transport.

The models contain 20 vertical layers with a small layer thickness of 1 cm, to enable hydraulic mixing in the

intertidal zone. Data on grain size distributions is obtained from Wittebrood (2017), see Figure A.7. To model changes in bed composition, the sieve curves from this figure must be divided into a number of fractions with different grain sizes. Broekema et al. (2016) advise a higher resolution at the fine tail of the sample, because finer grains are easier to be transported and play a large role in morphologic development. Because it is important to take armouring into account, coarse grains must also be included. The sediment fractions in their study represented [5%, 5%, 5%, 5%, 10%, 20%, 36%, 14%] of the cumulative mass fraction of the original sample, corresponding to percentile 2.5, 7.5, 12.5, 17.5, 25, 40, 68 and 93.

The grain sizes corresponding to these percentiles are calculated from the sieve numbers trough log-uniform interpolation, see equation 3.5. This interpolation requires the measured grain sizes corresponding to the percentiles directly below and above the wanted percentile. These grain sizes are indicated as D^- and D^+ respectively, and their percentiles are denoted as P^- and P^+.

$$D_P = 2^{\log_2(D^-) + \frac{P-P^-}{P^+-P^-}\left(\log_2(D^+) - \log_2(D^-)\right)} \tag{3.5}$$

where:

P	Percentile
D_P	Grain size of percentile P
D^-	Largest measured grain size that is smaller than D_P
D^+	Smallest measured grain size that is larger than D_P
P^-	Percentile of D^-
P^+	Percentile of D^+

The result of this interpolation to the sediment samples of P2N, P4 and P3S is depicted in Figure 3.8 and shown in Table 3.2. In model runs where only a single grain size is modelled, the median grain sizes of D_{50} = 316, 338 and 221 µm are used respectively, based on Figure A.6.

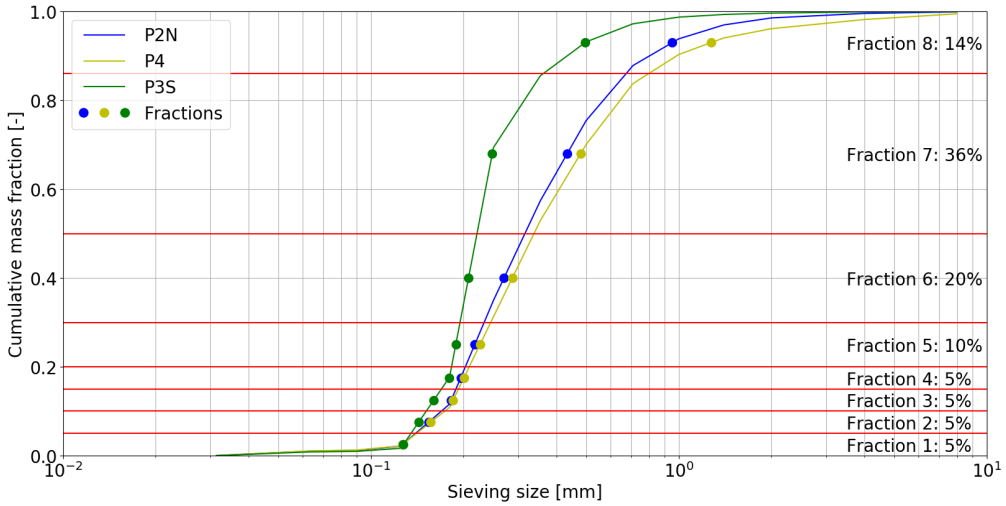

Figure 3.8: Division of the original sediment sample of P2N, P4 and P3S in eight sediment fractions

Datasets of the wind, waves and tide are obtained from the Royal Netherlands Meteorological Institute [4] and RWS, see Figure 3.9. Wind and tide data enable modelling of soil moisture content, hydraulic mixing and wave runup.

[4] 'Koninklijk Nederlands Meteorologisch Instituut' in Dutch, hereafter referred to as KNMI

Table 3.2: Grain size distribution in the AeoLiS models of P2N, P4 and P3S

Mass fraction (%)	Sample's percentile (-)	Grain size (µm)		
		P2N	P4	P3S
5	2.5	127	127	127
5	7.5	154	156	143
5	12.5	182	185	160
5	17.5	196	200	179
10	25	217	226	189
20	40	271	288	207
36	68	434	480	248
14	93	952	1,272	496

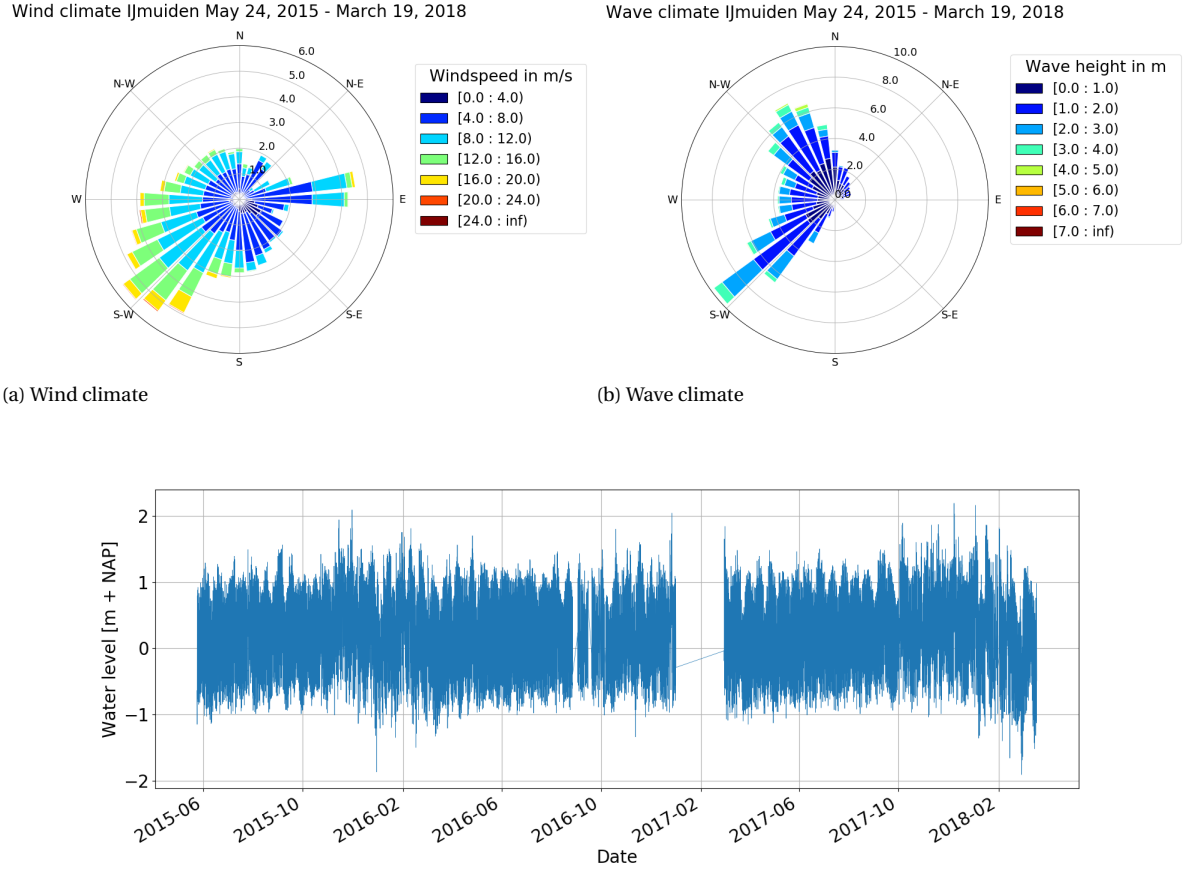

(a) Wind climate

(b) Wave climate

(c) Tidal water levels

Figure 3.9: Climate of IJmuiden between May 25, 2015 and March 19, 2018. Wind data is obtained from KNMI. Wave and tide data is obtained from RWS.

Simulations

The following simulations with the coupled AeoLiS-bathymetry model are modelled for each profile type:

- A default simulation. This simulation does not contain transport effects due to wave forcing or soil moisture content. However, grains are assumed immobile when they are located below the still water line, which depends on the tide. The grain size distribution for each model contains eight sediment fractions, which are given in Table 3.2.
- Simulations with wave forcing, which consists of hydraulic mixing and wave runup. Hydraulic mixing in the intertidal zone averages the sediment distribution over the depth of disturbance, using equation

E.10. Wave runup affects sediment availability in the intertidal zone and the lower part of the beach. AeoLiS does not model wave propagation, but takes into account the maximum level the waves reach when approaching the coast relative to still water level.

- A simulation with an increased threshold wind velocity due to the soil moisture content, following the formulation of Belly (1962) (equation 2.19) and equation E.11.
- A simulation with a single grain with the median grain size, as stated in subsection 3.2.1. This simulation investigates the effect of beach armouring, see subsection 2.2.2.
- A simulation where the bed is updated every time step, based on bed level measurements. This simulation resembles the effect of marine sediment supply. The monthly echo sounder measurements are linearly interpolated to update the bed level in the intertidal zone every 600 s.

Updating of the bathymetry of the shoreface and intertidal zone of the AeoLiS models is possible through the Basic Model Interface[5]. BMI provides a set of functions that allows the user to communicate with the underlying model during run time (Peckham et al., 2013). For example, the function model.*set_var( )* enables the user to change the spatial grid or a model parameter.

3.2.2. Dune growth

Dune growth is assessed by presenting a bar chart of the modelled increase in dune volume of every simulation in 302 days (expressed in m^3/m). This bar chart is constructed separately for all modelled profile (P2N, P4 and P3S). The dune growth volume is defined as the sum of all modelled bed level changes beyond the dune foot, see equation 3.6.

$$\Delta V = \sum_{m=x_1}^{x_2} \left(z_{t_2,m} \cdot \Delta x_{t_2,m}\right) - \sum_{m=x_1}^{x_2} \left(z_{t_1,m} \cdot \Delta x_{t_1,m}\right) \tag{3.6}$$

where the seaward and landward boundaries (x_1 and x_2) are set to the dune foot and the connection to the HPZ respectively. The measured dune growth is added as a solid black line in all bar charts.

The dune growth capacity with multiple sediment fractions, which is based on the transport capacity for aeolian sediment transport with following Bagnold (1941) (equation 2.8), is marked as a dashed black line in all bar chart. This formulation uses the grain size distributions as stated in 3.2. The dune growth capacity with a single grain size is different, because equation 2.8 takes beach armouring into account, through the factor $\sqrt{d_n/D_n}$ (B.M. Hoonhout, personal communication, January 30, 2019). This factor should not be accounted for when a single grain is considered. The dune growth capacity with a single grain size following Bagnold (1941), where $\sqrt{d_n/D_n}$ is set to 1, is marked as a dash-dotted line.

These dune growth capacities volumes indicate whether sediment transport in a simulation is supply limited or transport limited. If dune growth is equal to the dune growth capacity, sediment transport is transport limited. Transport is supply limited when the dune growth is lower, because supply-limiting factors have reduced sediment transport to the dune. The formulation of Bagnold (1941) is simplified, because it does not account for changes in the grain size distribution.

3.2.3. Profile development

Aeolian sediment transport changes the bed level, because erosion and sedimentation is space- and time-dependent, and the bed composition, because fine grains are easier transported than coarse grains. The results on erosion and sedimentation patterns, and bed composition are presented separately.

A study on erosion and sedimentation patterns provides insight into transport of sediment within the model domain, and how this depends on several marine processes. Erosion and sedimentation patterns are presented by plotting the difference between the initial bed level and the final bed level of every grid cell in the model domain. This is done separately for every simulation. The measured bed level change is marked as a black line. For clarification, the intertidal zone and the dune foot of the initial profile are marked.

[5]hereafter referred to as BMI

A study on bed composition provides insight into how the transport of fine and coarse grains over the model domain depends on several marine processes. Changes in bed composition are assessed by plotting the median grain size of every grid cell in the model domain at the final time step. This is done separately for every simulation. The median grain size is calculated from the grain size distribution through log-uniform interpolation, see equation 3.5. The initial median grain size is marked as a horizontal black line. For clarification, the intertidal zone and the dune foot of the initial profile are marked.

3.2.4. Time scale

Aeolian sediment transport is affected by wind velocity and wind direction, but also by supply-limiting marine processes. Short-term storm events are capable of transporting a large amount of sediment onshore, while high storm surge levels prevent initiation of aeolian sediment transport. Changes in wind conditions also occur within a year, where mild winds in during summer can only transport fine grains and stronger winds in winter are able to transport coarse grains as well. Typical time scales for changes in dune morphology or bed composition could be in the order of hours to months.

The bed levels in the dune have only been measured by the echo sounder in eight of the first twelve months, which is insufficient to assess a time scale for changes in dune development. Measurements of bed composition after construction have only been taken once, by Fortuijn (2018). The evolution of dune volume and bed composition in time can therefore only be assessed through the modelling study.

This part of the modelling study determines dune growth and changes in bed composition at every time step of the models, which are run for 360 days. Dune growth is defined as the increase in dune volume between the current time step and the first time step, according to equation 3.6. Changes in bed composition are assessed by calculating the median grain size at the current time step for one grid cell at the beach and one at the dune. The grid cell at the beach is located one grid cell seaward of the dune foot, the grid cell at the dune one grid cell landward of the dune foot.

4

Results: Data analysis

This chapter presents and discusses the results of the morphological evolution of the HD, obtained through a data analysis. It gives the volume balance of the different zones at the HD and sediment transport rates between these zones, using the methodology from chapter 3. Maps of the bed level difference of the entire domain in the first three years since construction, as well as each separate year, are given in appendix C. They show the exact locations of sedimentation and erosion.

4.1. Volume changes of cross-shore zones

Figure 4.1 presents the beach and dune growth per unit width for the first three years after construction. The volume changes of the domain of interest are shown in bright red and bright green. The growth rates per measurement interval are presented in section B.1 and per year in section B.2. Dune growth is positive for the entire domain of interest and every measurement interval, see Figure B.1. This figure also shows that the growth rates per unit time are more or less constant over time. However, a summer-winter variation can be observed, as the dune growth in March to September 2016 (Figure B.1c) and April to August 2017 (Figure B.1f) is smaller than the other intervals.

The highest accumulation of sediment in the dunes is observed in the south of the HD. Towards the north, the dune growth gradually decreases. This decrease follows from the correlation of the dune growth on the wind angle of incidence, see Figure 4.2 (with r^2 = 0.690 and p = 6.8e-15). The wind angle of incidence gradually increases from south to north due to a change in dunefoot orientation. Unlike the other profiles, the dune growth in P2S increases from south to north while the wind angle of incidence increases. This behaviour does not agree with the relation mentioned above, but can be explained with the presence of willow screens and a beach pavilion in the north of P2S, which trap sediment, and a gradual decrease of outer dune slope from south to north (Bodde et al., 2019).

The beach shows alternating periods of sedimentation and erosion (see Figure B.2), but generally erodes. However, sedimentation of the beach can be observed at two locations at the HD. In March 2018, an additional nourishment was constructed at P2S and the southern part of P3S, see appendix D. The discontinuity of beach profile in P3S can have led to net northward aeolian sediment transport and sedimentation in the northern part of P3S (around transect 4400), see Figure B.2h. Sedimentation around transect 6200 can result from maintenance works in summer 2015, where the dune and beach were reprofiled, see Figure B.2a.

Figure 4.3 shows the change of sediment volume in the offshore zone, shoreface and intertidal zone. The growth rates for every year since construction are shown in Section B.2. The additional nourishment in March 2018 also affected the bed levels at P2S and P3S of the intertidal zone. Therefore, the intertidal zone growth rates are locally calculated using the second to last echo sounder measurement and linearly extrapolated such that the time span matches that of the rest of the intertidal zone growth. Also, the measured bed levels are interpolated to create a northing and easting coordinate system, instead of a cross-shore and longshore system. This results in minor but negligible errors in the growth rates per unit width. The boundaries of the profile types in Figure 4.3 also slightly deviate between the different cross-shore zones.

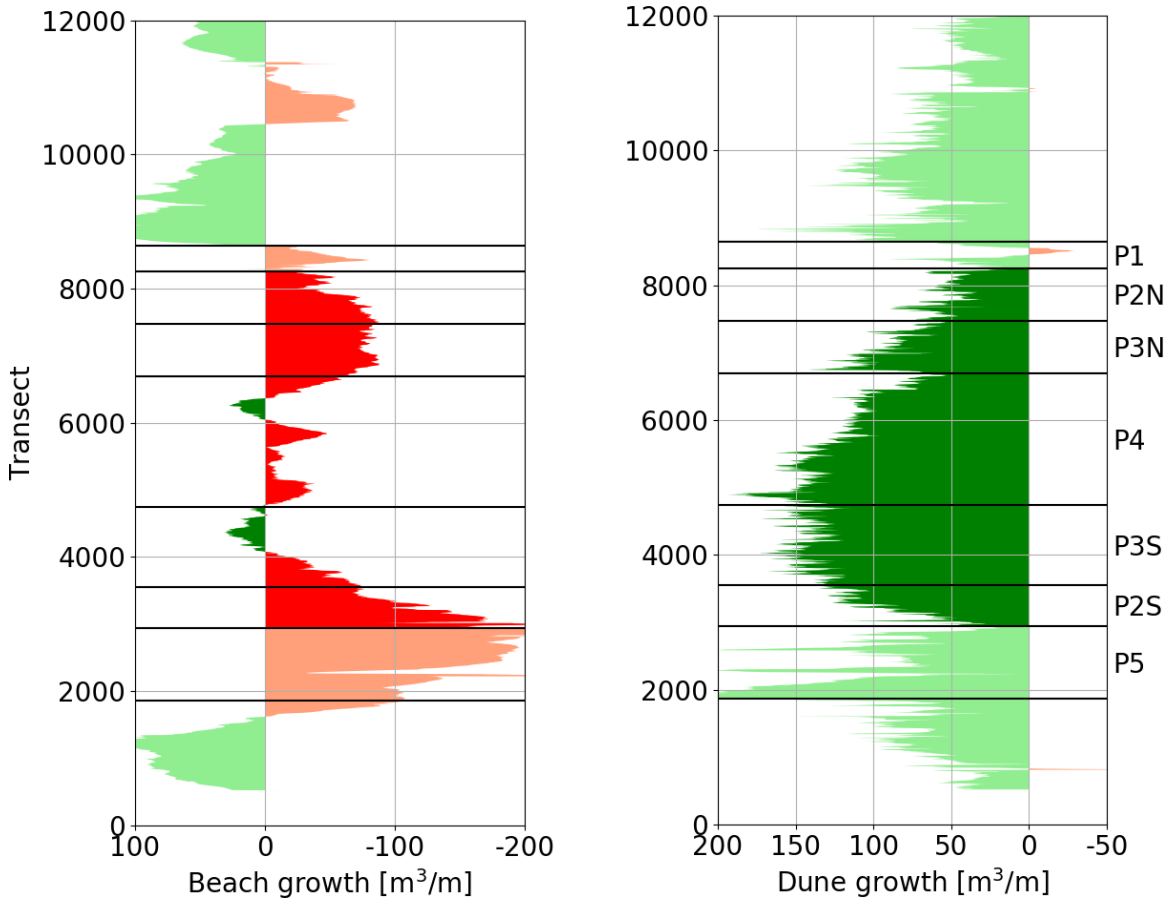

(a) Beach growth

(b) Dune growth

Figure 4.1: Volume changes of the beach and dunes of the HD per unit width between May 25, 2015 and March 19, 2018, based on LiDAR measurements.

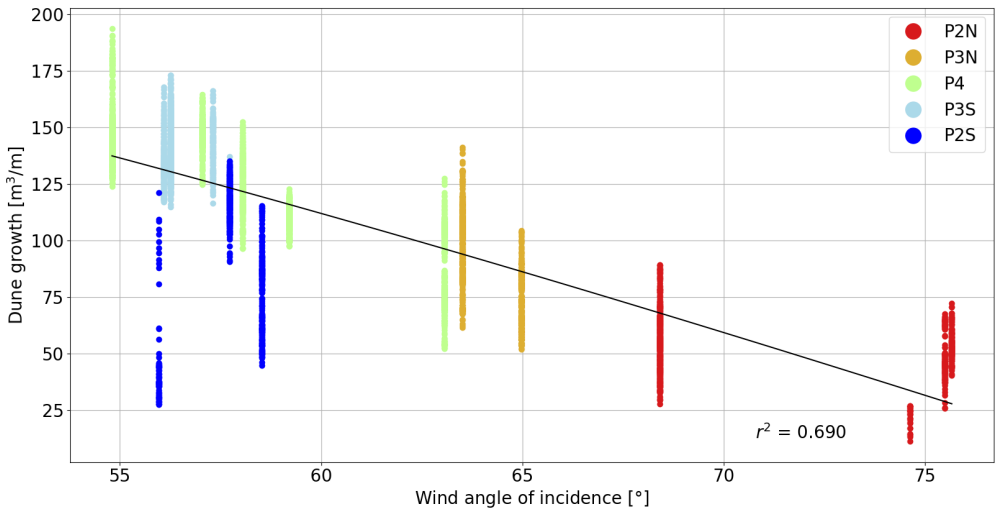

Figure 4.2: Dune growth between May 25, 2015 and March 19, 2018 of every longshore meter depending on the wind angle of incidence. The measured dunefoot orientation is discrete due to the resolution of the LiDAR dataset.

Erosion is observed in the shoreface and intertidal zone of the entire study area, see Figures 4.3b and 4.3c. Erosion rates are smallest in P3S, where sedimentation in the dune is largest. The dependency of the dune growth on de sediment transport rate from the shoreface to the intertidal zone rates is discussed in subsection 4.3. The offshore zone generally silts up, see Figure 4.3a. Although the offshore zone is defined beyond the closure depth, there is some morphological development. Possible causes for these developments are listed in subsection 2.1.3.

Figure 4.3a shows that the offshore zone growth is zero at some locations north and south of the HD. This is not necessarily true, because the measurement at those locations did not exceed NAP -10.9 m. Although the deepest measured bed level differs between each transect, NAP -10.9 is reached at all transects within the domain of interest (the bright red and bright green areas).

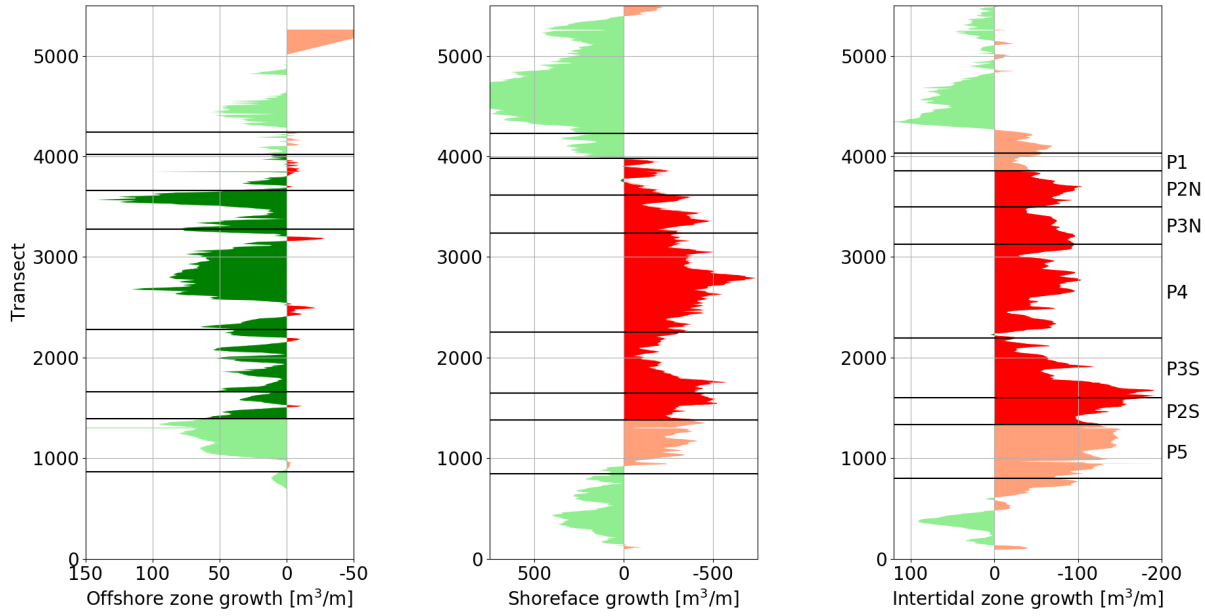

(a) Offshore zone growth (b) Shoreface growth (c) Intertidal zone growth

Figure 4.3: Volume changes of the offshore zone, shoreface and intertidal zone of the HD per unit width between May 3, 2015 and April 9, 2018, based on echo sounder measurements.

4.2. Sediment volume balance

The total volume changes of every domain for each profile type are calculated using equation 3.1 and shown in Table 4.1. In terms of coastal safety, a total of 1,479,000 m^3/m of sediment is lost in the domain of interest in the first three years after construction. The main sediment sink is assumed to the shoreface, where approximately 1,600,000 m^3 of sediment is lost in the first three years since construction. Figure 4.4 presents the net sediment transport rates between every domain for each profile type.

Table 4.1: Volume changes of every domain for each profile type between May 2015 and April 2018, based on LiDAR and echo sounder measurements

	Change in sediment volume (10^3 m^3)				
Profile	Offshore zone	Shoreface	Intertidal zone	Beach	Dunes
P2N	7	-112	-53	-47	41
P3N	47	-225	-53	-61	70
P4	86	-757	-95	-29	238
P3S	30	-316	-99	-13	169
P2S	22	-227	-73	-72	55
HD	192	-1,647	-374	-223	573

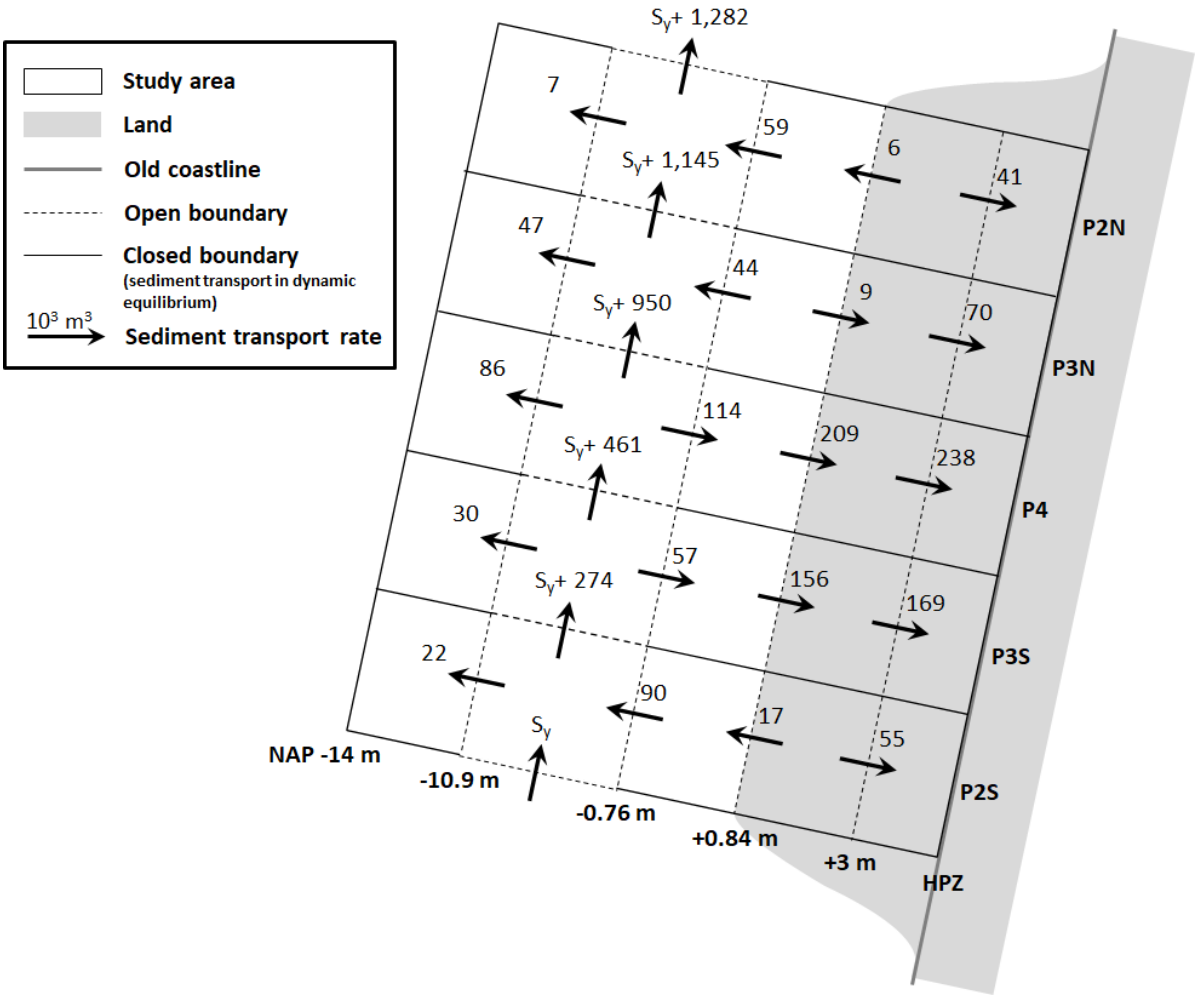

Figure 4.4: Net sediment transport rates ($*10^3$ m^3) between May 2015 and April 2018, based on LiDAR and echo sounder measurements

Section B.5 presents the sediment balance of the HD of every year since construction. The most notable results of these sediment balances are:

- The most substantial loss of sediment takes place in the first year after construction: Approximately 1,000,000 m^3 is lost, mainly transported northward through longshore sediment transport. Sediment loss is much lower in the second and third year. This can be explained through the development of the shoreline planform through alongshore spreading (see Figure 2.10), winnowing or settlements, which mainly took place during the first year after construction, or a severe wave climate (Arends, 2018). De Jongh (2017) stated that sediment at the HD is mainly lost through alongshore spreading.
- The offshore zone erodes during the first year after construction, but silts up in the second and third year. A possible cause for this shift is flow contraction, where longshore flow velocities are highest at the tip of the nourishment and longshore sediment transport increases. The peak flow velocity reduces once the shoreline planform has adjusted.

4.3. Sediment transport from the shoreface to the intertidal zone

Large longshore gradients in sediment transport from the shoreface to the intertidal zone can be observed in Figure 4.4, where landward directed transport rates in P4 and P3S are observed together with seaward transport rates in P2N, P3N and P2S. However, the net sediment transport rate between the intertidal zone and the shoreface for the entire domain is relatively small: approximately 22,000 m^3 seaward in three years. Figure 4.5 depicts the sediment transport rate from the shoreface to the intertidal zone per unit width. This transport rate shows atypical behaviour at the HD in relation to its surrounding coast. The sediment transport rates from the shoreface to the intertidal zone per year are presented in Figure B.8.

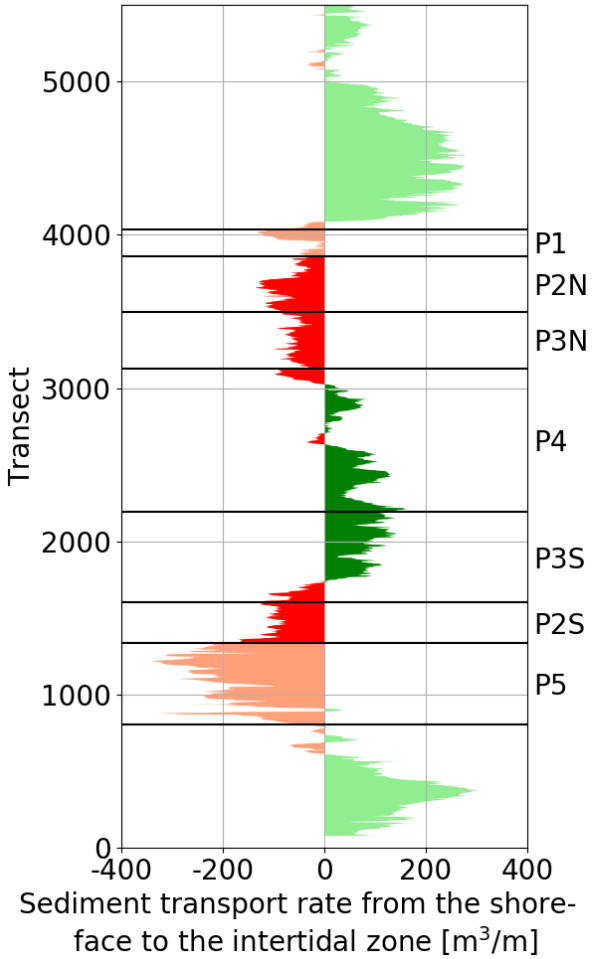

Figure 4.5: Sediment transport rate from the shoreface to the intertidal zone of the HD between May 2015 and April 2018, based on LiDAR and echo sounder measurements. Positive values correspond to landward and negative values to seaward transport.

Identifying which hydraulic process(es) caused these gradients in sediment transport is not straightforward, because cross-shore hydrodynamics and morphodynamics are very complex and contain many hydraulic processes, as discussed in subsection 2.1.3. One of the hydraulic processes that could cause both onshore and offshore sediment transport are long waves, as discussed in section 3.1. Sediment transport from the shoreface to the intertidal zone may depend on the crest level of sandbars in the shoreface.

Figure 4.6 presents the sediment transport rate from the shoreface to the intertidal zone depending on the offshore wave height of the smallest wave that will break on top of the sandbar, taking into account wave shoaling and wave refraction (see equation 2.17), and the level of the sandbar. The correlation between the variables in this figure is strong: r^2 = 0.574 and p = 4.99e-11. The result agrees with the hypothesis: The onshore directed sediment transport rate is highest where the highest number of waves break on top of the sandbar, and the sediment transport rate is offshore directed where the sandbar breaks only a few short waves. This result suggests that long waves that reach the intertidal zone of P2N, P3N and P2S are primarily bound long waves, and that mainly free long waves arrive at the intertidal zone of P4 and P3S.

The correlation of sediment transport rate from the shoreface to the intertidal zone and the offshore wave height for every year since construction are shown in Figure B.9 in appendix B. The first year shows a weak correlation: r^2 = 0.274, which is plausible due to the absence of sandbars in this year. A natural barred profile was being developed, and free and bound long waves were not the most influential sediment transport mechanism. This barred profile was fully developed in a few months after construction, but was not yet present in the north of the HD at the first BIP measurement. The correlation of the second and third year is stronger: r^2 is 0.481 and 0.483 respectively. In those years, the sediment transport rate from the shoreface to the intertidal

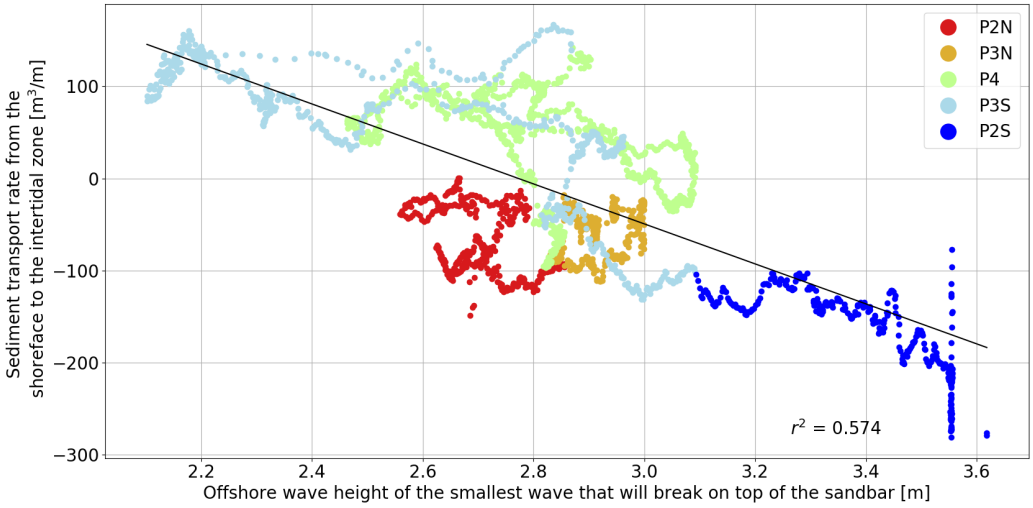

Figure 4.6: Sediment transport rate from the shoreface to the intertidal zone between May 2015 and April 2018 of every longshore meter depending on the offshore wave height of the smallest wave that will break on top of the sandbar

zone in P2S and P3S was disproportionally low. The intertidal zone locally eroded significantly during the second year (see Figure B.5b) and sediment was transported in longshore direction (see Figure B.12b). This resulted in the construction of the additional nourishment as shown in appendix D.

The sediment transport rate from the shoreface to the intertidal zone is positively correlated to the dune growth, see Figure 4.7. The correlation is moderate to strong (r^2 = 0.513 and the p-value = 1.67e-9), indicating that sediment transport from the shoreface to the intertidal zone is likely to result in dune growth. The profile types seem to have their own stronger correlation. This can be explained by the fact that, in this analysis, the dune growth and the sediment transport rate from the shoreface to the intertidal zone are by definition correlated: Both variables are calculated using the bed levels in the dunes.

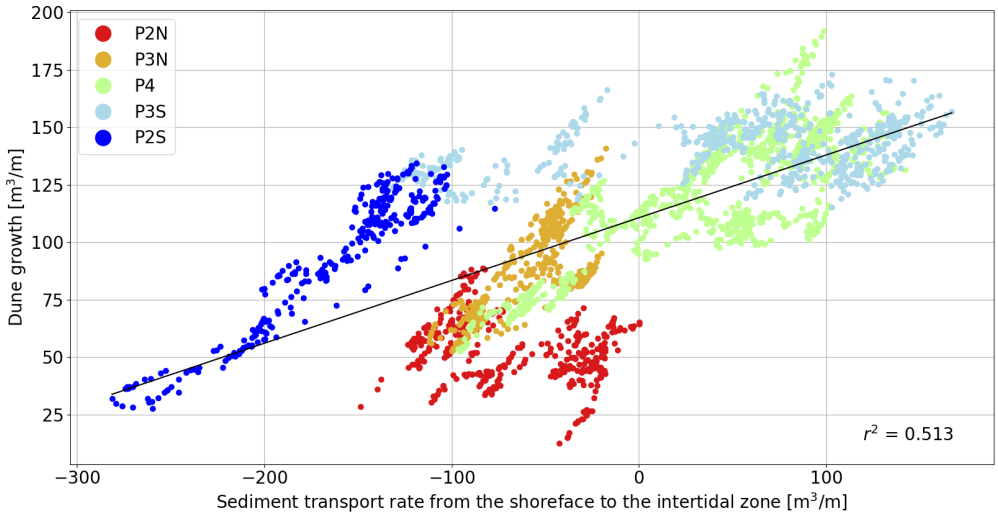

Figure 4.7: Dune growth between May 25, 2015 and March 19, 2018 of every longshore meter depending on the sediment transport rate from the shoreface to the intertidal zone

Figure B.10 presents the sediment transport rate from the shoreface to the intertidal zone, depending on the dune growth for every year since construction. In the first and third year, this correlation is moderate to strong: r^2 = 0.427 and r^2 = 0.381 respectively. The low correlation coefficient for the second year (r^2 = 0.080)

mainly is the result of relatively high dune growth rates in P2S and P3S, while the sediment transport rate from the shoreface to the intertidal zone is negative. As mentioned above, the intertidal zone has eroded significantly during that year.

The combination of Figures 4.6 and 4.7 relates the dune growth to the offshore wave height of the smallest wave that will break on top of the sandbar, through the sediment transport rate from the shoreface to the intertidal zone. When this 'intermediate step' is skipped and these parameters are directly plotted against each other, the correlation is much lower, see Figure 4.8 (with r^2 = 0.147 and the p-value = 4.61e-3). The following causes may explain this weak correlation:

- Sediment transport in the HD can be both supply limited and transport limited, see section 4.5. Therefore, dune growth depends on many other parameters, like the wind velocity, beach width, soil moisture content, wave runup, or sediment sorting in the intertidal zone. They are expected to contribute to deviations in aeolian sediment transport. The impact of these processes is discussed in chapter 5.
- The profile orientation gradually changes from south to north, which causes longshore gradients in aeolian sediment transport. This means that the sediment transport rate from the shoreface to the intertidal zone does not automatically result in changes in dune volume at the same transect. The largest longshore component of aeolian sediment transport is in the north (P2N and P3N) due to the large wind angle of incidence, so the largest deviations in Figure 4.8 are also found there.

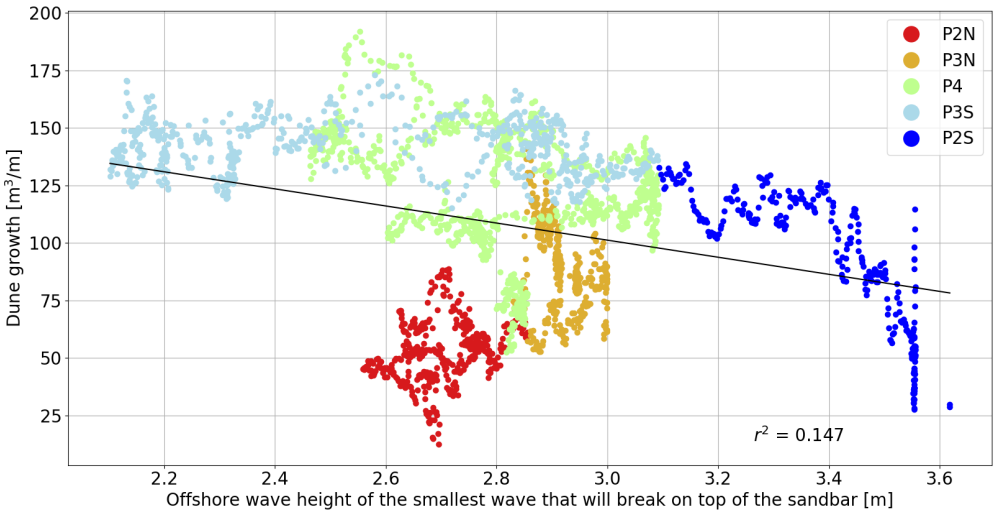

Figure 4.8: Dune growth between May 25, 2015 and March 19, 2018 of every longshore meter depending on the offshore wave height of the smallest wave that will break on top of the sandbar

Figure B.11 presents the correlation of dune growth and the offshore wave height of the smallest wave that will break on top of the sandbar for every year. The correlation in the first year is weak (r^2 = 0.034), but stronger in the second and third year (r^2 = 0.145 and r^2 = 0.354 respectively). As mentioned above, long waves were not the most influential sediment transport mechanism in the first year, due to the absence of sandbars. In the figures, the largest deviations are also found in the north (P2N and P3N).

4.4. Longshore sediment transport

The longshore sediment transport is the last calculated value, to close the sediment volume balance. It is the main sediment transport mechanism of the HD and approximately a factor 5 larger than the largest cross-shore sediment transport rate, see Figure 4.4. Figure 4.9 depicts the longshore sediment transport rate per unit width. Green areas indicate an increase in northward sediment transport and a loss of sediment for coastal safety. The longshore sediment transport rate per year is shown in Figure B.12.

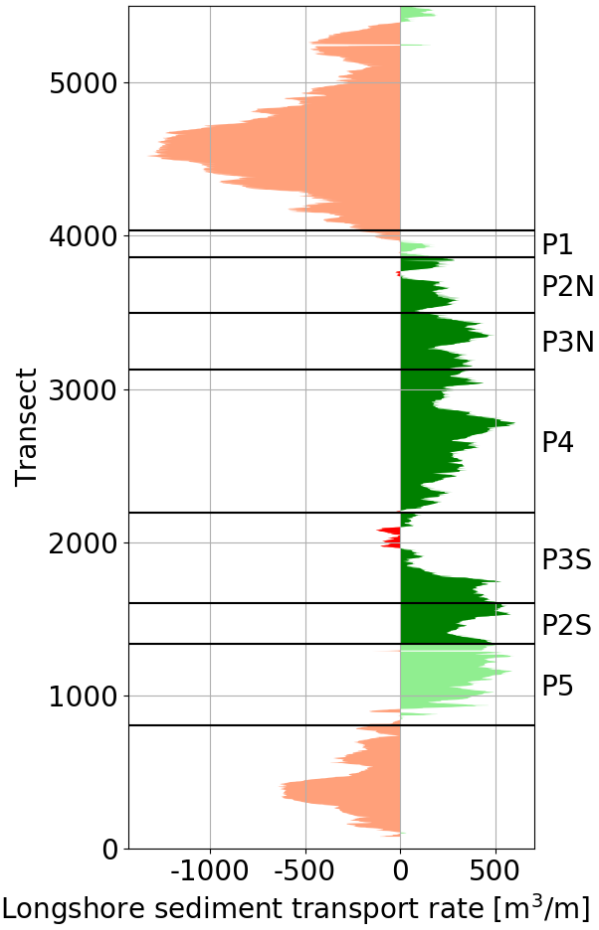

Figure 4.9: Longshore sediment transport rate of the HD per unit width $\left(\frac{\partial S_y}{\partial y}\right)$ between May 2015 and April 2018, based on LiDAR and echo sounder measurements. Positive values correspond to increased and negative values to decreased northward transport rates.

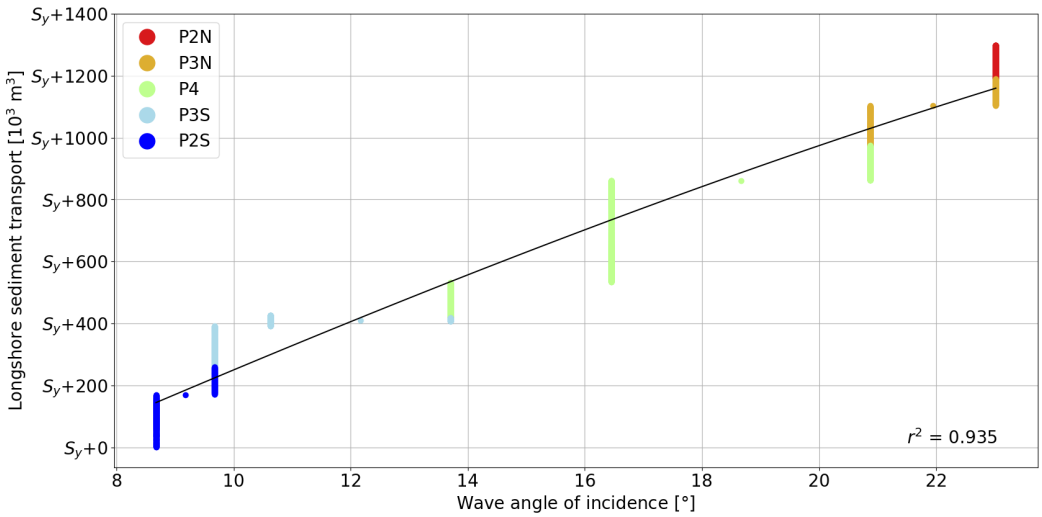

Figure 4.10: (S-φ)-curve of the longshore sediment transport between May 2015 and April 2018 of every longshore meter depending on the wave angle of incidence. The black curve corresponds to the (S-φ)-relation according to CERC (2008). The measured transect orientation is discrete due to the resolution of the LiDAR dataset.

Figure 4.9 shows that the longshore sediment transport rate is positive in the greater part of the domain of interest, which implies an increase in longshore sediment to the north, and a sediment loss for coastal safety. The longshore transport is negative directly north and south of the HD, which means sediment has settled in one or more of the cross-shore zones there.

Figure 4.10 shows the relation between the longshore sediment transport relative to the mean longshore transport S_y and the wave angle of incidence. The fitted black curve corresponds to the (S-φ)-relation according to CERC (2008), see equation 2.16 and Figure 2.6b. The correlation is very strong: r^2 = 0.935 and p = 1.37e-33, indicating that longshore sediment transport is related to the wave angle of incidence.

4.5. Supply limited and transport limited sediment transport

Figure 4.11a depicts the volume increase in the dunes as a function of the beach width, which represents the fetch distance for aeolian sediment transport, for every measurement interval. The dates of every measurement is given in Table A.1. The graph shows some correlation: r^2 = 0.326 and p = 9.47e-39. This figure shows a linear increase in dune growth as a function of the beach width, up to a beach width of approximately 120 m. From that point, dune growth seems to be independent of the beach width. This assumption agrees with the conceptual representation of the fetch effect of De Vries et al. (2014b).

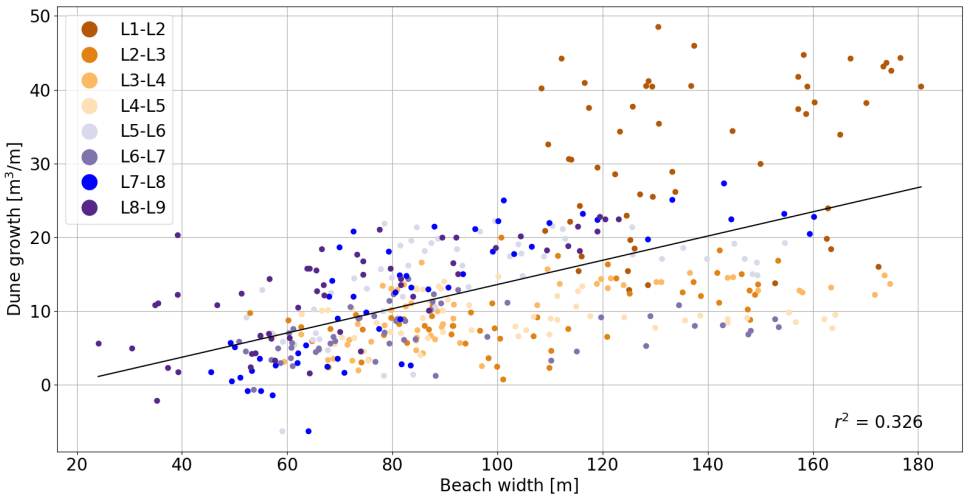

(a) Supply limited: Mean dune growth between depending on the beach width at the first of the two measurements

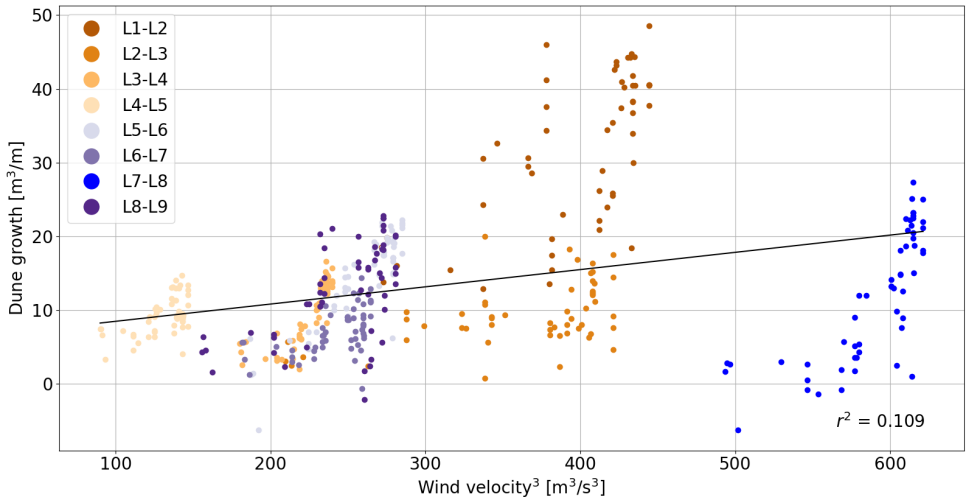

(b) Transport limited: Mean dune growth depending on the cross-shore component of the third power of the wind velocity

Figure 4.11: Supply limited and transport limited conditions of every 100 m of the HD for every LiDAR measurement interval. The intervals in the legend are denoted by two numbers, see Table A.1 for the corresponding dates. Wind data is obtained from KNMI.

Figure 4.11b shows the dune growth as a function of the cross-shore component of the third power of the wind velocity, which stems from the equilibrium sand flow of Bagnold (1941) (equation 2.8), also for each measurement interval. The correlation in this figure is weak, but significant: r^2 = 0.109 and p = 1.73e-12. However, the significance of the result is statistically not completely valid, as discussed in section 4.1. These figures suggest that aeolian sediment transport at the HD can better be described as supply limited than transport limited, although the limiting process is space- and time-dependent. The effect of transport capacity and supply-limiting processes on aeolian sediment transport is further assessed in chapter 5.

4.6. Volume changes and sediment transport of the North-Holland coast

The volume changes between November 8, 2015 and November 24, 2017 of the North-Holland coast (from Den Helder to IJmuiden) are provided in Figures 4.12 and 4.13. The HD are located between RSP 20.38 and RSP 26.95.

Figure 4.12b shows that the dunes along the entire North-Holland coast increase in volume. Sediment volumes in the dunes of the HD have increased more than their surrounding coast, even though the first seven months after construction where not accounted for in the JARKUS measurements. The beach shows increased erosion rates compared to their surrounding coast, see Figure 4.12a. Beach volumes along the North-Holland coast have roughly stayed the same. However, three beach nourishments (between RSP 12.13 and RSP 14.21, between RSP 31.25 and RSP 34.25, and between RSP 37.00 and RSP 39.00) have resulted in local growth peaks in the beach north and south of the HD (Rijkswaterstaat, 2017).

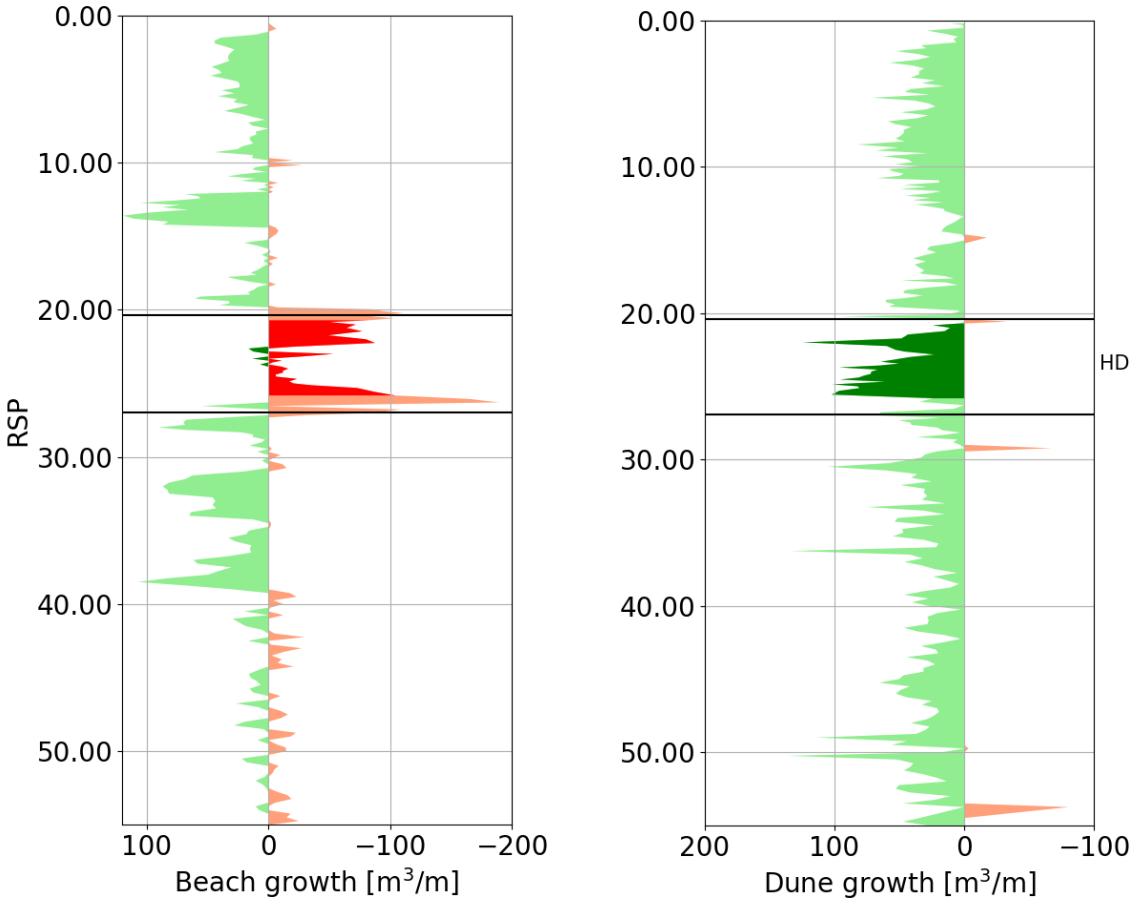

(a) Beach growth

(b) Dune growth

Figure 4.12: Volume changes of the beach and dunes of the North-Holland coast per unit width between November 8, 2015 and November 24, 2017, based on JARKUS measurements.

The shoreface and intertidal zone also show increased erosion rates compared to their surrounding coast. The intertidal zone can also be affected by the three beach nourishments, as described above.

A shoreface nourishment between RSP 31.00 and RSP 40.00 (Rijkswaterstaat, 2017) explains large positive sedimentation rates in the shoreface south of the HD. However, large sedimentation rates were also observed in the shoreface directly north and south of the HD (see Figure 4.13b), which may confirm that a large volume of sediment has been transported from the HD to those zones, through longshore transport. This large increase in sediment volume in the north and south of the HD is not observed in the other cross-shore zones.

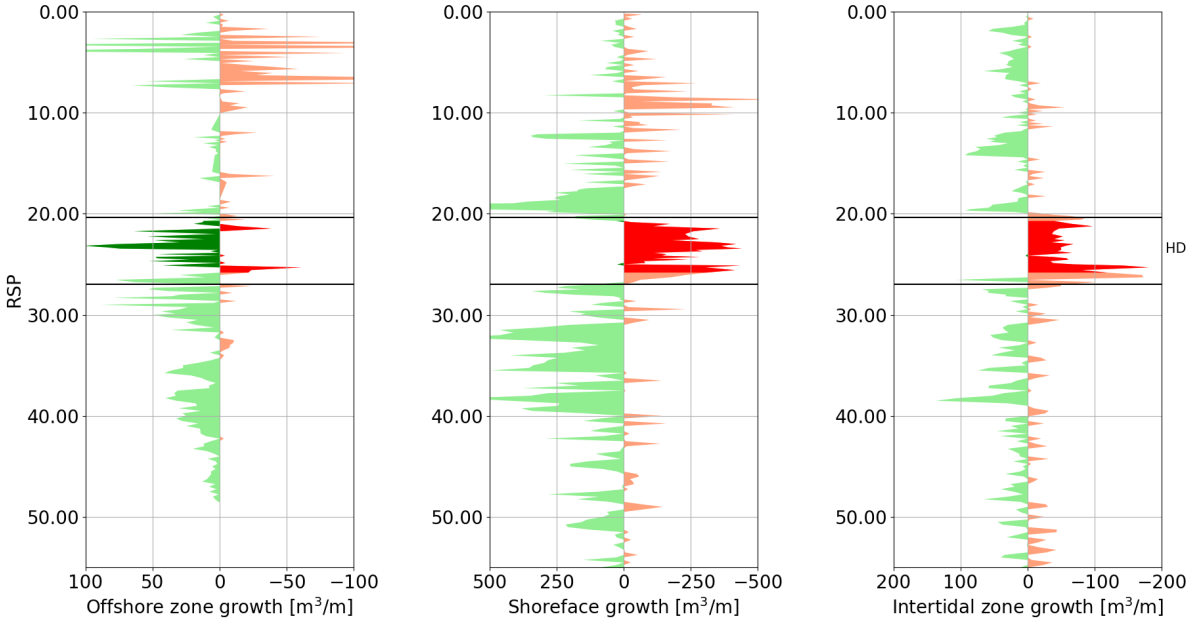

(a) Offshore zone growth (b) Shoreface growth (c) Intertidal zone growth

Figure 4.13: Volume changes of the offshore zone, shoreface and intertidal zone of the North-Holland coast per unit width between November 8, 2015 and November 24, 2017, based on JARKUS measurements.

The sediment transport rate from the shoreface to the intertidal zone of the entire North-Holland coast is shown in Figure 4.15a. North and south of the HD, this transport rate is directed landward. This is a very different behaviour compared to the transport rate at the HD, which is relatively small and locally seaward directed. Figure 4.14 presents the sediment transport rate from the shoreface to the intertidal zone depending on the offshore wave height of the smallest wave that will break on top of the sandbar. The transects within the HD are marked with bright blue dots. The correlation in this figure is very weak (r^2 = 0.001 and p = 0.577), indicating that bound and free long waves are not the main driver for sediment transport between the shoreface and the intertidal zone. Because the HD is a man-made nourishment, it is plausible that its morphodynamics are different than that of other profiles of the North-Holland coast, especially in the first years after construction. De Schipper (2014) discovered that a different (generally steeper) cross-shore profile in the shoreface of nourishments induces stronger low-frequency fluctuations in flow in the first phase after construction.

The longshore sediment transport rate for the North-Holland coast is shown in Figure 4.15b. The transport rates in this figure are generally negative, which corresponds to a gradual decrease in northward sediment transport from south to north. This suggests an increase of sediment volume in one or more of the cross-shore zones. Only the longshore sediment transport rate at the HD shows an increasing trend from south to north, hence a longshore loss of sediment. This increase in longshore transport has resulted in erosion of the shoreface, intertidal zone and beach (see Figures 4.12a, 4.13b and 4.13c). Causes for the dissimilar longshore sediment transport at the HD can be differences in coastal orientation or a decrease in median grain size. According to Mangor et al. (2017), coarser sand is more stable in terms of longshore loss.

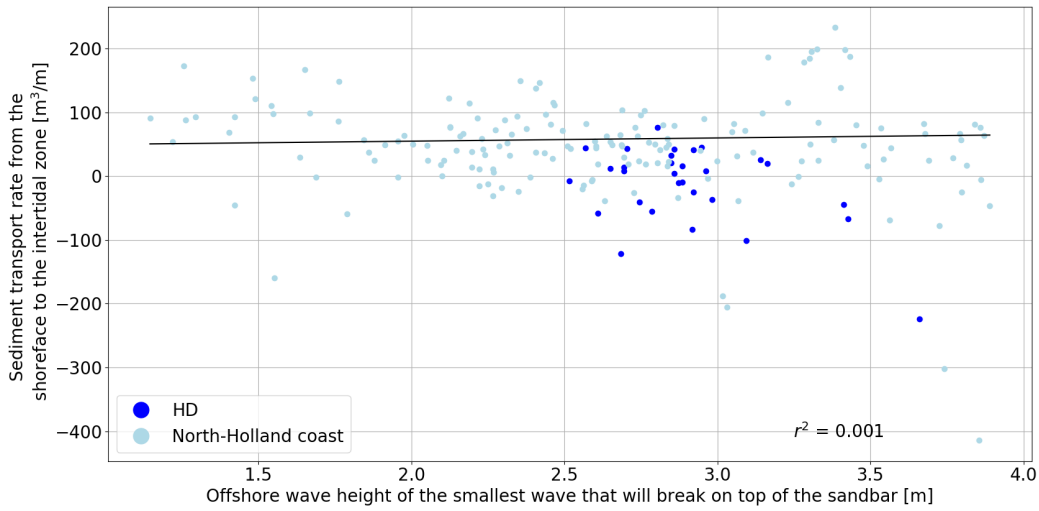

Figure 4.14: Sediment transport rate from the shoreface to the intertidal zone of the North-Holland coast between November 8, 2015 and November 24, 2017, based on JARKUS measurements, depending on the offshore wave height of the smallest wave that will break on top of the sandbar

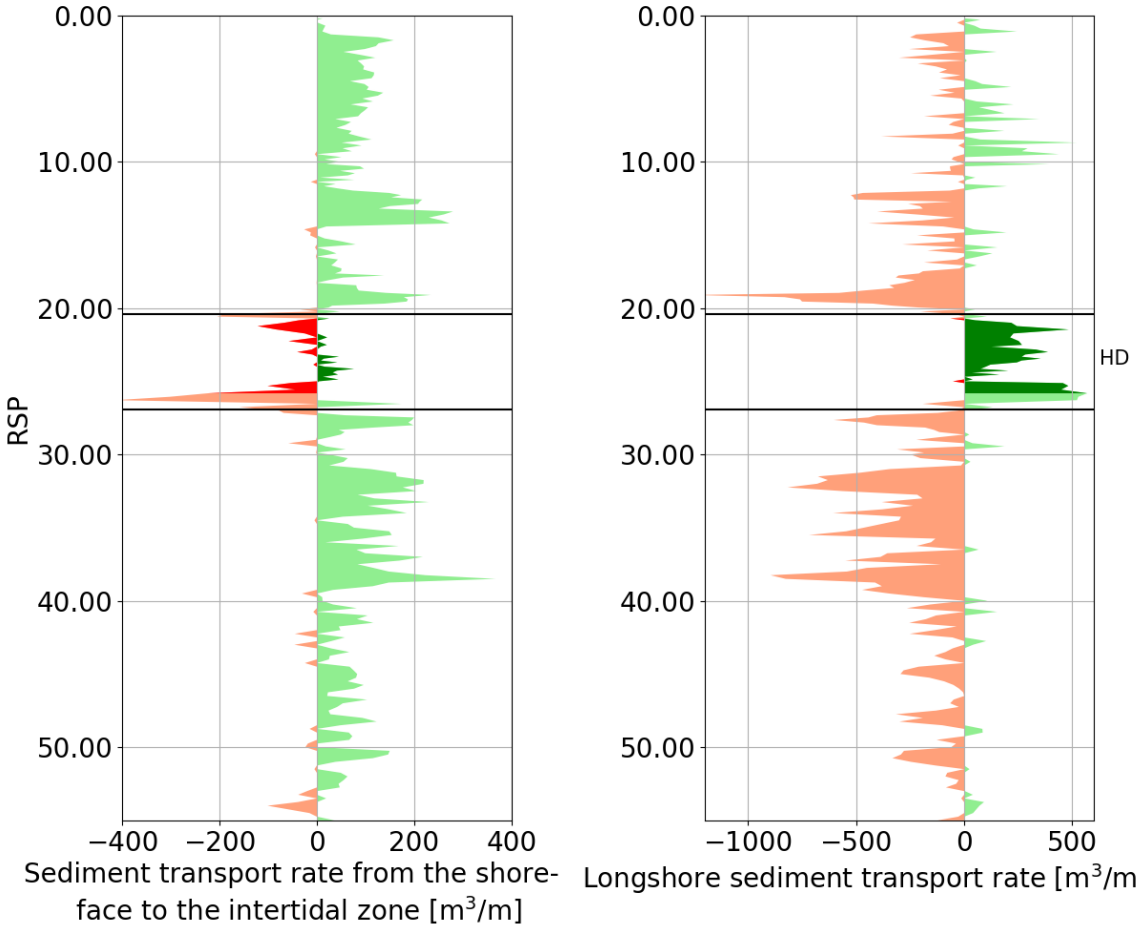

(a) Sediment transport rate from the shoreface to the intertidal zone. Positive values correspond to landward and negative values to seaward transport.

(b) Longshore sediment transport rate $\left(\frac{\partial S_y}{\partial y}\right)$. Positive values correspond to increased and negative values to decreased northward transport rates.

Figure 4.15: Sediment transport of the North-Holland coast per unit width between November 8, 2015 and November 24, 2017, based on JARKUS measurements.

4.7. Conclusions

Based on the results of this data analysis, the following conclusions can be drawn:

- Dune growth is positive for the entire HD. The total increase in sediment volume in the dunes is approximately 573,000 m^3 in three years. Dune growth can be related to the wind angle of incidence, which depends on the dunefoot orientation. The beach, intertidal zone and shoreface generally erode, while the offshore zone silts up.
- The net sediment transport rate from the shoreface to the intertidal zone is negative in the north and south of the domain of interest (P2N, P3N and P2S), and positive in the middle (P4 and P3S). This behaviour may depend on the crest level of the sandbars in the shoreface, which affects the breaking of short waves and 'freeing' of long waves. The sediment transport rate from the shoreface to the intertidal zone is correlated to dune growth, although these variables could not be calculated independently in this analysis.
- Northward longshore sediment transport increases from south to north. This increase can be related to a gradual increase of wave angle of incidence, which depends on the profile orientation. The sediment loss in longshore direction in the first three years after construction is approximately 1,300,000 m^3. This sediment volume was mainly transported in northward direction, and deposited directly north of the HD. A small fraction of sediment was transported southward and deposited directly south of the HD.
- Aeolian sediment transport in the HD is to a higher extent supply limited than transport limited, because the relation between dune growth and beach width is stronger than the relation between dune growth and the third power of the wind velocity. However, the limiting factor is time- and space-dependent.
- Dune growth in the HD is larger than in the rest of the North-Holland coast. In the other cross-shore zones, volume changes in the North-Holland coast are approximately zero at locations where no nourishments have been constructed, while the HD shows large sedimentation (offshore zone) or erosion rates (shoreface, intertidal zone, beach). The net sediment transport rate from the shoreface to the intertidal zone is positive in the North-Holland coast, but shows fluctuations within the HD. Northward longshore transport decreases in the North-Holland coast, but increases in the HD.

5

Results: Numerical modelling

Chapter 4 showed a weak correlation between dune growth and net sediment transport from the shoreface to the intertidal zone, which suggests that other processes influence sediment transport to the dune. This chapter presents and discusses the results of the morphological evolution of the HD based on several marine processes in the intertidal zone, obtained through numerical modelling. The results can be divided into three topics: Dune growth, erosion and sedimentation patterns, and bed composition.

5.1. Dune growth

The data analysis of chapter 4 showed that dune growth is positive for the entire domain of interest. Marine processes that increase or decrease the sediment availability of the intertidal zone and the lower beach can affect dune growth, depending on whether sediment transport is supply limited or transport limited. The dune growth volumes for every profile and every simulation is presented and discussed below.

Profile 2 North
Figure 5.1 reveals the modelled and measured dune growth volumes (in m^3/m), as well as the calculated dune growth capacity based on the transport equation of Bagnold (1941): Equation 2.8. All simulations overestimate the measured dune growth. These overestimations may result from the impossibility to model erosion during storm events and high soil moisture contents due to rainfall. The volume changes and their under- or overestimation relative to the measured dune growth are presented in Table 5.1.

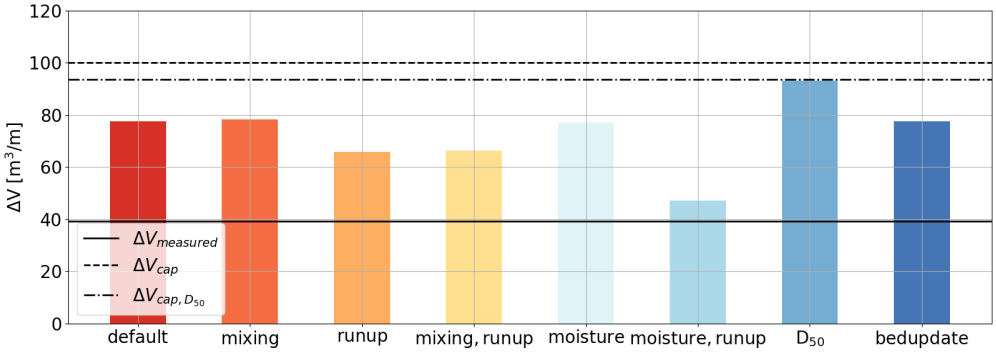

Figure 5.1: Effect of marine processes on dune growth of P2N in 302 days. The measured dune growth (solid black line) and dune growth capacity for multiple grains (dashed black line) and a single grain (dash-dotted black line) are marked.

Dune growth with hydraulic mixing is slightly higher than without, as shown in the first two bars of Figure 5.1, as a result of increased availability of fine grains in the intertidal zone. Wave runup reduces dune growth

due to a lower sediment availability landward of the still water level. Aeolian transport is supply limited when wave runup is so high that the wind is unable to pick up its capacity of sediment. Similar to the first two bars, the fourth bar shows a slight increase in dune growth as a result of hydraulic mixing. The inclusion of the soil moisture content in the intertidal zone reduces aeolian sediment transport to the dunes. Due to a high soil moisture content, grains in the intertidal zone are immobile. The combination of soil moisture content and wave runup gives the lowest sediment availability in the intertidal zone and beach, and the lowest dune growth volume. The simulation with the median grain size does not take into account beach armouring, and shows a significant increase in dune growth. Based on the last bar of Figure 5.1, dune growth does not seem to affected by bed updating in the intertidal zone. Section 5.2 elaborates on this.

The dune growth capacity is greater than all modelled dune growth volumes with multiple sediment fractions. This indicates that sediment transport of P2N is supply limited, even without hydraulic mixing, wave runup and soil moisture content. The dune growth volume of the simulation with a single grain size equals the dune growth capacity with D_{50}, indicating that sediment transport in that simulation, without beach armouring, is transport limited. All observations are quantified in Table 5.1.

Profile 4

Figure 5.2 reveals the modelled and measured dune growth volumes (in m^3/m). The first seven bars correspond to the simulations described in the introduction of this chapter. All simulations slightly overestimate the measured dune growth, but the general representation of the dune growth is good.

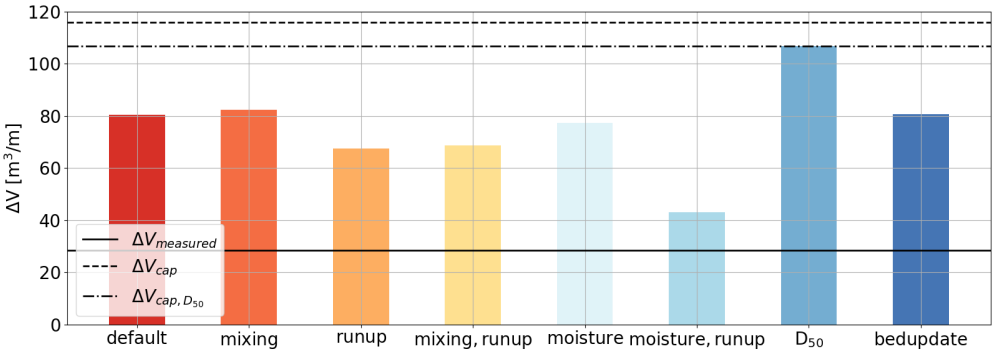

Figure 5.2: Effect of marine processes on dune growth of P4 in 302 days. The measured dune growth (solid black line) and dune growth capacity for multiple grains (dashed black line) and a single grain (dash-dotted black line) are marked.

Dune growth with hydraulic mixing is slightly higher than without, as shown in the first two bars of Figure 5.2. Wave runup reduces dune growth. Similar to the first two bars, the fourth bar shows a slight increase in dune growth as a result of hydraulic mixing. Similar to P2N, the inclusion of the soil moisture content in the intertidal zone reduces dune growth. The combination of soil moisture content and wave runup gives the lowest sediment availability in the intertidal zone and beach, and the lowest dune growth volume. The simulation with the median grain size shows a significant increase in dune growth. This simulation overestimates the measured dune growth volume. Based on the last bar of Figure 5.2, dune growth does not seem to affected by bed updating in the intertidal zone.

The dune growth capacity is greater than all modelled dune growth volumes with multiple sediment fractions. This indicates that sediment transport of P2N is supply limited, even without hydraulic mixing, wave runup and soil moisture content. The dune growth volume of the simulation with a single grain size equals the dune growth capacity with D_{50}, indicating that sediment transport in that simulation, without beach armouring, was transport limited. All observations are quantified in Table 5.1.

Profile 3 South

Figure 5.3 reveals the modelled and measured dune growth volumes (in m^3/m). The first seven bars correspond to the simulations described in the introduction of this chapter. The dune growth volumes in P3S are much higher than those of P2N and P4. The most likely cause of this difference is the finer grain size distribution of P3S relative to the other profiles. Most simulations overestimate the measured dune growth, but the representation of dune growth of the sixth bar is good.

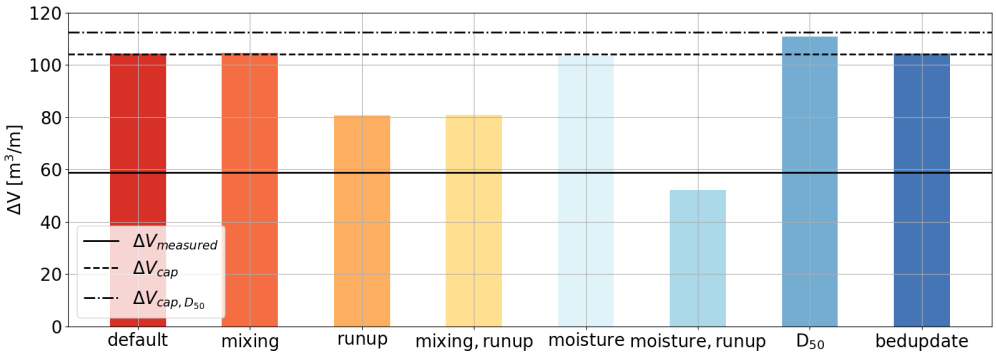

Figure 5.3: Effect of marine processes on dune growth of P3S in 302 days. The measured dune growth (solid black line) and dune growth capacity for multiple grains (dashed black line) and a single grain (dash-dotted black line) are marked.

The dashed line in this model, corresponding to Bagnold's dune growth capacity with multiple sediment fractions, is smaller than the dash-dotted line, indicating the dune growth capacity with a single grain size, because the median grain size of P3S is smaller than the reference grain size in equation 2.8. However, this is physically incorrect because beach armouring generally reduces aeolian sediment transport.

The effect of hydraulic mixing and soil moisture content on dune growth seems insignificant. A likely cause for these minor differences is that aeolian sediment transport is transport limited, because the modelled dune growth volumes are equal to the dune growth capacity. These different simulations have affected the erosion and sedimentation patterns in the intertidal zone and the beach, as will be explained in section 5.2, but have not affected the quantity of sediment that has been transported to the dune. The lower impact of supply-limiting factors on dune growth in P3S may be explained through the finer grain size distribution (see Figure 3.8) and the wider beach (see Figure C.1). The correlation between dune growth and beach width at the HD has been proven by Van Maanen (2018). Similar to the first five bars, the dune growth volume of the simulation with a single grain size equals the dune growth capacity with D_{50}, indicating that sediment transport in that simulation, without beach armouring, was transport limited. Only wave runup and the combination of soil moisture content and wave runup give a reduction in dune growth volume. This combination affects sediment availability in the intertidal zone and beach to such a degree that sediment transport becomes supply limited within 302 days. All observations are quantified in Table 5.1.

To illustrate that the impact of supply-limiting factors on dune growth is a time-dependent process, Figure 5.4 compares the modelled dune growth volumes after 180 days with the sediment transport capacity during that period. It reveals that sediment transport with wave runup and the combination of hydraulic mixing wave runup was predominantly transport limited as well. Erosion from the intertidal zone and the beach has gradually shifted the waterline location landward over time. Between the 180th and 302nd day, the beach has become so narrow that wave runup was able to limit aeolian sediment transport to the dune and decrease dune growth.

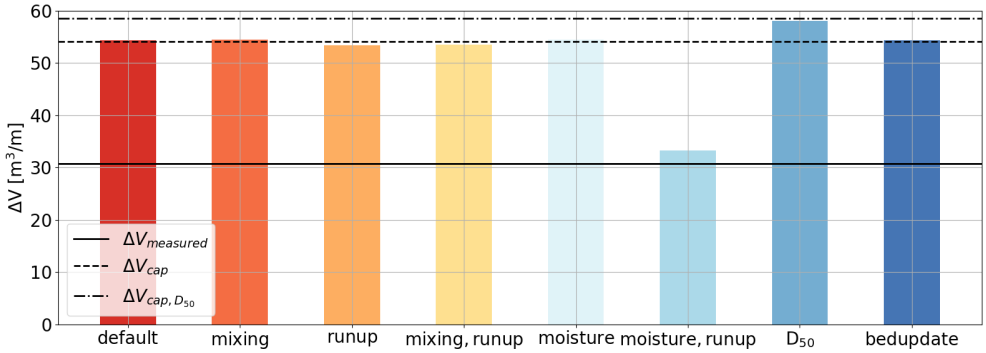

Figure 5.4: Effect of marine processes on dune growth of P3S in 180 days. The measured dune growth (solid black line) and dune growth capacity for multiple grains (dashed black line) and a single grain (dash-dotted black line) are marked.

Comparison
Table 5.1 compares the modelled dune growth volumes to the measured dune growth volume and the dune growth capacity following Bagnold (1941) (equation 2.8). The error is the absolute difference between the modelled and the measured dune growth volumes ($|\Delta V - \Delta V_m|$). Whether modelled sediment transport was supply limited or transport limited is indicated by the ratio between the modelled dune growth volume and the dune growth capacity ($\Delta V / \Delta V_{max}$). If this ratio is approximately 1, sediment transport is mainly transport limited. If the ratio is smaller than 1, sediment transport is mainly supply limited.

Values for $\Delta V / \Delta V_{max}$ of 0.99 or 0.98 can also be considered transport-limited, but the hand-calculated transport capacity does not use the same calculation method as AeoLiS. While AeoLiS accounts for beach armouring through redistribution of the weighting factors $\hat{w}$ (equation E.5), the transport capacity uses a simplified interaction between grains of different sizes through the factor $\sqrt{d_n / D_n}$, see equation 2.8. Although these methods should derive the same transport capacity, some minor deviations may arise.

Table 5.1: Modelled dune growth volumes in 302 days (in m^3/m) and their under- or overestimation. The first column of each model gives the dune growth volumes. The second column gives the absolute difference between the modelled and the measured dune growth. The third column gives the ratio between the modelled dune growth and the dune growth capacity.

	P2N			P4			P3S		
Simulation	ΔV	$\lvert\Delta V - \Delta V_m\rvert$	$\Delta V / \Delta V_{cap}$	ΔV	$\lvert\Delta V - \Delta V_m\rvert$	$\Delta V / \Delta V_{cap}$	ΔV	$\lvert\Delta V - \Delta V_m\rvert$	$\Delta V / \Delta V_{cap}$
Default	77.5	38.3	0.78	80.3	51.9	0.69	104.4	45.6	1.00
Mixing	78.2	39.0	0.78	82.3	53.9	0.71	104.7	45.9	1.00
Runup	65.8	26.6	0.66	67.5	39.1	0.58	80.6	21.8	0.77
Mixing, runup	66.2	27.0	0.66	68.6	40.2	0.59	80.8	22.0	0.78
Moisture	77.2	38.0	0.77	77.4	49.0	0.67	103.4	44.6	0.99
Moisture, runup	47.0	7.8	0.47	43.1	14.7	0.37	52.2	6.6	0.50
D_{50}	93.1	53.9	0.99	106.7	78.3	1.00	110.9	52.1	0.98
Bed update	77.6	38.4	0.78	80.6	52.2	0.70	104.4	45.6	1.00
Measured	39.2	-	-	28.4	-	-	58.8	-	-
Capacity	100.0	-	-	115.9	-	-	104.2	-	-
Capacity, D_{50}	93.6	-	-	106.8	-	-	112.6	-	-

5.2. Erosion and sedimentation patterns

The data analysis of chapter 4 showed that the dunes silted up, the beach and intertidal zone eroded. The erosion and sedimentation patterns for every profile and every simulation is presented and discussed below.

Profile 2 North
The measured transect used for the AeoLiS model of P2N is located in the middle of the domain P2N. The grain size distribution has a median grain size of 316 µm, see Table A.6. Figure 3.7a shows the initial bed level of the profile, corresponding to the echo sounder measurement of May 2015.

Bed level changes of the default run of 302 days, which does not include effects of soil moisture content, wave runup or hydraulic mixing, are shown in Figure 5.5. This figure shows erosion in the intertidal zone and the beach, and sedimentation in the dune. Beach erosion gradually decreases from the seaward side to the landward side, due to a gradual increase in sediment concentration in the air. The representation of morphological development in the intertidal zone is poor, in particular at the seaward side, because no marine processes have been taken into account. Erosion on the landward side of the beach is the result of the artificially increased threshold velocity, which prevents erosion from the dunes during periods with offshore directed wind, see Figure 3.9a. AeoLiS is not able to simulate the effect of dune geometry on aeolian sediment transport, because the interaction between morphology and wind field is not described in AeoLiS (Van Westen, 2018). Therefore, modelled dune development is very atypical, because the effects of vegetation and bed slope on sediment transport are implemented artificially. All sediment that is transported beyond the dune foot is deposited at the seaward side of the dunes.

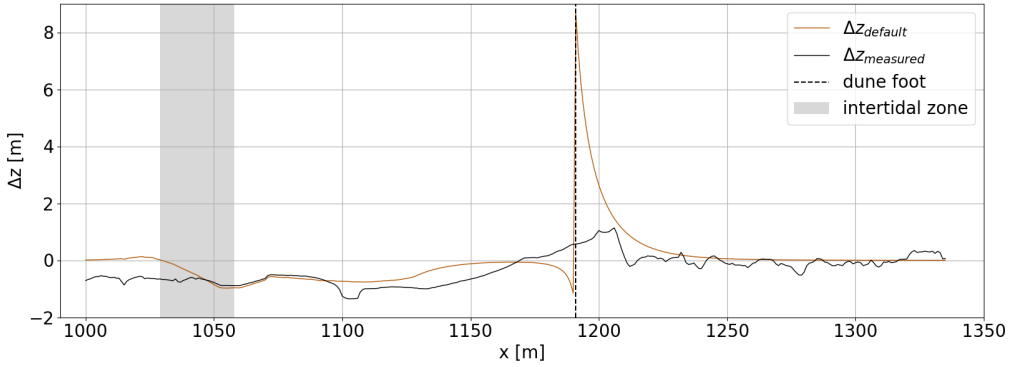

Figure 5.5: Modelled and measured bed level changes of P2N in 302 days. The intertidal zone (grey area) and dune foot (dashed black line) are marked.

Wave forcing (hydraulic mixing and wave runup) affects the availability of sediment for aeolian transport in the intertidal zone and the seaward side of the beach. Figure 5.6 presents the bed level changes of P2N with hydraulic mixing, wave runup, and the combination of the two. This figure shows that hydraulic mixing has an insignificant contribution to morphological development of the profile. Although barely visible, erosion of the intertidal zone with hydraulic mixing is slightly higher than without mixing. Wave runup reduces sediment availability for aeolian transport in the intertidal zone and seaward side of the beach. As a result, erosion at that domain is lower and the wind picks up sediment from the landward side of the beach. The dune growth volume is smaller, as discussed in section 5.1.

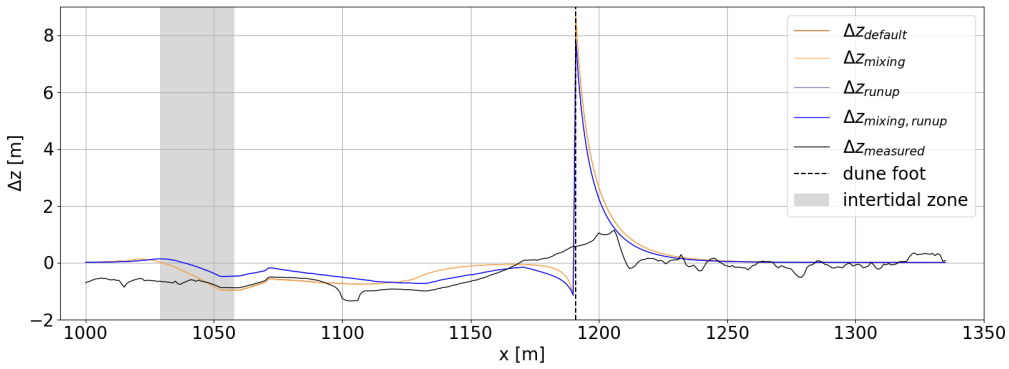

Figure 5.6: Effect of hydraulic mixing and wave runup on bed level changes of P2N in 302 days. The intertidal zone (grey area) and dune foot (dashed black line) are marked.

Figure 5.7 shows that the soil moisture content reduces sediment transport in the intertidal zone significantly. The erosion pattern is very similar to that of the run with wave runup, but the reduction of erosion in the intertidal zone and the increase of erosion at the beach are greater with moisture content. Because wave runup increases the domain that is moistened, the combination of soil moisture content and wave runup shows very little sediment transport in the intertidal zone and lower beach. Also, the dune growth volume is greatly reduced.

Beach armouring prevents fine grains from being transported, because they are not exposed to the wind when they are located behind a (much) coarser grain. In the model run with a single grain size, beach armouring as a result of winnowing cannot take place. This results in a small increase in erosion of the intertidal zone and beach, and an increase of sedimentation in the dune, see Figure 5.8.

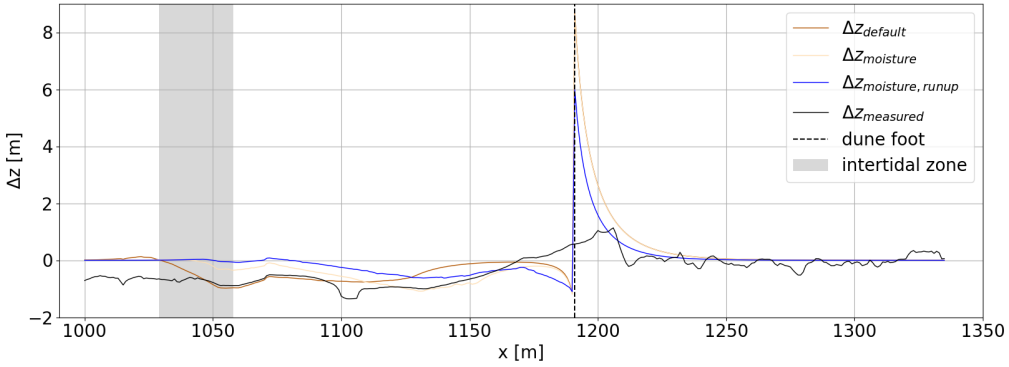

Figure 5.7: Effect of soil moisture content on bed level changes of P2N in 302 days. The intertidal zone (grey area) and dune foot (dashed black line) are marked.

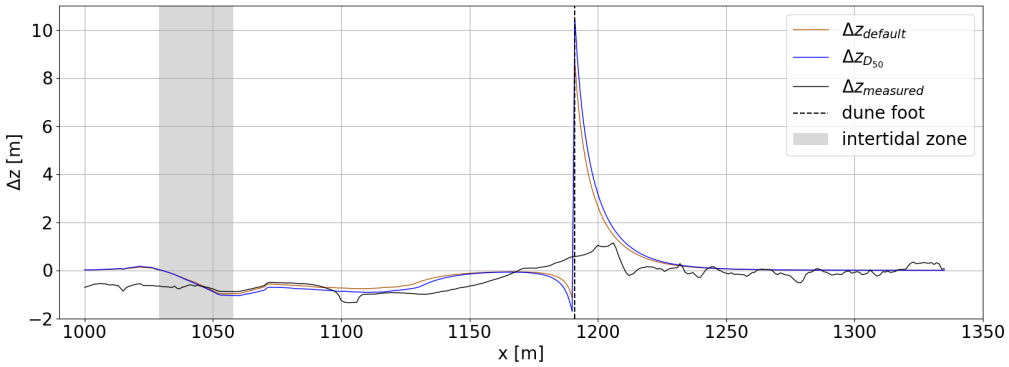

Figure 5.8: Effect of the grain size distribution on bed level changes of P2N in 302 days. The intertidal zone (grey area) and dune foot (dashed black line) are marked.

Figure 5.9 provides the bed level changes of P2N with bed updating in the intertidal zone, based on interpolated echo sounder measurements. In case of sediment supply to the intertidal zone, the grain size distribution of the supplied sediment is not taken into account because this distribution is not known. This figure shows that the modelled bed level equals the measured bed level up to $x \approx 1{,}110$ m, which roughly corresponds to the most landward waterline location at that period. From that point, the modelled bed level difference gradually approaches the default bed level difference. The bed level difference with bed updating does not instantly match the default bed level difference after the jump, because the bed updating affects the domain that lies below the still water level. This was proven to be of great importance for a hydro-aeolian model at the Sand Engine, because the volume of the dry beach varied over time to a large extend Van het Hooft (2018), but the significance for the HD seems to be moderate within 302 days. However, it is unknown whether this significance increases after modelling multiple years.

Aeolian sediment transport as a function of the bed slope is currently not implemented in AeoLiS. Therefore, the morphology of the landward side of the beach and the dune is not affected by bed updating in the intertidal zone. According to the AeoLiS manual (Hoonhout, 2018), the wind velocity threshold based on bed slopes will be modified following Dyer (1986). His formulation is based on laboratory experiments with unidirectional flow and is not easily modified to varying wind conditions.

The evolution of the beach and dune following the morphology of the intertidal zone can be predicted based on the physics of aeolian transport. If sediment erodes from the intertidal zone and the intertidal zone gradually decreases in altitude, the threshold velocity for transport to the beach increases, because an onshore directed wind needs a higher lift force to lift or roll a grain over another, see Figure 2.1. On the other hand, if the intertidal zone silts up due to onshore transport from the shoreface to the intertidal zone and increases in altitude, a grain is easier lifted or rolled over another grain, which facilitates aeolian transport to the beach. Be-

cause sediment is transported from the intertidal zone to the shoreface in P2N (see Figure B.8a), dune growth is expected to be lower with bed updating than without, although this cannot currently be modelled.

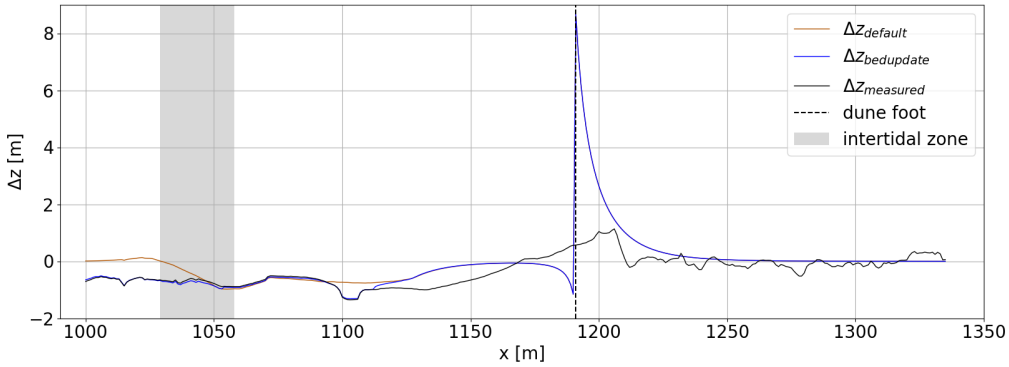

Figure 5.9: Effect of bed updating in the intertidal zone on bed level changes of P2N in 302 days. The intertidal zone (grey area) and dune foot (dashed black line) are marked.

Profile 4

The measured transect used for the AeoLiS model of P4 is located in the northern side of the domain P4. The grains in this model are relatively coarse: The median grain size of its distribution is 338 µm, see Table A.6. Figure 3.7b shows the initial bed level of the profile, corresponding to the echo sounder measurement of May 2015.

Bed level changes of the default run of 302 days, which does not include effects of soil moisture content, wave runup or hydraulic mixing, are shown in Figure 5.10. Erosion and sedimentation patterns of this profile are very similar to those of P2N. Erosion is observed in the intertidal zone and the beach, and sedimentation is observed in the dune. Beach erosion gradually decreases from the seaward side to the landward side, due to a gradual increase in sediment concentration in the air.

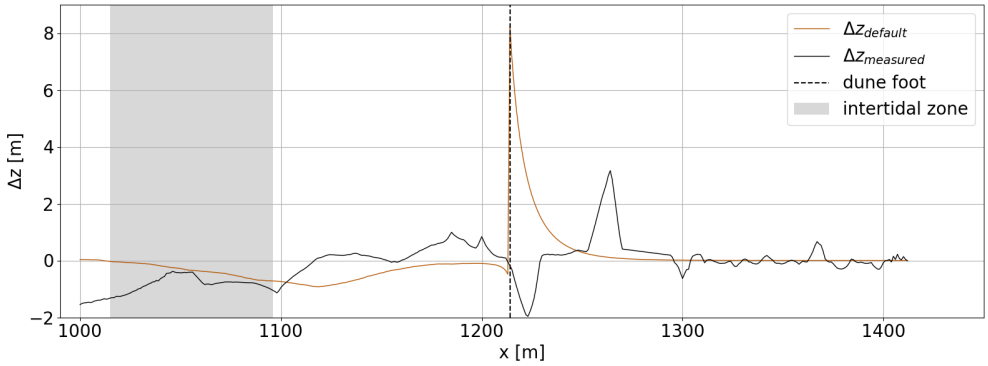

Figure 5.10: Modelled and measured bed level changes of P4 in 302 days. The intertidal zone (grey area) and dune foot (dashed black line) are marked.

Figure 5.11 presents the bed level changes of P4 with hydraulic mixing, wave runup, and the combination of the two. Similar to P2N, this figure shows that hydraulic mixing has a small contribution to morphological development of the profile. However, the contribution is more significant than that of P2N due to the broader grain size distribution of P4. Because the difference between fine grains and coarse grains in P4 is larger than that of P2N, the change in bed composition due to hydraulic mixing, and therefore the change in aeolian sediment transport, is more significant. Wave runup reduces sediment availability for aeolian transport in the intertidal zone and seaward side of the beach. As a result, erosion at that domain is lower and the wind picks up sediment from the landward side of the beach.

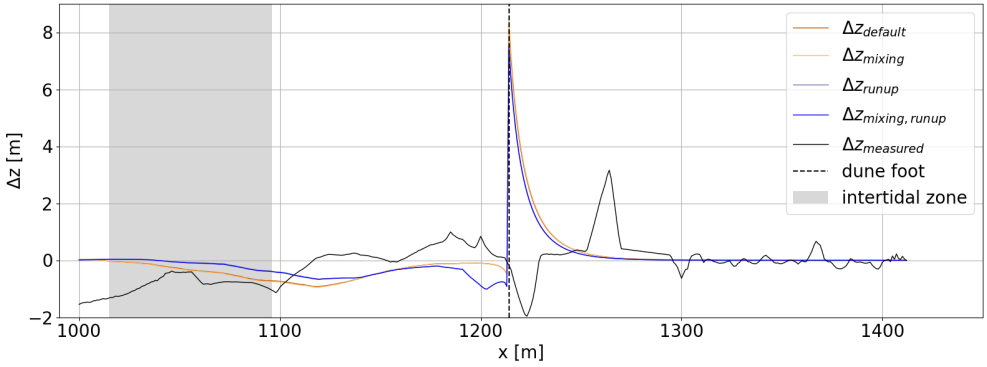

Figure 5.11: Effect of hydraulic mixing and wave runup on bed level changes of P4 in 302 days. The intertidal zone (grey area) and dune foot (dashed black line) are marked.

Figure 5.12 shows that the soil moisture content reduces sediment transport in the intertidal zone significantly. However, the erosion pattern is not similar to that of the run with wave runup: The soil moisture content caused erosion along the entire beach, while wave runup only resulted in erosion at the seaward side of the beach. Because wave runup increases the domain that is moistened, the combination of soil moisture content and wave runup shows very little sediment transport in the intertidal zone and lower beach. Also, the dune growth volume is greatly reduced.

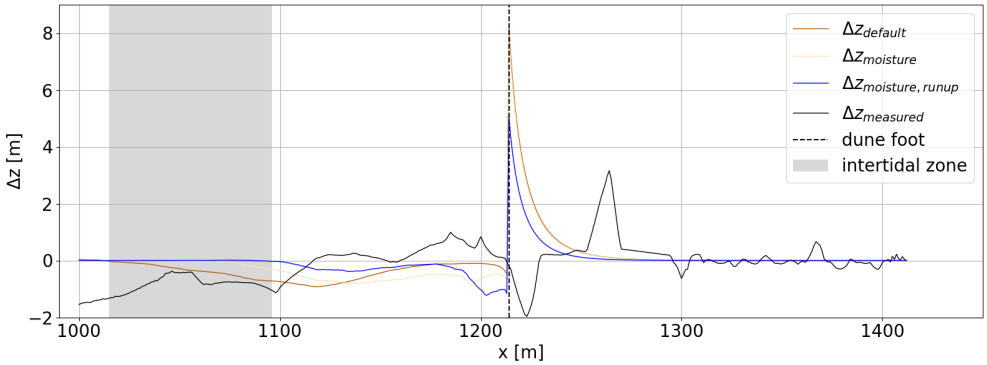

Figure 5.12: Effect of soil moisture content on bed level changes of P4 in 302 days. The intertidal zone (grey area) and dune foot (dashed black line) are marked.

Similar to P2N, the model run with a single grain size has resulted in a small increase in erosion of the intertidal zone and beach, and an increase of sedimentation in the dune, see Figure 5.13. However, the difference in sediment volume change between a single and multiple grain sizes is more significant in P4 than in P2N. The reason for this is a broader grain size distribution in P4, which amplifies the effect of beach armouring.

Figure 5.14 provides the bed level changes of P4 with bed updating in the intertidal zone, based on interpolated echo sounder measurements. This figure shows that the modelled bed level equals the measured bed level up to $x \approx 1{,}120$ m, which roughly corresponds to the highest still water level at that period. At that point, there is a steep decline in bed level, after which the bed level difference gradually approaches the default bed level difference.

Because sediment is transported from the shoreface to the intertidal zone in P4 (see Figure B.8a), dune growth is expected to be higher with bed updating than without, although this cannot currently be modelled in AeoLiS.

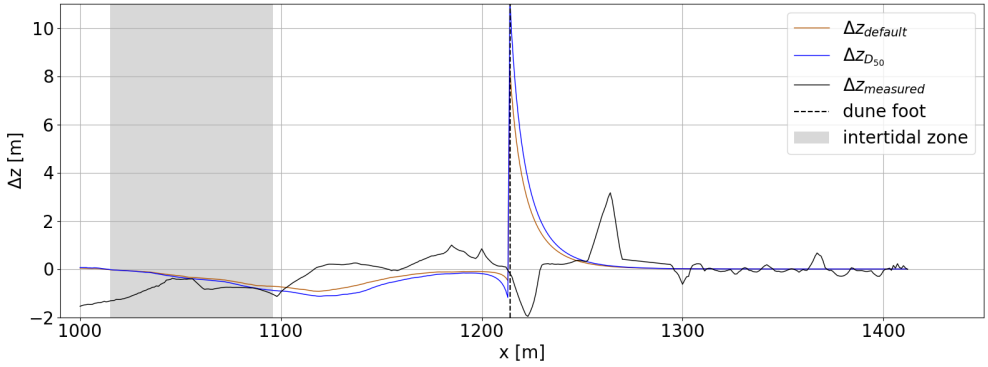

Figure 5.13: Effect of the grain size distribution on bed level changes of P4 in 302 days. The intertidal zone (grey area) and dune foot (dashed black line) are marked.

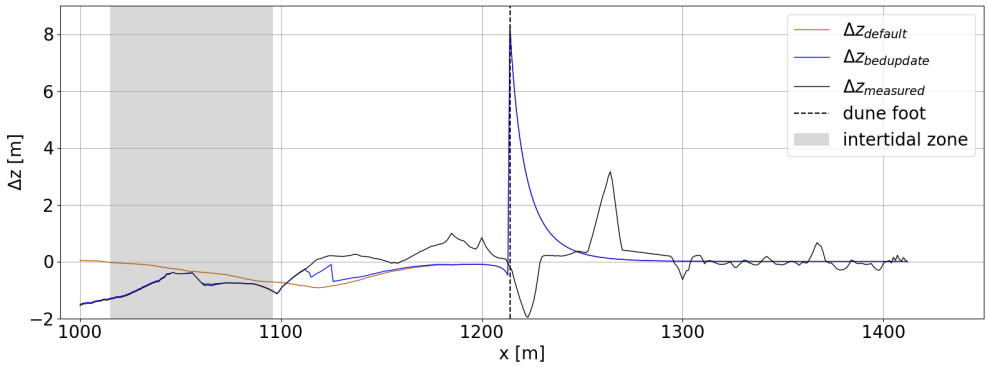

Figure 5.14: Effect of bed updating in the intertidal zone on bed level changes of P4 in 302 days. The intertidal zone (grey area) and dune foot (dashed black line) are marked.

Profile 3 South

The measured transect used for the AeoLiS model of P3S is located in the middle of the domain P3S. The grain size distribution is much finer than in the other two models: D_{50} = 221 µm, see Table A.6. Figure 3.7c shows the initial bed level of the profile, corresponding to the echo sounder measurement of May 2015.

Bed level changes of the default run of 302 days, which does not include effects of soil moisture content, wave runup or hydraulic mixing, are shown in Figure 5.15. Erosion and sedimentation patterns slightly deviate from those of P2N and P4. Erosion is still observed in the intertidal zone, and sedimentation is observed in the dune. However, the landward side of the beach shows little morphological development. Erosion on the landward side of the beach is larger than that of P2N and P4, because P3S has many fine grains that can be transported under mild offshore wind conditions.

Figure 5.16 presents the bed level changes of P3S with hydraulic mixing, wave runup, and the combination of the two. Similar to P2N and P4, this figure shows that hydraulic mixing has an insignificant contribution to morphological development of the profile. This change is smaller than that of P2N and P4 due to the narrower grain size distribution of P3S. Because the difference between fine grains and coarse grains in P3S is smaller than that of P2N and P4, the change in bed composition due to hydraulic mixing, and therefore the change in aeolian sediment transport, is less significant. Wave runup reduces sediment availability for aeolian transport in the intertidal zone. As a result, erosion at that domain is lower and the wind picks up more sediment from the beach.

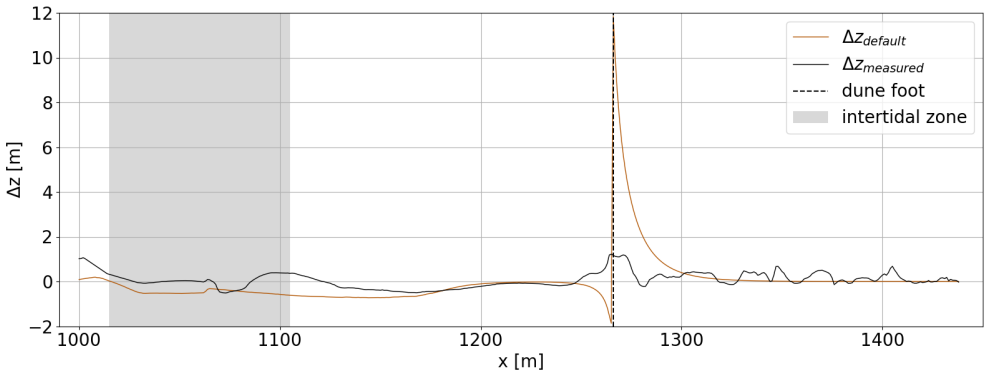

Figure 5.15: Modelled and measured bed level changes of P3S in 302 days. The intertidal zone (grey area) and dune foot (dashed black line) are marked.

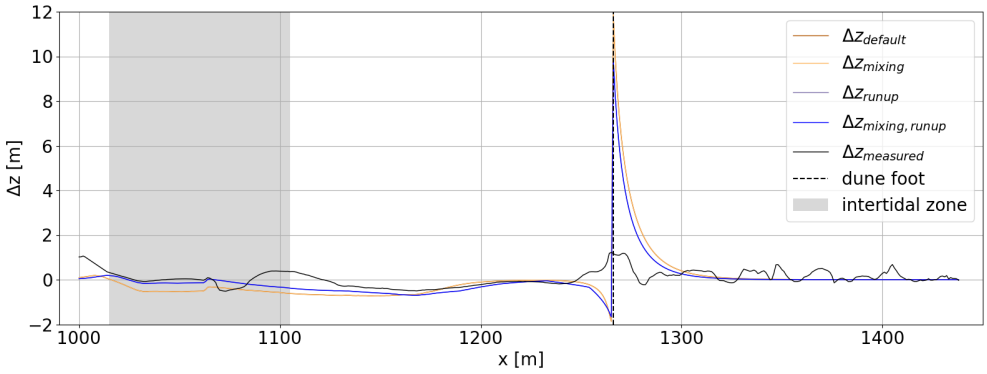

Figure 5.16: Effect of hydraulic mixing and wave runup on bed level changes of P3S in 302 days. The intertidal zone (grey area) and dune foot (dashed black line) are marked.

Figure 5.17 shows that the soil moisture content reduces sediment transport in the intertidal zone significantly. The erosion pattern is very similar to that of the run with wave runup, but the reduction of erosion in the intertidal zone and the increase of erosion at the beach are greater with moisture content. Because wave runup increases the domain that is moistened, the combination of soil moisture content and wave runup shows very little sediment transport in the intertidal zone and lower beach. Also, the dune growth volume is greatly reduced.

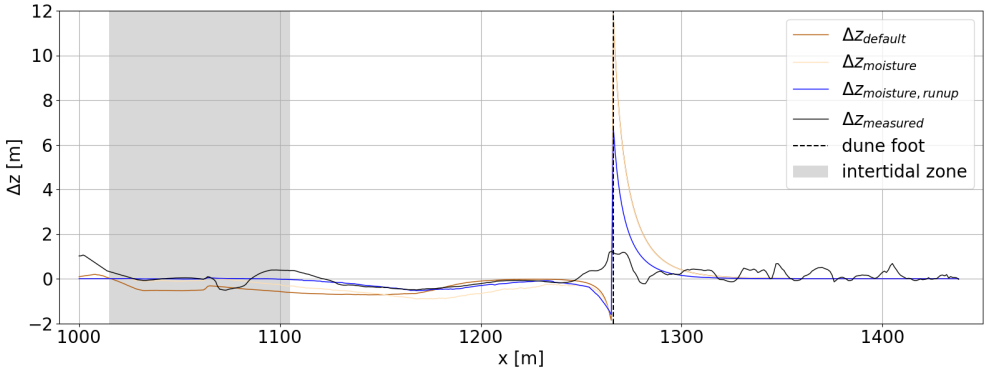

Figure 5.17: Effect of soil moisture content on bed level changes of P3S in 302 days. The intertidal zone (grey area) and dune foot (dashed black line) are marked.

Similar to P2N and P4, the model run with a single grain size has resulted in a small increase in erosion of the intertidal zone and beach, and sedimentation in the dune, and a decrease of sedimentation in the dune, see Figure 5.18. However, the difference in sediment volume change between a single and multiple grain sizes is smaller in P3S than in P2N or P4. The reason for this is a narrower grain size distribution in P3S, which weakens the effect of beach armouring.

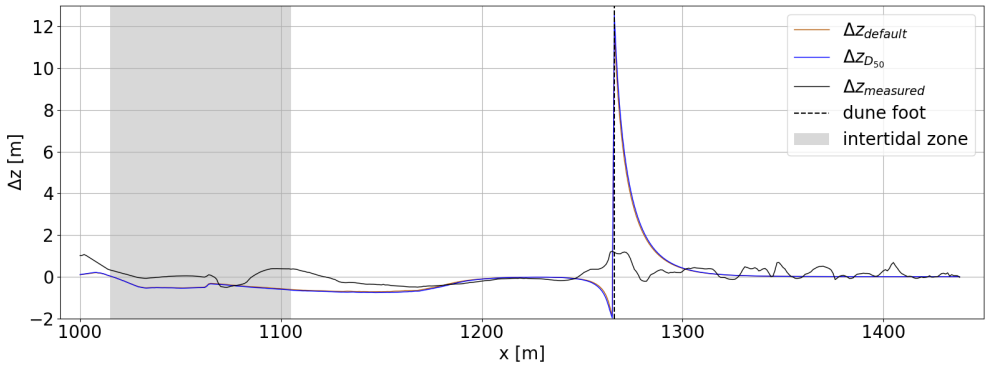

Figure 5.18: Effect of the grain size distribution on bed level changes of P3S in 302 days. The intertidal zone (grey area) and dune foot (dashed black line) are marked.

Figure 5.19 provides the bed level changes of P3S with bed updating in the intertidal zone, based on interpolated echo sounder measurements. This figure shows that the modelled bed level equals the measured bed level up to $x \approx 1{,}120$ m, which roughly corresponds to the highest still water level at that period. At that point, the bed level difference gradually approaches the default bed level difference.

Because sediment is transported from the intertidal zone to the shoreface in P3S (see Figure B.8a), dune growth is expected to be lower with bed updating than without, although this cannot currently be modelled in AeoLiS.

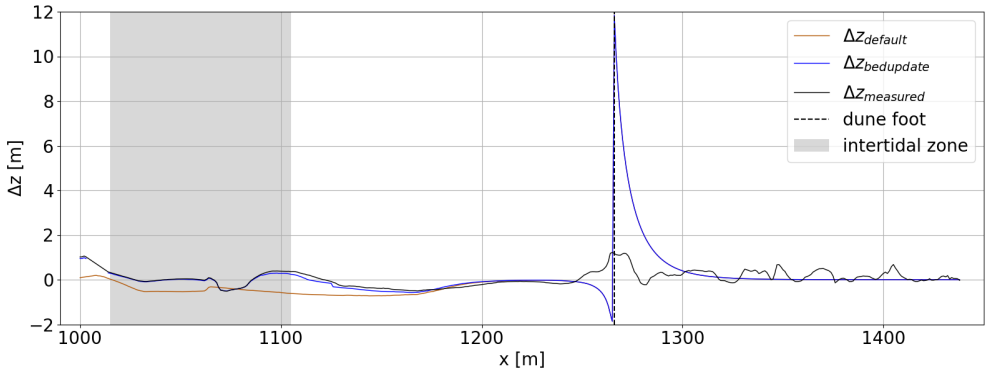

Figure 5.19: Effect of bed updating in the intertidal zone on bed level changes of P3S in 302 days. The intertidal zone (grey area) and dune foot (dashed black line) are marked.

5.3. Bed composition

Because fine grains are easier to be transported than coarse grains, aeolian transport has also changed the bed composition of the intertidal zone, beach and dunes. The changes in bed composition for every profile and every simulation is presented and discussed below.

Profile 2 North

Figure 5.20 presents the median grain size at the final time step of every grid cell of the model of P2N. This figure reveals that the intertidal zone and the beach have coarsened. This coarsening may have resulted

from landward aeolian sediment transport of fine sediments from the intertidal zone and beach to the dune. These fine sediments have subsequently settled in the dune, where the median grain size at the final time step is finer than the initial median grain size. This redistribution of sediment has resulted in a more natural system, with finer grains in the dunes and coarser grains in the intertidal zone and beach, and agrees with the grain size measurements of Fortuijn (2018).

The upper part of the shoreface contains a relatively fine grain size distribution, which resulted from settlement of fine grains during periods with offshore directed wind. However, this modelling study does not take into account the grain size distribution of marine sediments that have migrated onshore, so the modelled grain size distribution in this domain is not accurate.

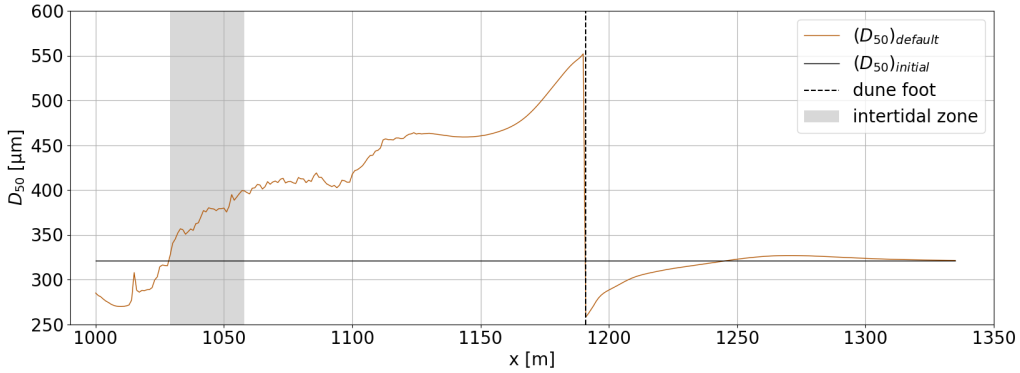

Figure 5.20: Modelled median grain size of P2N in 302 days. The intertidal zone (grey area) and dune foot (dashed black line) are marked.

Hydraulic mixing redistributes the sediment at the top layer of grid cells below the water surface towards its original distribution, by averaging the grains within the depth of disturbance. Figure 5.21 clearly shows that the median grain size at the intertidal zone and lower beach of the model runs with hydraulic mixing ($(D_{50})_{mixing}$ and $(D_{50})_{mixing,\ runup}$) are closer to the initial median grain size than those without mixing ($(D_{50})_{default}$ and $(D_{50})_{runup}$). Because relatively many fine sediments could be picked up from the intertidal zone and the lower beach for model runs that include hydraulic mixing, the median grain size in the dune is lower for those runs.

Wave runup decreases sediment availability at the region directly landward of the still water level. Because sediment in that region is immobile, the wind picks up sediment further onshore. When comparing a model run with wave runup to a run without runup, for example $(D_{50})_{default}$ and $(D_{50})_{runup}$ in Figure 5.21, it is clear that the spatial distributions of the median grain size show great similarities, but that the distribution of $(D_{50})_{runup}$ has shifted approximately 10 m onshore relative to that of $(D_{50})_{default}$, especially in the intertidal zone.

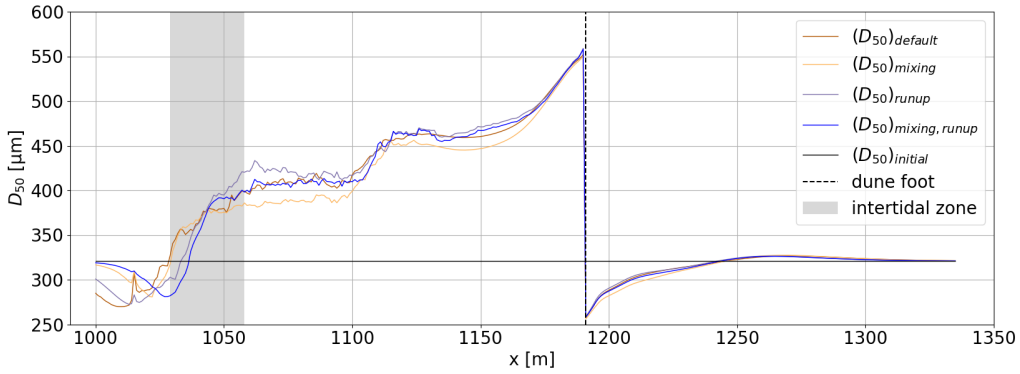

Figure 5.21: Effect of hydraulic mixing and wave runup on the median grain size of P2N in 302 days. The intertidal zone (grey area) and dune foot (dashed black line) are marked.

Similar to wave runup, the soil moisture content shifts the spatial distribution of the grain size onshore. Furthermore, inclusion of the soil moisture content increases the difference between the threshold velocity of fine grains and coarse grains, because the threshold velocities are multiplied by the same factor if the formulation of Belly (1962) is used (see equation 2.19). This multiplication increases the range of wind velocities where transport of fine grains can initiate and transport of coarse grains cannot. Therefore, relatively many fine particles are transported in the intertidal zone and lower beach, see Figure 5.22. The combination of soil moisture content and wave runup results in coarsening of the entire beach because grains at the intertidal zone were predominantly immobile. Figure 5.22 also shows a wide trough around x = 1,070 m. This trough can be related to the shape of the initial beach profile, see Figure 3.7a, where the bed level has a trough at the same location. The combination of soil moisture content and wave runup may have caused that that location is almost permanently moist, and that erosion from that location seldom occurred.

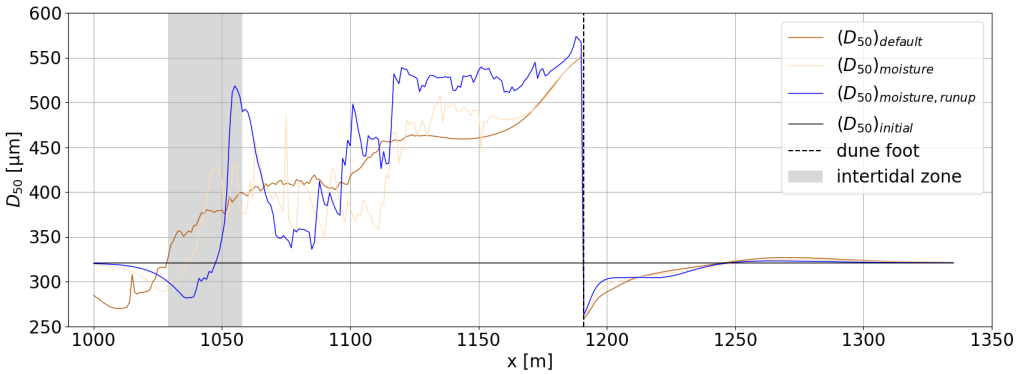

Figure 5.22: Effect of soil moisture content on the median grain size of P2N in 302 days. The intertidal zone (grey area) and dune foot (dashed black line) are marked.

Profile 4

Figure 5.23 presents the median grain size at the final time step of every grid cell of the model of P4. This figure reveals that the intertidal zone and the beach have coarsened, and that the dune has refined. This redistribution of sediment has resulted in a more natural system, with finer grains in the dunes and coarser grains in the intertidal zone and beach, and agrees with the grain size measurements of Fortuijn (2018).

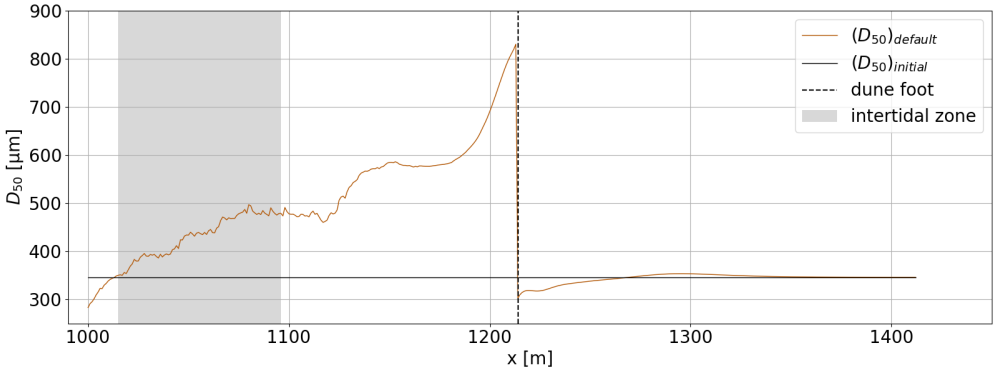

Figure 5.23: Modelled median grain size of P4 in 302 days. The intertidal zone (grey area) and dune foot (dashed black line) are marked.

Figure 5.24 clearly shows that the median grain size at the intertidal zone and lower beach of the model runs with hydraulic mixing ($(D_{50})_{mixing}$ and $(D_{50})_{mixing,\ runup}$) are closer to the initial median grain size than those without mixing ($(D_{50})_{default}$ and $(D_{50})_{runup}$).

When comparing a model run with wave runup to a run without runup, for example $(D_{50})_{default}$ and $(D_{50})_{runup}$ in Figure 5.24, it is clear that the spatial distributions of the median grain size show great similarities, but that

the distribution of $(D_{50})_{runup}$ has shifted approximately 20 m onshore relative to that of $(D_{50})_{default}$, especially in the intertidal zone.

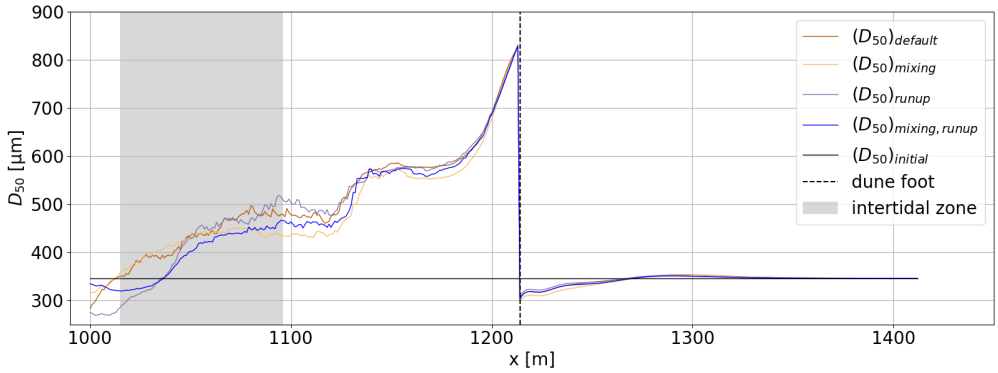

Figure 5.24: Effect of hydraulic mixing and wave runup on the median grain size of P4 in 302 days. The intertidal zone (grey area) and dune foot (dashed black line) are marked.

Similar to wave runup, the soil moisture content shifts the spatial distribution of the grain size onshore. Also, relatively many fine particles are transported in the intertidal zone and lower beach, see Figure 5.25. The combination of soil moisture content and wave runup results in coarsening of the entire beach.

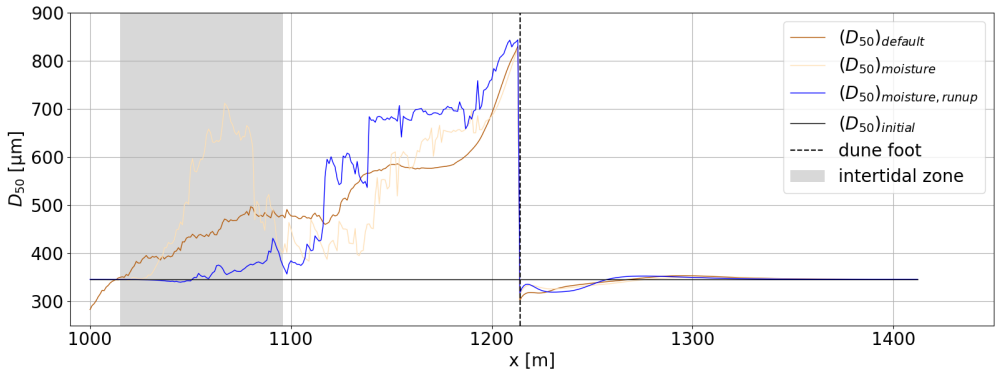

Figure 5.25: Effect of soil moisture content on the median grain size of P4 in 302 days. The intertidal zone (grey area) and dune foot (dashed black line) are marked.

Profile 3 South

Figure 5.26 presents the median grain size at the final time step of every grid cell of the model of P3S. This figure reveals that the intertidal zone and the beach have coarsened, and that the dune has refined. This redistribution of sediment has resulted in a more natural system, with finer grains in the dunes and coarser grains in the intertidal zone and beach, and agrees with the grain size measurements of Fortuijn (2018).

Figure 5.27 clearly shows that the median grain size at the intertidal zone and lower beach of the model runs with hydraulic mixing ($(D_{50})_{mixing}$ and $(D_{50})_{mixing,\,runup}$) are closer to the initial median grain size than those without mixing ($(D_{50})_{default}$ and $(D_{50})_{runup}$).

When comparing a model run with wave runup to a run without runup, for example $(D_{50})_{default}$ and $(D_{50})_{runup}$ in Figure 5.27, it is clear that the spatial distributions of the median grain size show great similarities, but that the distribution of $(D_{50})_{runup}$ has shifted approximately 10 m onshore relative to that of $(D_{50})_{default}$, especially in the intertidal zone.

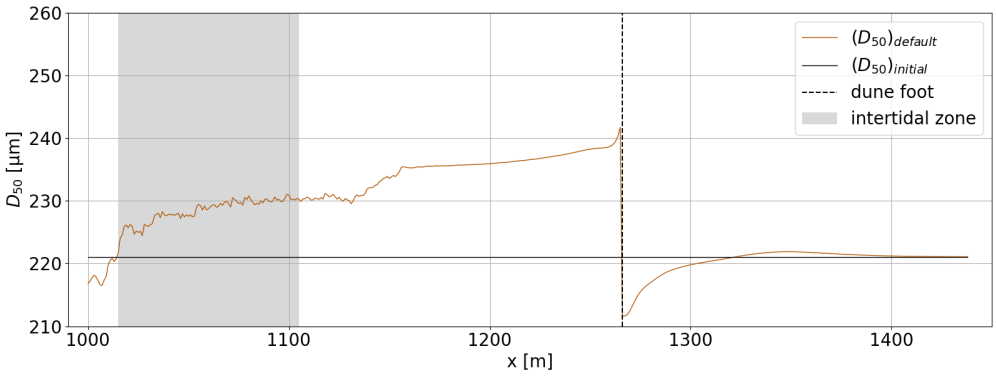

Figure 5.26: Modelled median grain size of P3S in 302 days. The intertidal zone (grey area) and dune foot (dashed black line) are marked.

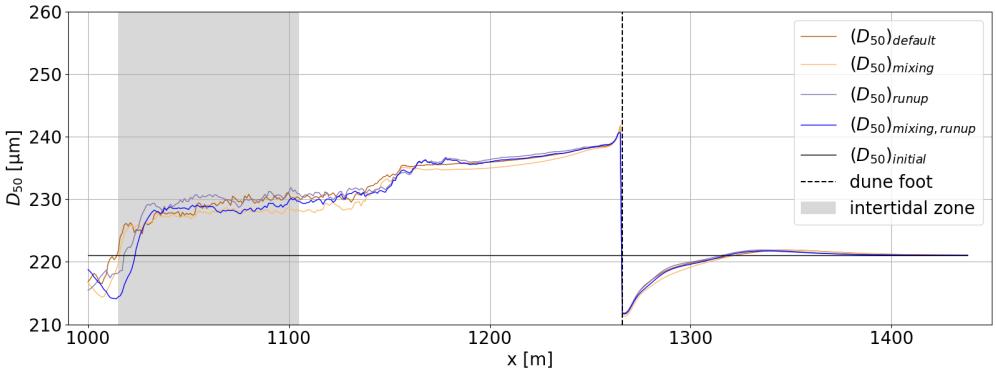

Figure 5.27: Effect of hydraulic mixing and wave runup on the median grain size of P3S in 302 days. The intertidal zone (grey area) and dune foot (dashed black line) are marked.

Similar to wave runup, the soil moisture content shifts the spatial distribution of the grain size onshore. Also, relatively many fine particles are transported in the intertidal zone and lower beach, see Figure 5.28. The combination of soil moisture content and wave runup results in coarsening of the entire beach because grains at the intertidal zone were predominantly immobile. Figure 5.28 also shows a wide trough around x = 1,060 m. This trough can be related to the shape of the initial profile, see Figure 3.7c, where the bed level has a trough at the same location. The combination of soil moisture content and wave runup may have caused that that location is almost permanently moist, and that erosion from that location seldom occurred.

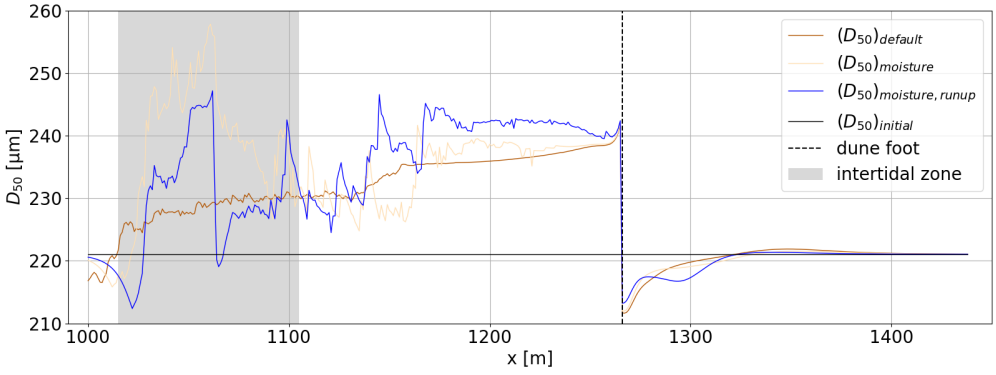

Figure 5.28: Effect of soil moisture content on the median grain size of P3S in 302 days. The intertidal zone (grey area) and dune foot (dashed black line) are marked.

5.4. Time scale

Figure 5.29 provides the temporal evolution of the dune volume for the default simulation of P2N, P4 and P3S. It shows a large increase in dune volume during the northern hemisphere winter (between November 2015 and March 2016), and little to no dune growth in summer (especially between August 2015 and November 2015). This volume increase is roughly evenly distributed over the winter season, and does not seem to be directly related to individual storm events. However, these models do not model dune erosion during storm events, where storm surge in combination with wave runup can exceed the dune foot level of NAP + 3 m and transport sediment offshore.

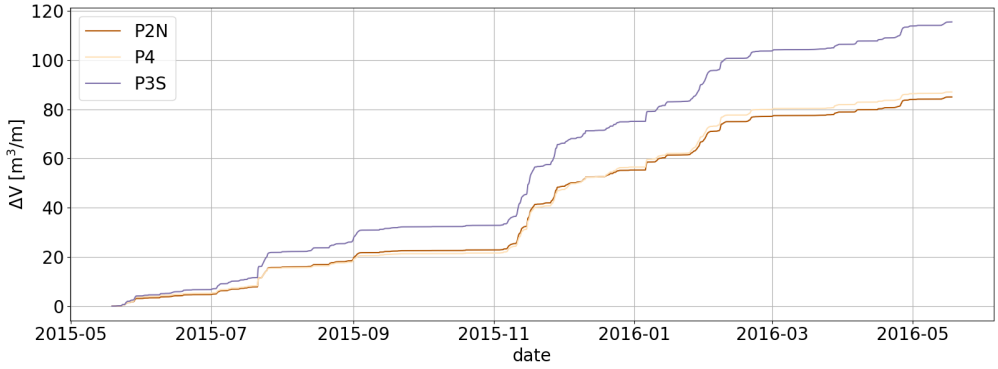

Figure 5.29: Temporal evolution of dune growth volume of P2N, P4 and P3S in 360 days

Figure 5.30 presents the temporal evolution of the median grain size at the beach and the dune for the default simulation of P2N, P4 and P3S. This figure shows many fluctuations for all profiles, both for the beach and the dune, indicating that the median grain size may directly be affected by changes in the wind velocity. Figure 5.31 relates the change of the median grain size in one time step on the beach and the dune to the cross-shore component of the wind velocity. The top panel shows that the median grain size on the beach generally increases when the wind is offshore directed. Because fine grains rarely erode from the dunes, fine grains from the beach are picked up and transported in offshore direction, coarsening the beach. On the other hand, the median grain size decreases during periods with onshore directed wind. Grains at the dune seem immobile when the wind is offshore directed, because the threshold velocity in the dune is higher than in the other zones. The grain size distribution changes when the wind is onshore directed. No relation is observed between changes in median grain size and the magnitude of the wind velocity.

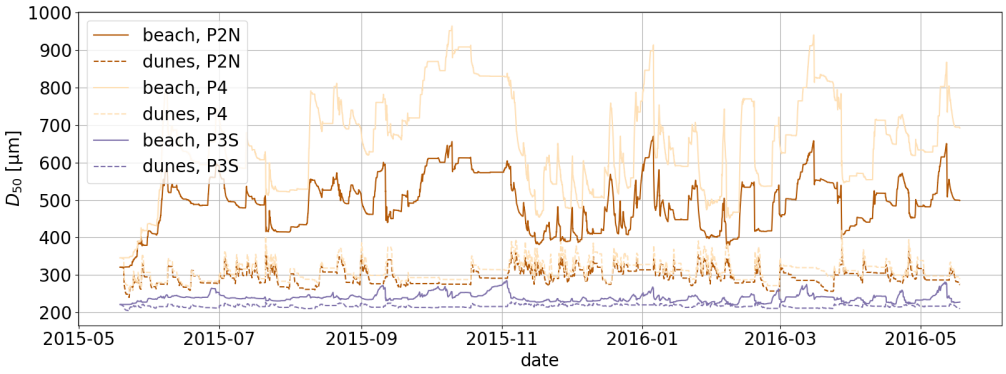

Figure 5.30: Temporal evolution of the median grain size at the beach (solid lines) and the dunes (dashed lines) of P2N, P4 and P3S in 360 days

In addition to short-term changes in median grain size, a seasonal variation is also noticeable. The median grain size at the beach is coarsest between August 2015 and November 2015, when mild winds in summer can

only transport the finest grains from the beach to the dunes, leaving coarse grains on the bed. During winter, stronger winds can also transport coarser grains from the beach, shifting the distribution of the resulting grains on the bed back towards its initial distribution.

Although not shown in this report, the typical time scales for changes in morphology and bed composition for simulations with one or more marine processes does not differ from the default simulation.

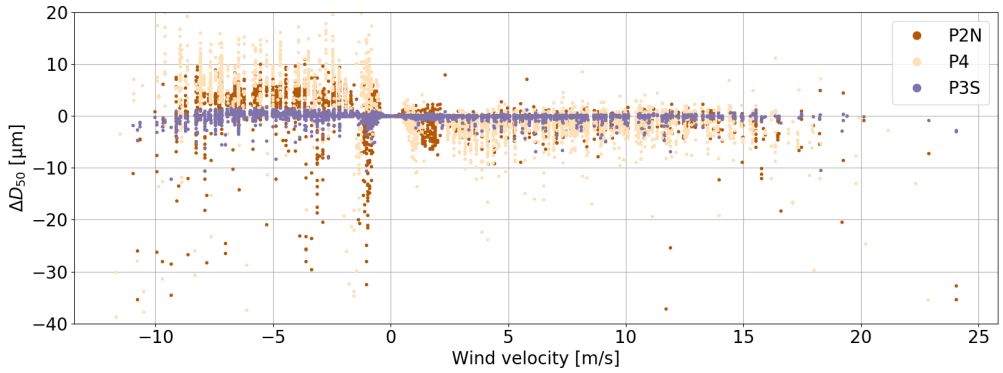

(a) Beach

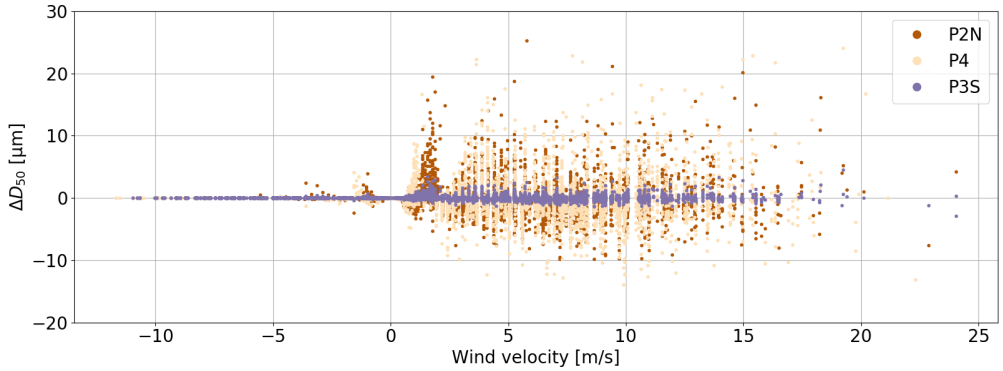

(b) Dune

Figure 5.31: Change in median grain size in one time step on the beach and the dune of P2N, P4 and P3S depending on the cross-shore component of the wind velocity

5.5. Conclusions

Based on the results of this modelling study, the following conclusions can be drawn:

- The intertidal zone and beach of the HD generally erode. Sediment is transport in cross-shore direction, to the dune. Because the model is mass conservative, the erosion volume in the intertidal zone and the beach equals the sedimentation volume in the dune.

  Hydraulic mixing does not contribute to significant bed level changes. Wave runup and the soil moisture content reduce erosion in the intertidal zone, because grains in the intertidal zone are immobile when they are moist. This causes more erosion in the (lower) beach and, in case of supply limited sediment transport, less sedimentation in the dune. Beach armouring decreases availability for aeolian transport of fine sediment, resulting in lower erosion and sedimentation volumes.

  Aeolian sediment transport as a function of the bed slope is currently not implemented in AeoLiS. Therefore, the morphology of the landward side of the beach and the dune is not affected by bed updating in the intertidal zone. Bed updating only affects the domain that lies below the still water level.

- The bed of the intertidal zone and beach of the HD becomes coarser over time, indicating that mainly fine grains are transported to the dunes. The median grain size in the dune is generally finer than the initial median grain size.

Hydraulic mixing refines the bed in the intertidal zone and the beach, up to the highest measured still water level, and coarsens the bed in the dune. With wave runup, the spatial variation of changes in grain size distribution shifts landward, because sediment is mainly picked up from the lower beach instead of the intertidal zone. The soil moisture content also shifts the spatial variation of changes in grain size distribution, and the combination of wave runup and soil moisture content fortifies this effect. The soil moisture content also significantly increases the median grain size in the intertidal zone and beach, because the difference in threshold for aeolian transport between fine and coarse grains becomes larger.

- Aeolian sediment transport in P2N and P4 is mainly supply limited, because supply-limiting factors (hydraulic mixing, wave runup, soil moisture content) either increasingly or decreasingly affect the dune growth volume. The dune growth volume of P2N and P4 with beach armouring is equal to the transport capacity following Bagnold (1941), indicating that aeolian sediment transport is transport limited.

  Aeolian sediment transport in P3S is mainly transport limited, because the dune growth volume in most simulations is equal to the dune growth capacity following the formulation of Bagnold (1941). Supply-limiting processes do not seem to affect dune growth in this profile. These results are likely to be related to the finer grain size distribution and wider beach at P3S. Wave runup and the combination of wave runup and soil moisture content seem to affect sediment transport to such a degree that transport is supply limited.

- The typical time scale for dune growth is seasonal. Dune growth in all models (P2N, P4 and P3S) was roughly evenly distributed over the winter season, whilst the majority of sediment settled in the dune. The temporal variation of the median grain size in the beach and the dune show many fluctuations, indicating that the bed composition directly reacts to changes in wind velocity or wind direction. Apart from short-term changes, a seasonal variation is also noticeable. The median grain size in the beach is higher during summer than during winter, because mild winds in summer can only transport the finest grains on the bed while storm winds in winter are able to transport coarser grains as well.

6

Discussion

In this study, the contribution of marine processes to changes in morphology and bed composition in the beach and dune was analysed and modelled. This chapter discusses the significance of the results of this study, as well as the limitations and assumptions that were required or made.

6.1. Significance of the results

As presented in chapter 4, the sediment volume in the dunes has increased by approximately 573,000 m^3 in three years. Meanwhile, the beach has eroded by 223,000 m in the same period. These findings agree with those of Bodde et al. (2019). Based on this study, the remaining sediment is expected to stem from the intertidal zone and the shoreface: These cross-shore zones have eroded by approximately 374,000 m^3 and 1,647,000 m^3 respectively. Based on these sediment volume changes, the total net sediment transport between the shoreface and the intertidal zone is approximately 22,000 m^3 in three years, directed seaward. However, this net sediment transport rate shows great variability in alongshore direction, where seaward directed transport in P2N, P3N and P2S (up to 150 m^3/m in three years) are observed together with landward directed transport in P3N and P4 (up to 150 m^3/m in three years).

The net sediment transport rate from the shoreface to the intertidal zone is related to the wave height of short waves that break on top of the sandbars in the shoreface. Short wave breaking affects the 'freeing' of long waves and the direction of cross-shore sediment transport. This study only assessed the contribution of bound and free long waves to cross-shore sediment transport from the shoreface to the intertidal zone, because that sediment transport mechanism is the only one that changes its cross-shore direction when approaching the coast. Although the net sediment transport rate from the shoreface to the intertidal zone is strongly correlated to the offshore wave height of the smallest short wave that will break on top of the sandbars, this study has been unable to prove that long waves govern this sediment transport, because it has not considered other transport mechanisms. Differences in sediment transport in the intertidal zone could also have been caused by longshore variations in, for example, the undertow or wave skewness. A further study on cross-shore sediment transport in the intertidal zone and its governing processes, including the undertow, wave skewness and long waves, would give insight into prediction of morphodynamics in the intertidal zone and its timescale.

The net sediment transport rate from the shoreface to the intertidal zone is not directly correlated to dune growth. The modelling study shows that several processes affect sediment availability in the intertidal zone, and enhance or reduce sediment transport from the intertidal zone to the dune. In the 1DH AeoLiS models of P2N and P4, dune growth is affected by hydraulic mixing, wave runup, soil moisture content en beach armouring. However, dune growth in P3S seems less dependent on these marine processes. Due to the presence of finer grains and a wider beach in P3S, aeolian sediment transport to the dune frequently reaches its capacity. To maximise dune growth for future coastal nourishment projects, a wide beach with fine grains at a small angle from the dominant wind direction must be constructed. However, a small nourished grain size negatively affects the beach width over time, as shown in Figure 2.11. Minimum beach width requirements must be met when designing a nourishment project with fine grains.

The effect of marine sediment supply on aeolian sediment transport or dune growth could not be assessed in this modelling study, because the wind velocity threshold based on the bed slope is currently not implemented in AeoLiS. Instead, the bed up to the waterline location is updated based on measurements. The representation of erosion in the intertidal zone and lower beach is poor, because the three models show a sudden decline in bed level at the highest modelled waterline location. However, this change in waterline location has affected sediment availability in the intertidal zone and lower beach. If the AeoLiS models would be coupled with a marine sediment transport model, the quality of the modelled morphology in the intertidal zone is expected to improve. Van het Hooft (2018) showed that a standalone AeoLiS model of the Sand Engine has a poor representation of the morphology of the intertidal zone, while a coupled AeoLiS-Delft3D model performs significantly better, because marine processes changed the dry beach volume of the Sand Engine to a large extent over time. Although this change is lesser for the HD, it is plausible that the contribution of marine processes becomes significant after modelling multiple years.

The typical timescale of changes in sediment transport and grain size distribution could be in the order of hours (storm events) to months (summer-winter cycle). However, the measurement frequency of the bed level data is not sufficient to assess the typical time scale for changes in dune morphology and bed composition. Also, literature on these topics is lacking. Based on the modelling study, the typical time scale for morphological changes in the dune is seasonal: Dune growth is roughly spread equally over the winter season, whilst the majority of sediment settled in the dune. The bed compositions show many short-term fluctuations, indication that the typical time scale for changes in bed composition is in the order of hours. Apart from short-term changes, a seasonal variation is also noticeable. The bed of the beach is coarser during summer than during winter.

6.2. Assumptions and limitations

Bed level data was analysed to create the sediment balance for the HD. The derivation of this sediment balance required several assumptions. Also, the bathymetry was measured at different moments in time by different parties, which introduced some limitations in this data analysis. The use of the numerical model AeoLiS, which modelled the contribution of supply-limiting (marine) processes on the morphology and bed composition of the beach and the dunes, introduced several limitations. These assumptions and limitations are discussed below.

6.2.1. Assumptions data analysis

Gradients in longshore sediment transport only take place in the shoreface, while longshore sediment transport between the other cross-shore zones is assumed to be in dynamic equilibrium, see Figure 3.3. This assumption is necessary to be able to calculate all sediment transport rates from the volume balance. If gradients in longshore sediment transport do take place in other cross-shore zones, some errors are induced in calculated cross-shore transport rates. A study by Radermacher et al. (2017) has proven that gradients in longshore sediment transport through flow contraction can take place in the offshore zone. However, this study is unable to quantify the effect of flow contraction to longshore sediment transport.

It is assumed that no cross-shore sediment transport takes place seaward of the offshore zone. Measurements showed that changes in sea bed level occurred at the deepest measured location. Because this location is located far beyond the closure depth, this sediment can be considered a sediment loss for coastal safety and irrelevant for this study. Also, cross-shore sediment transport landward of the dunes is assumed to be none, while in fact up to 5% of aeolian transport from the beach to the dune flows over the dunes of the HD (Bodde et al., 2019). This quantity is assumed negligibly small. Only the cross-shore sediment transport rate from the offshore zone to the shoreface and from the beach to the dunes would change if these bed level changes were taken into account.

For simplicity, settlement of the subsoil is assumed to occur only in the shoreface, while in reality this settlement took place over the entire cross-sectional domain, as quantified by De Jongh (2017). However, the quantification of settlements in her study was very simplified (P.G.F. Brandenburg, personal communication, January 8, 2019). The majority of the settled volume settled in the dunes (Wittebrood, 2017). This assumption has not caused errors in calculated volume changes, longshore transport or sediment loss for coastal safety, but has induced some errors in calculated net cross-shore sediment transport rates.

6.2.2. Limitations data analysis

The interpolated BIP dataset uses a northing and easting coordinate system, instead of a cross-shore and longshore coordinate system. Therefore, the transects of the offshore zone, shoreface and intertidal zone in the data analysis are horizontal instead of perpendicular to the coastline, which causes a maximum deviation of a few dozen meters. The use of the northing and easting system induces only small errors in growth and transport rates per unit meter, because the bed levels are strongly autocorrelated.

The LiDAR measurements contain the bed levels from March 2015 onwards, directly after completion of the HD. However, construction works started one year earlier in the southern end of the domain. The southern part already experienced a significant amount of morphological development during that year, but all developments before March 2015 have not been captured in these LiDAR measurements. Also, the first JARKUS measurement since the construction of the nourishment was executed eight months after the construction was finished. This means that a significant amount of volume changes could not be calculated based on these JARKUS measurements.

The latest echo sounder measurement was executed after an additional nourishment constructed in March 2018, which impedes the calculation of volume changes. This issue was resolved by using the second to last echo sounder measurement and linearly extrapolating the growth rates. The latest LiDAR measurement was carried out directly before construction of the additional nourishment.

If cross-shore sediment transport between the shoreface and the intertidal zone is proven to depend on the level of sandbars in the shoreface, sandbar dynamics will greatly affect this transport. Sandbars may have a life cycle of 10 to 15 years, whilst it generally migrates offshore, although the return period can differ by a factor of 3 to 4 (Walstra, 2016). The current measurement period is too short to assess sandbar dynamics.

Some scatter plots are distorted, because the BIP data used in these calculations was interpolated from data with a lower resolution. Because the correlation coefficients require independently sampled data points, they are calculated based on data of every 100 longshore meter. However, this does not guarantee statistically independent variables, because bed levels that follow from two independent measurements could still be autocorrelated. Based on the data analysis, a sample resolution of at least 1,500 m is required to obtain statistically independent data points. This sample resolution would only give four data points in the HD, which is insufficient to draw statistically valid conclusions on significance. Therefore, the sample resolution of the data is unchanged, but the significance of the results is statistically not fully valid.

6.2.3. Model limitations

As mentioned in section 6.1, the wind velocity threshold based on the bed slope is not yet implemented in AeoLiS. AeoLiS will implement this feature following the formulation of Dyer (1986). Because of this, AeoLiS is unable to model the contribution of the sediment transport rate from the shoreface to the intertidal zone on aeolian sediment transport, which was accounted for by updating the bed of the intertidal zone based on measurements. Bed updating only affected the domain that lies below the still water level. This was proven to be of great importance for a hydro-aeolian model at the Sand Engine, because the volume of the dry beach varied over time to a large extent (Van het Hooft, 2018). The significance for the HD seems to be moderate within the modelling time of 302 days, because the coastline only shows minor deviations. However, it is unknown whether this significance increases after modelling multiple years.

AeoLiS is not able to simulate the effect of dune geometry on aeolian sediment transport, because the interaction between morphology and wind field is not described in AeoLiS: The wind field is spatially uniform. (Van Westen, 2018). Therefore, modelled dune development is very atypical, because the effects of vegetation on sediment transport is implemented artificially. In the models, all sediment that is transported beyond the dune foot is deposited at the seaward side of the dunes.

The grain size distributions directly after construction of the HD in 2015 varied in cross-shore and alongshore direction (Fortuijn, 2018). However, AeoLiS only accepts a single grain size distribution in the entire domain as initial condition. The grain size distribution used in the models is representative for all measured grain size distributions in cross-shore direction (P.G.F. Brandenburg, personal communication, January 8, 2019). Because the median grain size in the intertidal zone and the beach was above average, the models are expected to overestimate the real aeolian transport rates.

1DH AeoLiS models are not able to account for longshore gradients in aeolian sediment transport. Similar to the data analysis, longshore aeolian sediment transport in the models is assumed to be in dynamic equilibrium. This assumption may under- or overestimate real bed level changes. AeoLiS calculates the cross-shore component of the wind velocity to model sediment transport.

The weighting factor of a sediment fraction in case of erosion depends on the grain size distribution on the bed and in the air. It takes into account the interaction between different sediment fractions, like sheltering or cascading. The ratio between these distributions is implemented in AeoLiS as the user-defined bed interaction parameter (ζ), because the exact interaction between sediment fractions is unknown.

7

Conclusions and Recommendations

This chapter derives the conclusion of this study, based on the results of the data analysis and numerical modelling, given in chapters 4 and 5. Next, recommendations for improvement of this and future studies are given, based on the conclusions and the discussion in chapter 6.

7.1. Conclusions

The conclusions of this study are based on the data analysis that calculates volume changes and net sediment transport rates for the entire Hondsbossche Dunes, and the modelling study on three profiles (Profile 2 north, Profile 4 and Profile 3 south) that qualifies the effect of marine processes (hydraulic mixing, wave runup, soil moisture content and beach armouring) on morphology and bed composition. The modelling study also assesses the typical time scale for changes in morphology and bed composition.

The main research question of this study is formulated as follows:

What is the causal relationship between marine processes and beach and dune evolution at the Hondsbossche Dunes?

This research question is answered by providing answers to the sub-questions. All conclusions are illustrated in Figure 7.1.

1. *What are the cross-shore and alongshore net sediment transport rates and which processes govern these transports?*

Along the entire Hondsbossche Dunes, sediment is transported from the beach to the dune, up to 190 m^3/m in three years. The total increase in sediment volume in the dunes in three years is approximately 573,000 m^3. The net sediment transport rate from the beach to the dune can be related to the wind angle of incidence, which depends on the dunefoot orientation.

In the north and south of the Hondsbossche Dunes (Profile 2 north, Profile 3 north and Profile 2 south), sediment is transported from the intertidal zone to the shoreface, up to 150 m^3/m in three years. This behaviour is different from the middle of the domain (Profile 4 and Profile 3 south), where up to 150 m^3/m of sediment is transported from the shoreface to the intertidal zone in the same period. The direction of cross-shore sediment transport between the shoreface and the intertidal zone may depend on the crest level of sandbars in the shoreface: The sandbars in the middle of the Hondsbossche Dunes break more short waves than those in the north and south, which causes 'freeing' of long waves and net landward sediment transport.

Northward longshore sediment transport increases from south to north. This increase can be related to a gradual increase in wave angle of incidence, which depends on the profile orientation. The sediment loss in longshore direction in the first three years after construction is approximately 1,300,000 m^3. This sediment volume was mainly transported in northward direction, and deposited directly north of the Hondsbossche Dunes. A small fraction of sediment was transported southward and deposited directly south of the Hondsbossche Dunes.

2. *How do the net sediment transport rate from the shoreface to the intertidal zone and marine processes influence dune growth?*

The sediment transport rate from the shoreface to the intertidal zone is positively correlated to the dune growth. However, these parameters are by definition correlated in this data study, because both variables are calculated using the bed levels in the dunes. The numerical models cannot verify the effect of the sediment transport rate from the shoreface to the intertidal zone on dune growth, because aeolian sediment transport as a function of the bed slope is not yet implemented in AeoLiS.

Wave runup and the presence of soil moisture reduce dune growth if aeolian sediment transport is supply limited, which is mainly the case for Profile 2 north and Profile 4. Beach armouring may have caused supply limited transport, because modelled sediment transport without beach armouring is transport limited for all profiles. Hydraulic mixing barely affects the dune growth volume, but refines the composition of the sediment that settles in the dune. Aeolian sediment transport in Profile 3 south is to a higher extent transport limited, because the dune growth volume in some simulations is equal to the dune growth capacity following the formulation of Bagnold (1941). Marine processes seem to have less effect on dune growth in this profile. These results are likely to be related to the finer bed composition and wider beach at Profile 3 south.

3. *How are changes in morphology and bed composition caused by marine processes in the intertidal zone?*

The intertidal zone of the entire Hondsbossche Dunes generally erodes, up to 200 m^3/m in three years. Also, the bed of the intertidal zone becomes coarser over time, because fine grains are eroded more easily than coarse grains. The redistribution of sediment results in a more natural system, with finer grains in the dunes and coarser grains in the intertidal zone and beach.

Wave runup and the presence of soil moisture reduce cross-shore aeolian sediment transport from the intertidal zone to the beach, because grains in the intertidal zone are immobile when they are moist. This reduction results in increased erosion at the dry part of the beach, because the wind picks up sediment from the beach instead of the intertidal zone. Hydraulic mixing does not contribute to significant morphological changes in the intertidal zone. Beach armouring decreases the availability of fine sediment for aeolian transport, resulting in lower erosion and sedimentation rates.

Hydraulic mixing redistributes grains on the bed of the intertidal zone toward its initial distribution. Wave runup locally increases the water level, so sediment is mainly picked up from the lower beach instead of the intertidal zone. Therefore, the spatial variation of changes in bed composition shifts landward. The combination of wave runup and soil moisture content fortifies this effect. The soil moisture content also significantly coarsens the bed composition in the intertidal zone, because the difference in threshold for aeolian transport between fine and coarse grains becomes larger.

4. *What is the typical timescale of changes in morphology and bed compositions in the coastal area?*

The typical time scale for morphological changes in the dune is seasonal. Dune growth is roughly spread equally over the winter season, whilst the majority of sediment settled in the dune as a result of more severe wind conditions.

The bed compositions show many short-term fluctuations, indicating that the bed composition directly reacts to changes in wind velocity or wind direction. The typical time scale is in the order of hours, the scale of storm events. Apart from short-term changes, a seasonal variation is also noticeable. The bed in the beach is coarser during summer than during winter, because mild winds in summer can only transport the finest grains on the bed while storm winds in winter are able to transport coarser grains as well.

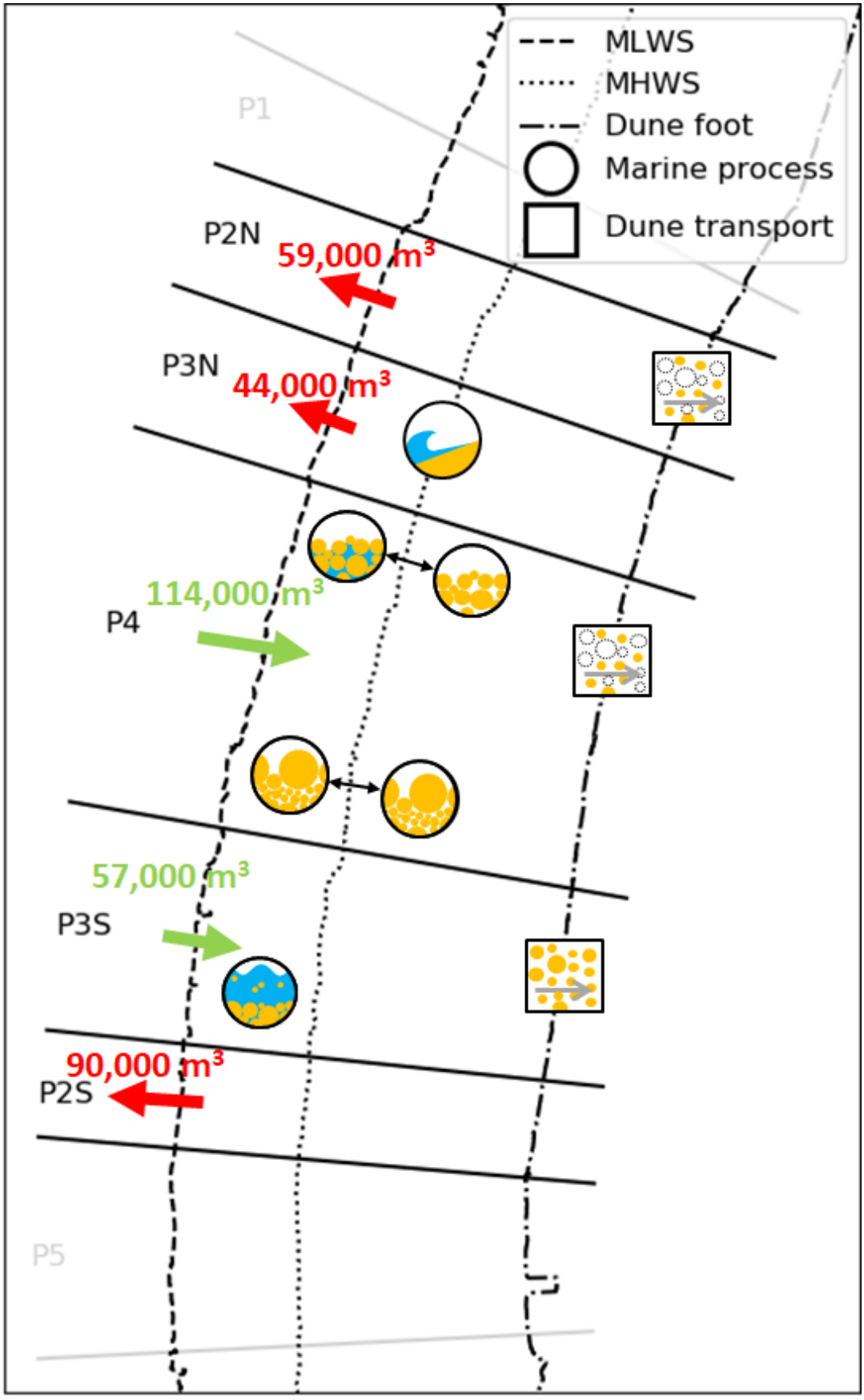

Figure 7.1: Schematic diagram of the Hondsbossche Dunes with net sediment transport rates from the shoreface to the intertidal zone between May 2015 and April 2018 (red and green arrows), marine processes (circles) and transport to the dunes (squares). Marine processes are wave runup (P3N), soil moisture content (P4 top), beach armouring (P4 bottom) and hydraulic mixing (P3S). Although these processes take place along the entire Hondsbossche Dunes, they are illustrated at a single location. Aeolian sediment transport to the dunes is supply limited in Profile 2 north and Profile 4, and transport limited in Profile 3 south.

7.2. Recommendations

Based on the drawn conclusions, it is recommended to construct a wide beach with fine grains at a small angle from the dominant wind direction to maximise natural dune growth in future coastal nourishment projects. However, a small nourished grain size negatively affects the beach width over time, as shown in Figure 2.11. Minimum beach width requirements must be taken into account when designing a nourishment project with fine grains.

Also, several simplifications and assumptions were made throughout this research, as discussed in chapter 6. Therefore, the following recommendations are given to increase the quality, integrality and reliability of further research:

- A study on cross-shore sediment transport in the intertidal zone and its governing processes would give insight into prediction of morphodynamics in the intertidal zone and its timescale. This study should examine the relative contributions of the undertow, wave skewness and long waves to cross-shore sediment transport between the shoreface and the intertidal zone.
- If cross-shore sediment transport between the shoreface and the intertidal zone is proven to depend on the crest level of sandbars in the shoreface, a further study on sandbar dynamics at the Hondsbossche Dunes could predict cross-shore sediment transport from the shoreface to the intertidal zone and improve the predictions of dune growth.
- Additional features in AeoLiS are recommended to improve the quality of further studies. Implementation of the wind velocity threshold based on the bed slope enables AeoLiS to model the contribution of the sediment transport rate from the shoreface to the intertidal zone on aeolian sediment transport and dune growth. According to the AeoLiS manual (Hoonhout, 2018), this feature will be implemented following the formulation of Dyer (1986). Implementation of the interaction between morphology and wind field enables AeoLiS to simulate the effect of dune geometry on aeolian sediment transport. Van Westen (2018) has initiated this implementation in AeoLiS.
- If the AeoLiS models would be coupled with a marine sediment transport model, the quality of the modelled morphology in the intertidal zone is expected to improve. Although the change in dry beach volume through marine processes is small for the Hondsbossche Dunes, it is plausible that the contribution of marine processes becomes significant after modelling multiple years.
- To predict the typical time scales for changes in morphology and bed composition at the Hondsbossche Dunes, a better general understanding of these time scales needs to be developed. Also, a higher bed level measurement frequency could enable the possibility to assess these typical time scales from a data study.

Bibliography

Archi (n.d.). De Hondsbossche Zeewering. `http://www.archi.nl/bergen-digitaal/index.php/attracties/natuur/bos-en-duinen/225-de-hondsbossche-zeewering`. Assessed: July 20, 2018.

Arends, I. (2018). Evaluating the applicability of 2DH models for the prediction of mega nourishments: A case study of the Hondsbossche Dunes. Master's thesis, Delft University of Technology.

Ashton, A. and Murray, A. (2006). High-angle wave instability and emergent shoreline shapes: 1. Modeling of sand waves, flying spits, and capes. *Journal of Geophysical Research: Earth Surface*, 111(F4).

Bagnold, R. (1937). The transport of sand by wind. *The Geographical Journal*, 89(5):409–438.

Bagnold, R. (1941). The Physics of Blown Sand and Desert Dunes. *London: Methuen*.

Belly, P. (1962). Sand movement by wind. Technical report, California University Berkeley Institute Of Engineering Research.

Bodde, W., Huiskes, R., IJff, S., Kramer, H., Kuiters, L., Lagendijk, G., Leenders, J., Ouwerkerk, S., Scholl, M., Smit, M., Smits, N., Stuurman, R., Van der Valk, B., Verheijen, A., De Vries, D., and Wegman, C. (2019). Innovatieproject Hondsbossche Duinen. Technical report, Ecoshape.

Bosboom, J. and Stive, M. (2012). *Coastal Dynamics I: Lectures Notes CIE4305*. VSSD.

Box, G. E., Jenkins, G. M., Reinsel, G. C., and Ljung, G. M. (2015). *Time series analysis: forecasting and control*. John Wiley & Sons.

Broekema, Y., Giardino, A., Van der Werf, J., Van Rooijen, A., Vousdoukas, M., and Van Prooijen, B. (2016). Observations and modelling of nearshore sediment sorting processes along a barred beach profile. *Coastal engineering*, 118:50–62.

Bruun, P. (1954). *Coast erosion and the development of beach profiles*, volume 44. US Beach Erosion Board.

Coastal Engineering Research Center (2008). *Coastal Engineering Manual*. US Army Corps of Engineers.

Cohn, N., Ruggiero, P., De Vries, S., and García-Medina, G. (2017). Beach growth driven by intertidal sandbar welding. In *Proceedings of the Coastal Dynamics Conference*, pages 1059–1069.

Cohn, N., Ruggiero, P., De Vries, S., and Kaminsky, G. (2018). New insights on coastal foredune growth: the relative contributions of marine and aeolian processes. *Geophysical Research Letters*.

De Jongh, L. (2017). Initial morphological evolution of a mega nourishment. Master's thesis, Delft University of Technology.

De Schipper, M. (2014). *Alongshore variability of nourished and natural beaches*. PhD thesis, Delft University of Technology.

De Schipper, M., De Vries, S., Ruessink, G., De Zeeuw, R., Rutten, J., Van Gelder-Maas, C., and Stive, M. (2016). Initial spreading of a mega feeder nourishment: Observations of the Sand Engine pilot project. *Coastal Engineering*, 111:23–38.

De Vries, S., Arens, S., De Schipper, M., and Ranasinghe, R. (2014a). Aeolian sediment transport on a beach with a varying sediment supply. *Aeolian Research*, 15:235–244.

De Vries, S., Southgate, H., Kanning, W., and Ranasinghe, R. (2012). Dune behavior and aeolian transport on decadal timescales. *Coastal Engineering*, 67:41–53.

De Vries, S., Van Thiel de Vries, J., van Rijn, L., Arens, S., and Ranasinghe, R. (2014b). Aeolian sediment transport in supply limited situations. *Aeolian Research*, 12:75–85.

Dean, R. (1991). Equilibrium beach profiles: characteristics and applications. *Journal of coastal research*, pages 53–84.

Dean, R. (2002). *Beach nourishment: theory and practice*, volume 18. World Scientific Publishing Company.

Dyer, K. (1986). Coastal and estuarine sediment dynamics. *John Wiley and sons, CHichester, Sussex(UK), 1986, 358*.

Elko, N. and Wang, P. (2007). Immediate profile and planform evolution of a beach nourishment project with hurricane influences. *Coastal Engineering*, 54(1):49–66.

Fortuijn, L. (2018). The effects of climate change on coastal management in the Hondsbossche Dunes: Analysis and modeling of aeolian sediment transport and dune growth. Master's thesis, Delft University of Technology.

Google Maps (2018). Dutch coast. `https://www.google.com/maps/@52.6059461,4.6909286,9z`. Assessed: November 15, 2018.

Hallermeier, R. (1981). A profile zonation for seasonal sand beaches from wave climate. *Coastal engineering*, 4:253–277.

Holland, K. and Elmore, P. (2008). A review of heterogeneous sediments in coastal environments. *Earth-Science Reviews*, 89(3-4):116–134.

Hoogwaterbeschermingsprogramma (n.d.). Hondsbossche en Pettemer Zeewering. `http://www.hoogwaterbeschermingsprogramma.nl/PersPress/Nederlands/Parelprojecten/Hondsbossche+en+Pettemer+Zeewering/default.aspx`. Assessed: July 20, 2018.

Hoonhout, B. (2018). *AeoLiS Documentation*.

Hoonhout, B. and De Vries, S. (2016). A process-based model for aeolian sediment transport and spatiotemporal varying sediment availability. *Journal of Geophysical Research: Earth Surface*, 121(8):1555–1575.

Hoonhout, B., De Vries, S., Baart, F., Van Thiel de Vries, J., Van der Weerd, L., and Wijnberg, K. (2013). Monitoring of beach surface properties with remote sensing. In *Coastal Dynamics 2013: 7th International Conference on Coastal Dynamics, Arcachon, France, 24-28 June 2013*. Bordeaux University.

Hotta, S., Kubota, S., Katori, S., and Horikawa, K. (1985). Sand transport by wind on a wet sand surface. In *Coastal Engineering 1984*, pages 1265–1281. ASCE.

Karman, P., Mijnders, I., Verbeek, I., and Argiolu, R. (2013). Milieueffectrapport Kustversterking Hondsbossche en Pettemer Zeewering. Technical report, Arcadis. client: Hoogheemraadschap Hollands Noorderkwartier and Provincie Nood Holland.

Leenders, J. and Smit, M. (2016). Ecoshape Hondsbossche en Pettemer Zeewering: B1-P1 - Inventarisatie maatregelen ontwerp HPZ. Technical report, Ecoshape.

Maidment, D. et al. (1993). *Handbook of hydrology*, volume 1. McGraw-Hill New York.

Mangor, K., Drønen, N., Kærgaard, K., Kristensen, N., Sørensen, P., and Kroon, A. (2017). Shoreline management guidelines. *DHI Water & Environment*.

Ministerie van Verkeer en Waterstaat (2006). Landelijke rapportage toetsing 2006. *Achtergrondrapport Deel 1: Dijkringgebieden*.

Muller, M., Roelvink, J., Luijendijk, A., De Vries, S., and Van Thiel de Vries, J. (2012). Process-based modeling of coastal dune development. *Coastal Engineering Proceedings*, 1(33):33.

Peckham, S., Hutton, E., and Norris, B. (2013). A component-based approach to integrated modeling in the geosciences: The design of CSDMS. *Computers & Geosciences*, 53:3–12.

Prodger, S., Russell, P., Davidson, M., Miles, J., and Scott, T. (2016). Understanding and predicting the temporal variability of sediment grain size characteristics on high-energy beaches. *Marine Geology*, 376:109–117.

Pye, K. (1987). *Aeolian dust and dust deposits*. Academic Press.

Radermacher, M., De Schipper, M., Swinkels, C., MacMahan, J., and Reniers, A. (2017). Tidal flow separation at protruding beach nourishments. *Journal of Geophysical Research: Oceans*, 122(1):63–79.

Rijkswaterstaat (2017). Kustlijnkaarten 2018.

Roelvink, J. and Stive, M. (1988). Large scale tests of cross-shore sediment transport on the upper shoreface. In *Symp. on Math. Mod. of Sed. Transp. in the Coastal Zone, Copenhagen, May*.

Schiereck, G. (1993). *Introduction to bed, bank and shore protection*. CRC Press.

Sherman, D. and Hotta, S. (1990). Aeolian sediment transport: theory and measurement. *Coastal Dunes: form and process*, 17:37.

Shields, A. (1936). Anwendung der Aehnlichkeitsmechanik und der Turbulenzforschung auf die Geschiebebewegung. *PhD Thesis Technical University Berlin*.

Simunek, J., Van Genuchten, M. T., and Sejna, M. (2005). The HYDRUS-1D software package for simulating the one-dimensional movement of water, heat, and multiple solutes in variably-saturated media. *University of California-Riverside Research Reports*, 3:1–240.

Sorgedrager, J. (2002). Cross-shore sediment transport on the shoreface. Master's thesis, Delft University of Technology.

Van de Rest, P. (2004). Morfodynamica en hydrodynamica van de Hollandse kust. Master's thesis, Delft University of Technology.

Van het Hooft, T. (2018). Predicting the dune growth at a meganourishment: By using a process based Integrated Hydro- Aeolian-Morphodynamic model. Master's thesis, Delft University of Technology.

Van Kesteren, D. and Smit, M. (2013). Initieel Aanlegprofiel, Prognose van eolisch zandverlies. Technical report, ZSNH Combinatie Van Oord – Boskalis. Zwakke Schakels Noord-Holland, Versterking en Onderhoud, Kustdeel RSP17.00 - RSP28.32.

Van Maanen, R. (2018). De samenhang van het intergetijdengebied op de duinaangroei van de Hondsbossche Duinen. Technical report, HKV Lijn in Water.

Van Rijn, L. (1997). Sediment transport and budget of the central coastal zone of Holland. *Coastal Engineering*, 32(1):61–90.

Van Rijn, L. (2007a). Unified view of sediment transport by currents and waves. I: Initiation of motion, bed roughness, and bed-load transport. *Journal of Hydraulic engineering*, 133(6):649–667.

Van Rijn, L. (2007b). Unified view of sediment transport by currents and waves. II: Suspended transport. *Journal of Hydraulic engineering*, 133(6):668–689.

Van Rijn, L. et al. (1993). *Principles of sediment transport in rivers, estuaries and coastal seas*, volume 1006. Aqua publications Amsterdam.

Van Westen, B. (2018). Numerical modelling of aeolian coastal landform development. Master's thesis, Delft University of Technology.

Verhagen, H. (1992). Method for artificial beach nourishment. In *Coastal Engineering 1992*, pages 2474–2485. ASCE.

Walstra, D. (2016). *On the anatomy of nearshore sandbars: A systematic exposition of inter-annual sandbar dynamics*. PhD thesis, Delft University of Technology.

Wang, P., Elko, N., and Roberts, T. (2009). Profile equilibration and longshore spreading associated with beach nourishment: a case study along west-central Florida coast. In *Proceedings Of Coastal Dynamics 2009: Impacts of Human Activities on Dynamic Coastal Processes (With CD-ROM)*, pages 1–13. World Scientific.

Wijnberg, K. (1997). On the systematic offshore decay of breaker bars. In *Coastal Engineering 1996*, pages 3600–3613. ASCE.

Wittebrood, M. (2017). Aeolian Sediment Transport at the Hondsbossche Dunes: The influence on beach and dune development. Master's thesis, Delft University of Technology.

Wright, L. and Short, A. (1984). Morphodynamic variability of surf zones and beaches: a synthesis. *Marine geology*, 56(1-4):93–118.

A

Data availability

A.1. Profile types

Profile type 1: High dune with variation in height
This profile type is located at a stretch of 750 m on the northern end of the HD, see Figure 1.3. The profile, called the panorama dune, consists of a single dune with an outer slope of 1:1.7 and an inner slope of 1:2.5. The crest height is at a level of NAP +26.2 m. The crest height gradually decreases at the north and south sides of the panorama dune until the geometry is similar to profile type 2. The panorama dune is fully vegetated and there are low-lying depositions areas at the dune crest. Because this profile type is constructed for touristic purposes instead of coastal safety or ecological development, they are excluded in this analysis.

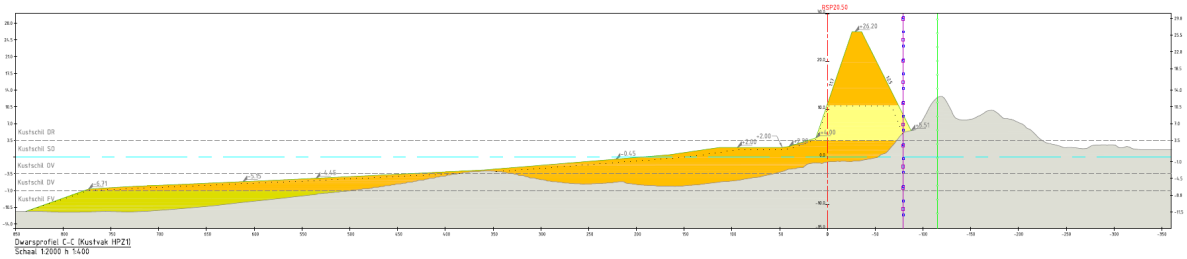

Figure A.1: Profile type 1 (Van Kesteren and Smit, 2013)

Profile type 2: High dune with restricted variation in height
This profile type is constructed at two locations along the HD, one in the north and one in the south (hereafter referred to as P2N and P2S respectively), see Figure 1.3. Both have a width of 500 m. Similar to profile type 1, this profile consists of a single dune row with an outer and inner slope of 1:2.1. The dune crest is located at NAP +12.5 m and is approximately 60 m wide. The dunes are only partly vegetated and there are no low-lying deposition areas.

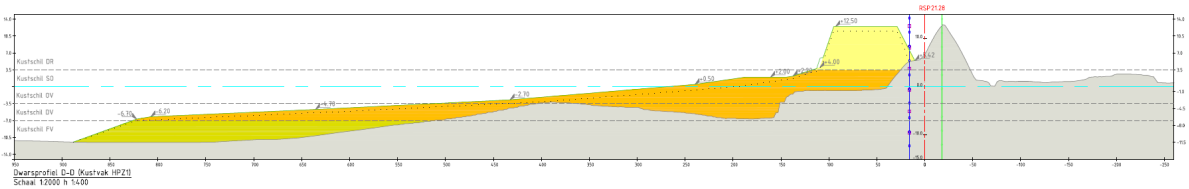

Figure A.2: Profile type 2 (Van Kesteren and Smit, 2013)

Profile type 3: Transition dune, low foredune with adjacent high dune
Similar to profile type 2, this profile type is constructed in the north and in the south (hereafter referred to as

P3N and P3S), see Figure 1.3. The dunes have a width of 1,000 and 1,500 m respectively. The profile consists of a high dune with a crest at NAP +10.4 m and a lower foredune at NAP +5.5 m. Both the dune and the foredune are partly vegetated and contain low-lying deposition areas.

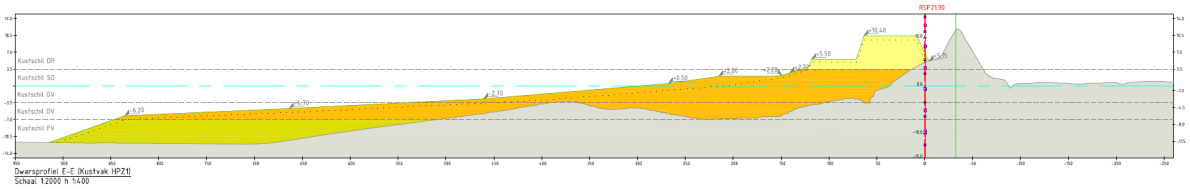

Figure A.3: Profile type 3 (Van Kesteren and Smit, 2013)

Profile type 4: Two dune rows with a dune valley
This dune type is constructed along a stretch of 1,500 m at the middle of the HD, see Figure 1.3. The profile consists of two dune rows, separated by a dune valley. The crest of the seaward dune is located at NAP +5.5 m and has small open areas. There is a longshore variation in vegetation pattern at the landward slope of the seaward dune. The landward dune has a foredune at approximately NAP +7 m and a higher dune at approximately NAP +11 m. Its seaward slope varies in longshore direction between 1:2.5 and 1:3.5. The landward dune is fully vegetated, except for the low-lying deposition areas. The valley between the dune rows is damp since construction.

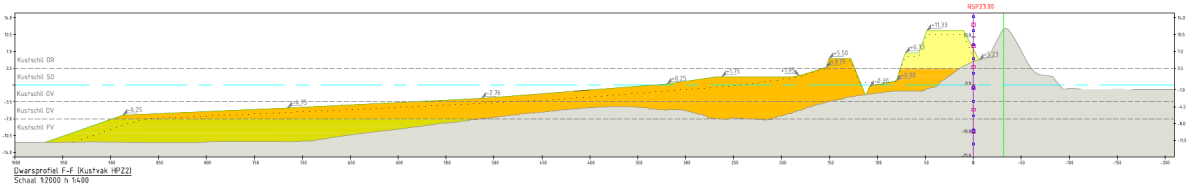

Figure A.4: Profile type 4 (Van Kesteren and Smit, 2013)

Profile type 5: Lagoon
This profile is located along a stretch of 1,000 m at the southern end of the HD, see Figure 1.3. The small dune has a crest at NAP +5.4 m and is fully vegetated at the inner slope and crest. A lagoon is located between the dune and the old dune of the HPZ. Similar to profile type 1, this profile type is constructed for touristic purposes and therefore excluded in this analysis.

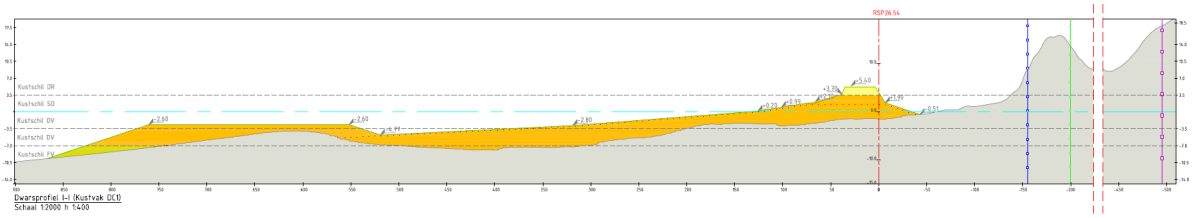

Figure A.5: Profile type 5 (Van Kesteren and Smit, 2013)

A.2. Topography and bathymetry measurements

Since the construction of the HD, nine topography measurements have been executed using LiDAR. These measurements present the cross-section of the dunes of every meter in longshore direction, with a spatial accuracy of 0.5 m. The coordinate system is based on the reference system of RWS: 'RijksStrandPaal' (hereafter referred to as RSP). The measurements cover the beach (from the high tide level) and the dunes of the whole study area, from RSP 17.08 in the north to RSP 28.30 in the south. Because LiDAR is not able to penetrate through water, it gives no information of the topography in the valley or below the water line. The

RSP-coordinates of the different profile types are shown in Figure 1.3. Table A.1 presents the date of every LiDAR-measurement.

Table A.1: LiDAR-measurements of the HD since construction

# measurement	Date
L1	May 24, 2015
L2	December 28, 2015
L3	March 21, 2016
L4	September 1, 2016
L5	December 5, 2016
L6	April 19, 2017
L7	August 11, 2017
L8	December 6, 2017
L9	March 19, 2018

Moreover, RWS conducts yearly measurements of the topography and bathymetry to a depth of approximately NAP -12 m, along the JARKUS-transects. The JARKUS-transects cover the entire Dutch coast, using the RSP reference system, with a cross-shore transect every 100 to 200 m. The measurements have a spatial accuracy of 5 m, and cover the shoreface, dry beach, intertidal zone and dunes. The dates of the JARKUS-measurement since construction of the HD are given in Table A.2.

Table A.2: JARKUS-measurements of the HD since construction

# measurement	Date
J1	November 8, 2015
J2	November 18, 2016
J3	November 24, 2017

The bathymetry of the lower shoreface of eleven transects along the HD is measured on a monthly basis by the contractor, using a single beam echo sounder. The vertical accuracy of the bed elevation measurements was of order 2-5 cm for the dry parts and 5-20 cm for the wet parts. To ensure that the entire cross-shore transect is measured, topographic surveys are executed around low tide and bathymetric surveys around high tide, resulting in overlap of both techniques (De Jongh, 2017). In addition to these eleven cross-shore transects above, eleven supplementary measurements surveys have been carried out, see Table A.3. These surveys cover the entire coastal zone. The dry part has been measured using LiDAR and the part below water level has been surveyed with a single beam echo sounder, on a longshore interval of 200 m. These transects are interpolated to create a BIP dataset, which has a horizontal accuracy of 2 by 2 m, using a northing and easting coordinate system. Re-interpolating this data to a cross-shore and longshore coordinate system is considered less accurate than using this data with a northing and easting coordinate system.

Table A.3: Echo sounder measurements of the HD since construction

# measurement	Date
E1	May 3, 2015
E2	January 6, 2016
E3	April 14, 2016
E4	August 27, 2016
E5	December 6, 2016
E6	January 20, 2017
E7	April 9, 2017
E8	August 16, 2017
E9	December 11, 2017
E10	January 11, 2018
E11	April 9, 2018

A.3. Grain size measurements

Directly after completion of the project, a measurement of the grain size distributions was conducted for the entire study area, to a depth of NAP -1 m. A total of 67 samples have been collected. The grain size distributions have been determined for five subdomains, which are indicated in Figure A.6. This figure also presents the RSP-coordinates between the subdomains and the median grain size D_{50} for every subdomain in µm. Figure A.7 presents the grain size distributions for every subdomain.

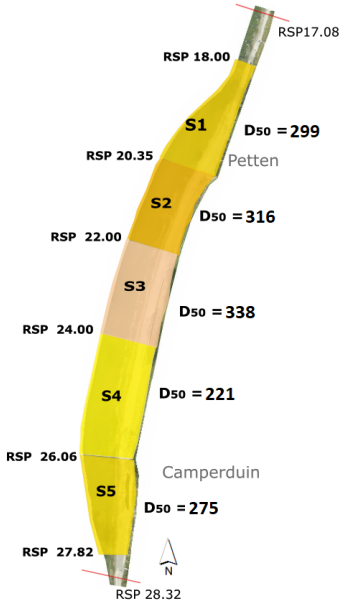

Figure A.6: Study area showing the median grain size D_{50} for every subdomain in µm (adapted from Wittebrood, 2017)

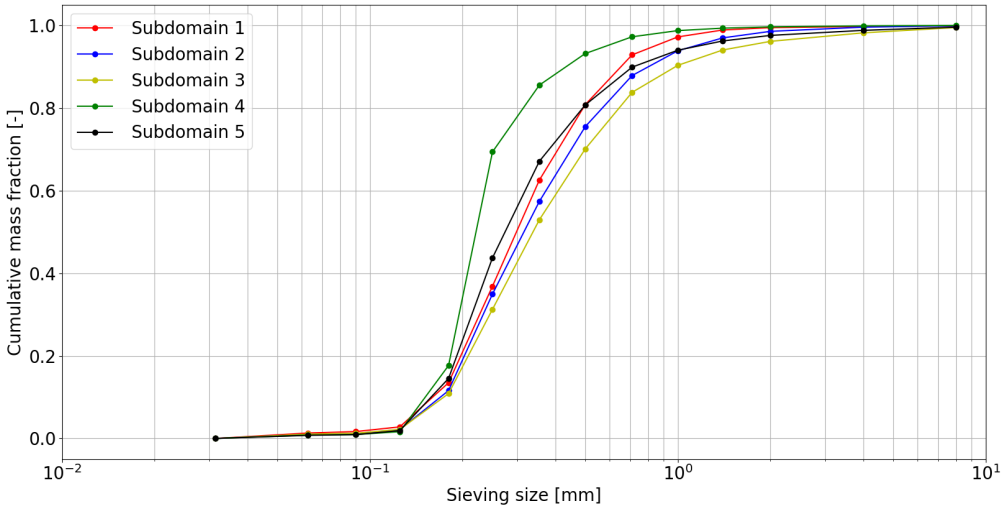

Figure A.7: Sieve curves showing the grain size distribution for every subdomain

Measurements on the grain size distribution along five transects have been taken by Fortuijn (2018) in 2018. These measurement can be used to qualitatively assess the redistribution of sediment over the domain.

B

Volume changes and sediment transport per interval

This appendix depicts the changes in sediment volume of each cross-shore zone for every measurement interval or every year. The dates of every LiDAR and echo sounder measurement are presented in Table A.1 and A.3.

B.1. Dune and beach volume changes per unit width per measurement interval

Figure B.1 presents the changes in sediment volume in the dunes per measurement interval, and B.2 the volume changes at the beach. The changes in sediment volume are scaled to $m^3/m/y$.

Dune growth

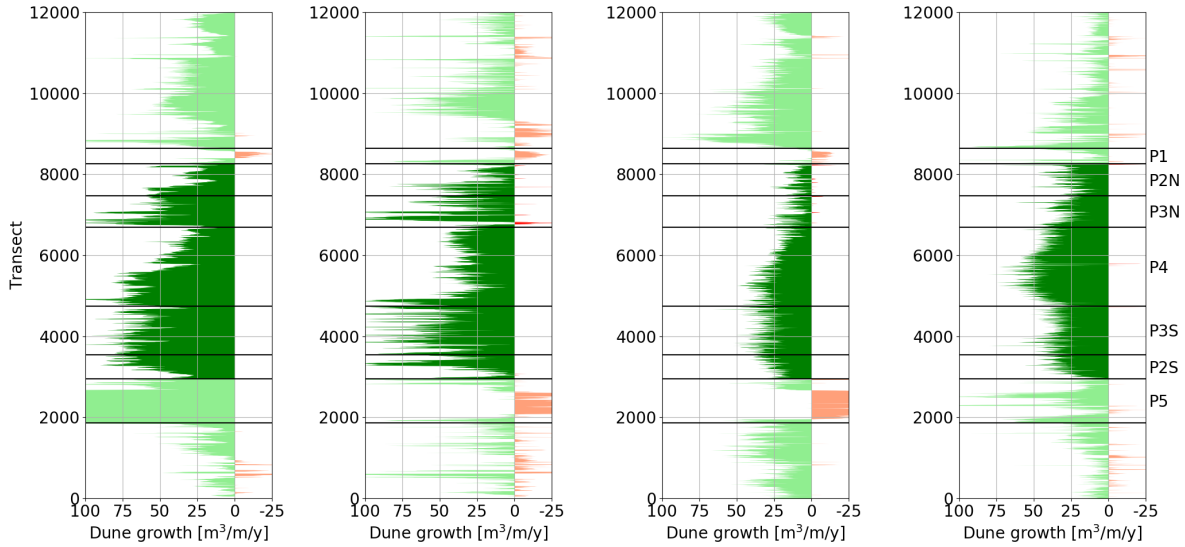

(a) May 24, 2015 to December 28, 2015

(b) December 28, 2015 to March 21, 2016

(c) March 21, 2016 to September 1, 2016

(d) September 1, 2016 to December 5, 2016

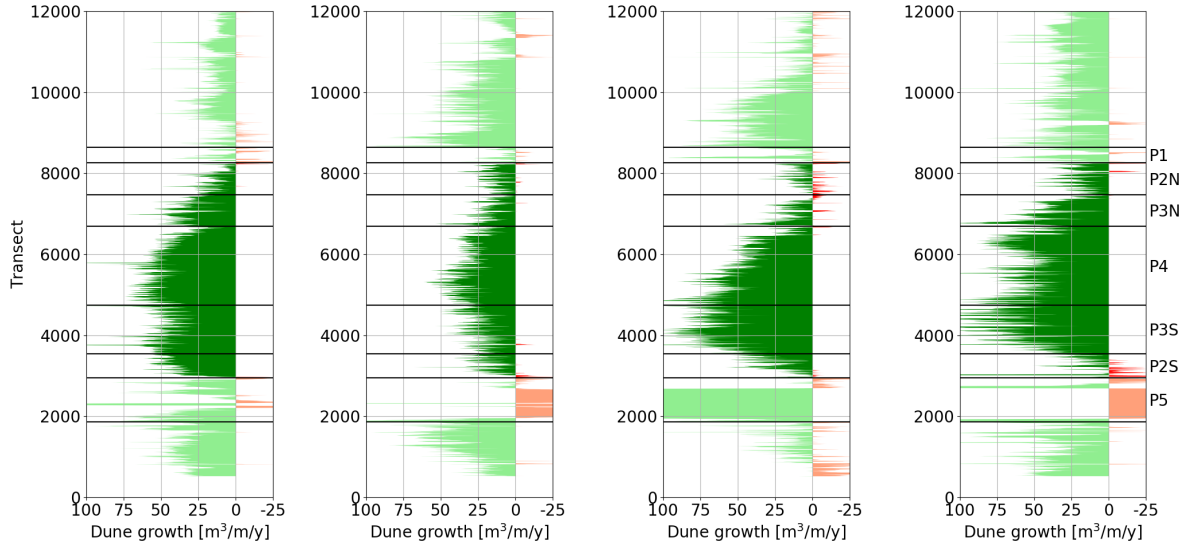

(e) December 5, 2016 to April 19, 2017

(f) April 19, 2017 to August 11, 2017

(g) August 11, 2017 to December 6, 2017

(h) December 6, 2017 to March 19, 2018

Figure B.1: Dune volume changes per unit width of every measurement interval between May 25, 2015 and March 19, 2018, based on LiDAR measurements

Beach growth

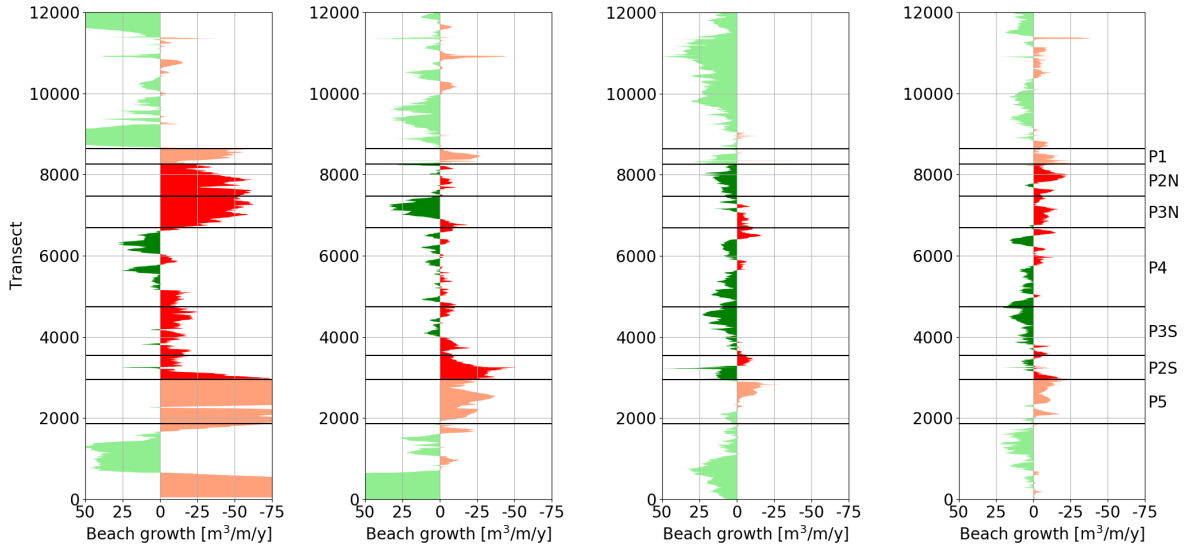

(a) May 24, 2015 to December 28, 2015

(b) December 28, 2015 to March 21, 2016

(c) March 21, 2016 to September 1, 2016

(d) September 1, 2016 to December 5, 2016

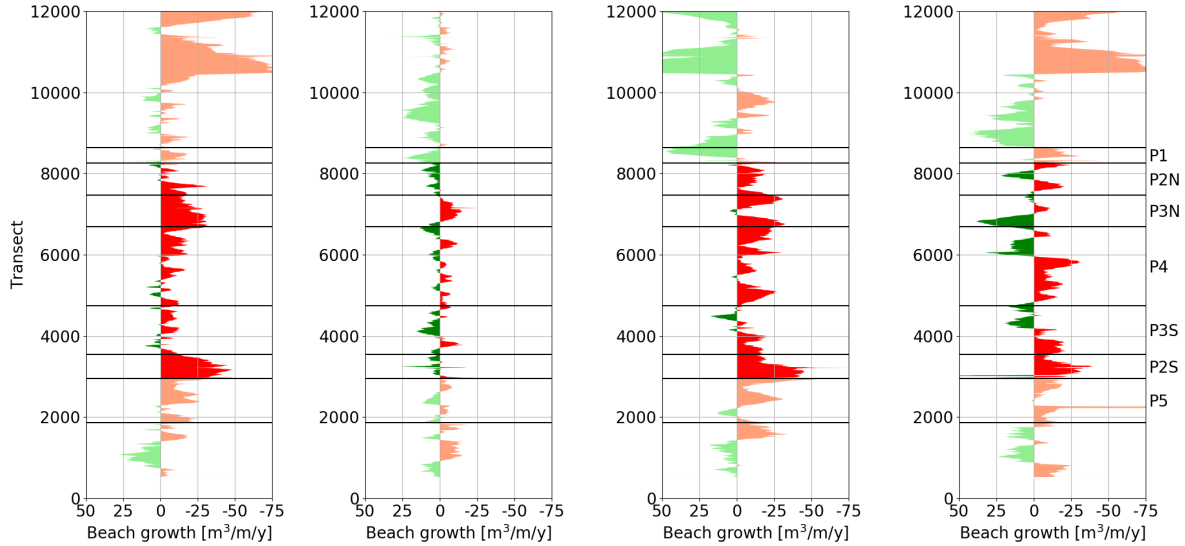

(e) December 5, 2016 to April 19, 2017

(f) April 19, 2017 to August 11, 2017

(g) August 11, 2017 to December 6, 2017

(h) December 6, 2017 to March 19, 2018

Figure B.2: Beach volume changes per unit width of every measurement interval between May 25, 2015 and March 19, 2018, based on LiDAR measurements

B.2. Volume changes of cross-shore zones per unit width per year

This section presents the changes in sediment volume in the dunes, beach, intertidal zone, shoreface and offshore zone for every year since construction of the HD.

Dune growth

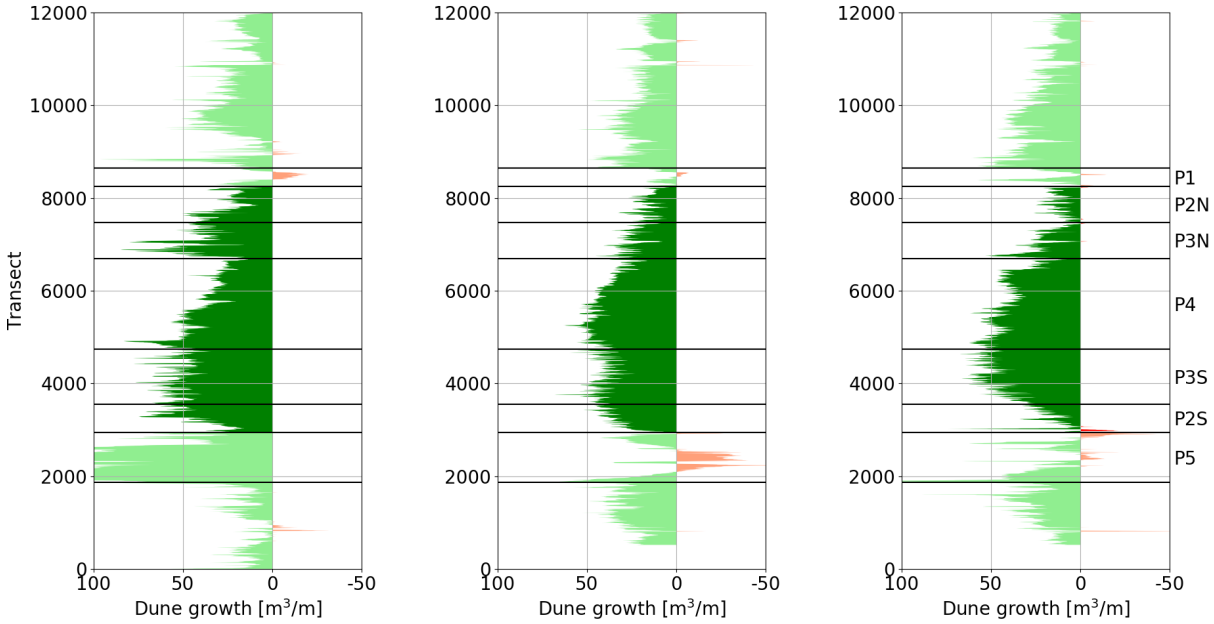

(a) Year 1 (b) Year 2 (c) Year 3

Figure B.3: Dune volume changes per unit width of every year since construction, based on LiDAR measurements

Beach growth

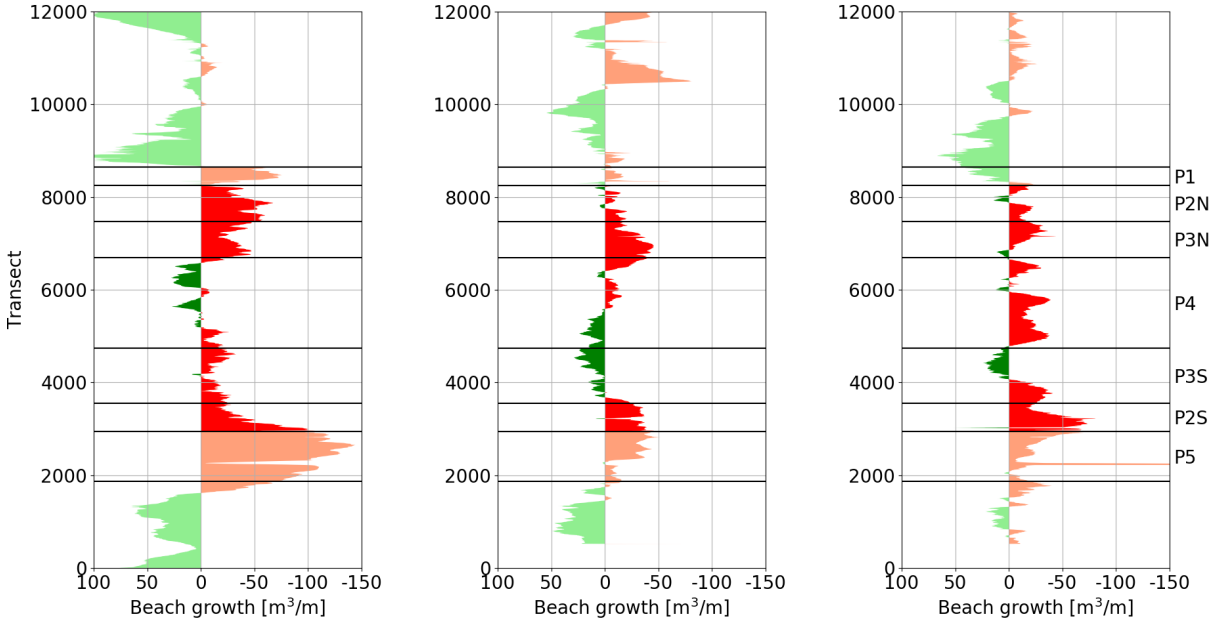

(a) Year 1 (b) Year 2 (c) Year 3

Figure B.4: Beach volume changes per unit width of every year since construction, based on LiDAR measurements

Intertidal zone growth

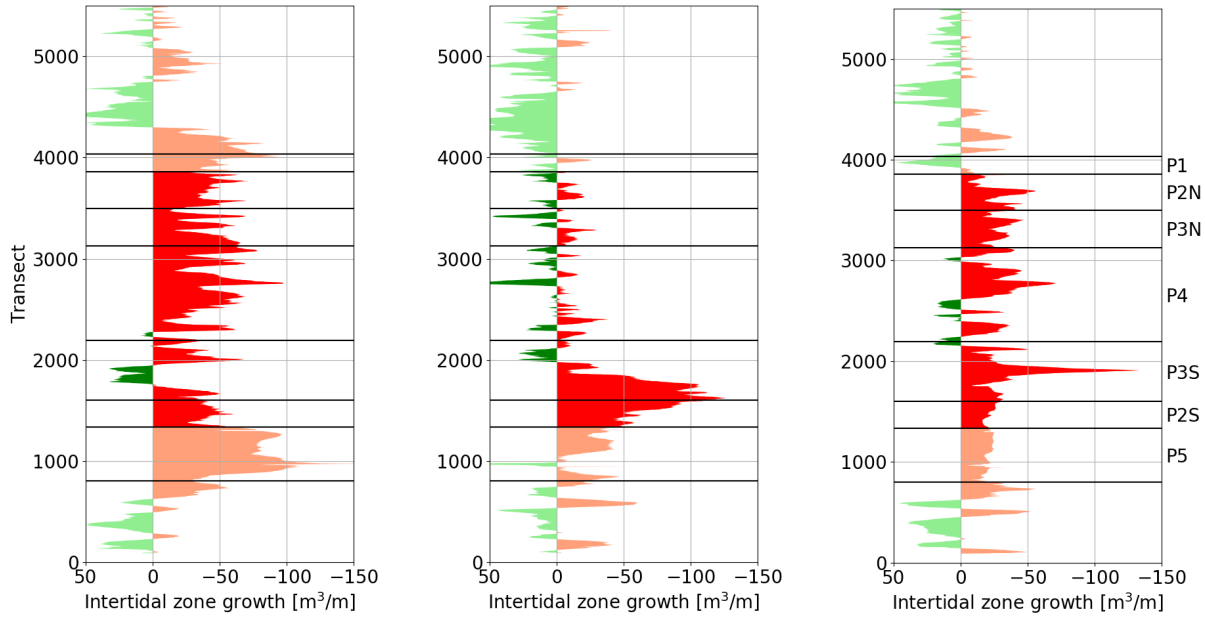

(a) Year 1 (b) Year 2 (c) Year 3

Figure B.5: Intertidal zone volume changes per unit width of every year since construction, based on echo sounder measurements

Shoreface growth

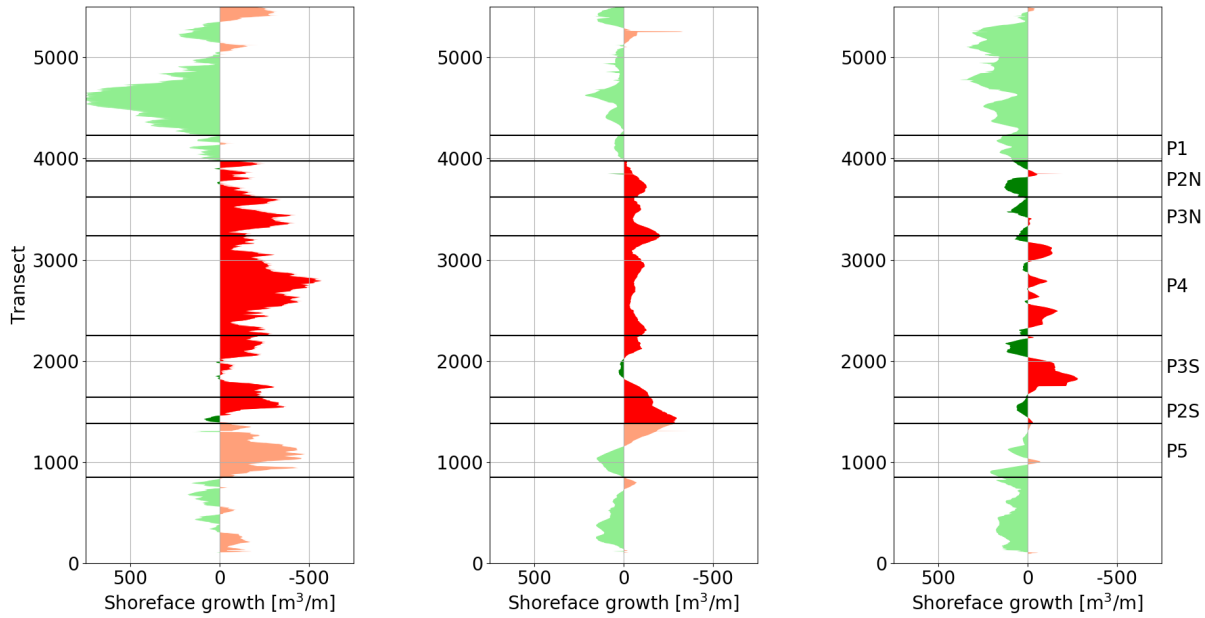

(a) Year 1 (b) Year 2 (c) Year 3

Figure B.6: Shoreface volume changes per unit width of every year since construction, based on echo sounder measurements

Offshore zone growth

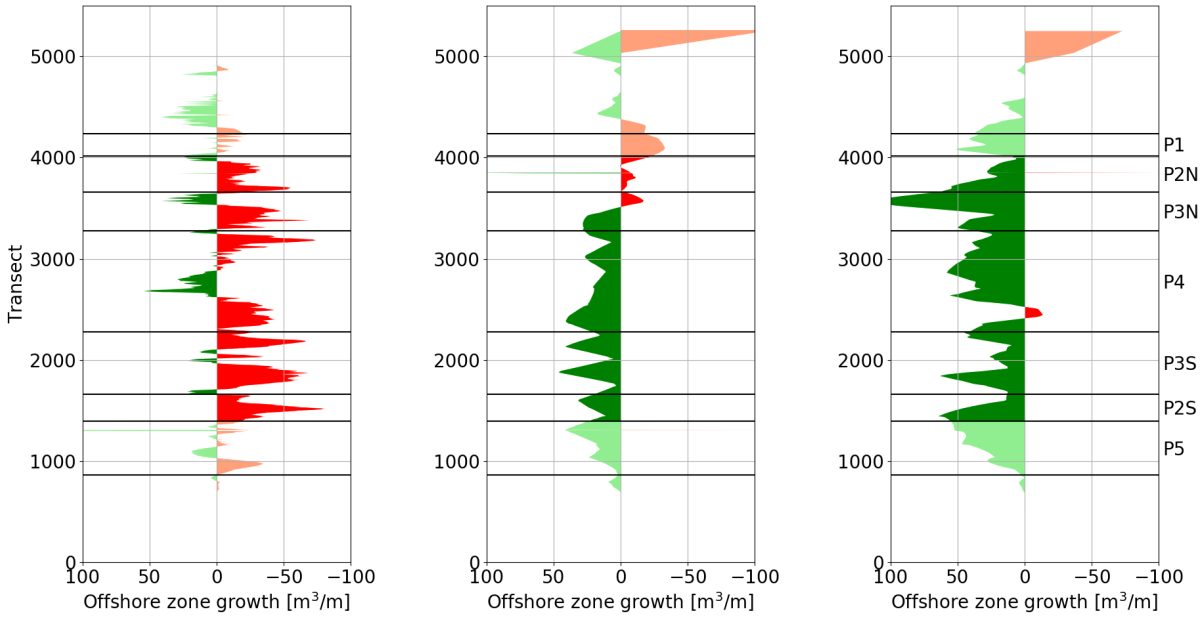

(a) Year 1 (b) Year 2 (c) Year 3

Figure B.7: Offshore zone volume changes per unit width of every year since construction, based on echo sounder measurements

B.3. Sediment transport rate from the shoreface to the intertidal zone per year

Figure B.8 shows the sediment transport rate from the shoreface to the intertidal zone for every year since construction of the HD. Figure B.10 shows the relation between the sediment transport rate from the shoreface to the intertidal zone and the offshore wave height of the smallest wave that will break on top of the sandbar for each year. Figure B.10 shows the relation between this transport rate the dune growth. The direct relation between the offshore wave height of the smallest wave that will break on top of the sandbar and dune growth for each year is presented in Figure B.11.

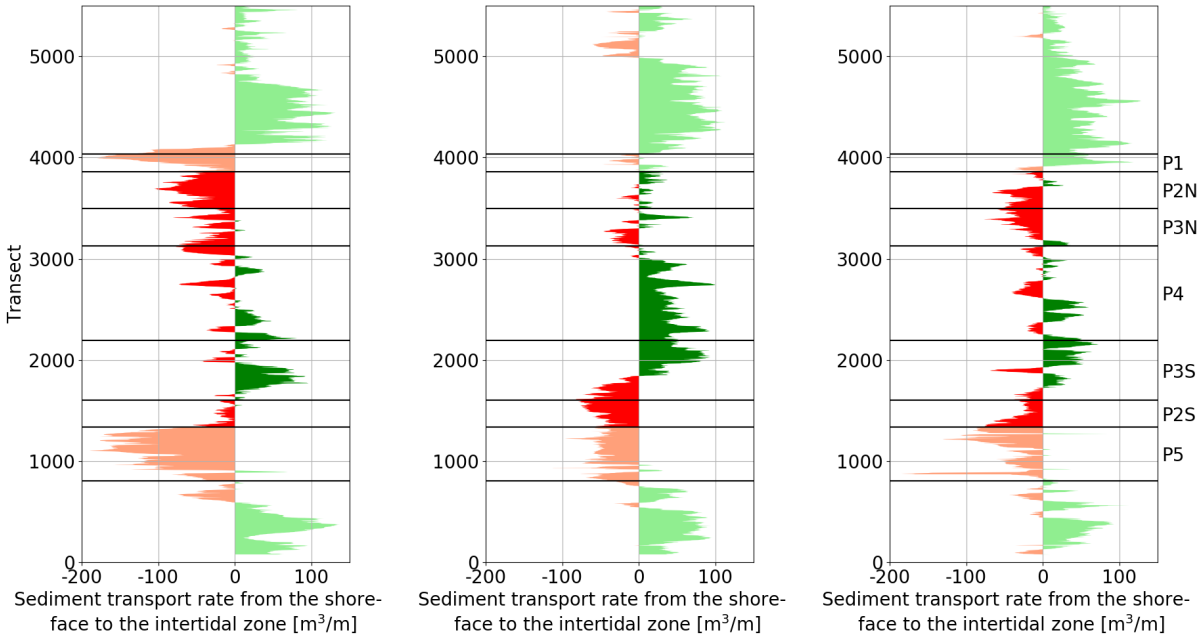

(a) Year 1 (b) Year 2 (c) Year 3

Figure B.8: Sediment transport rate from the shoreface to the intertidal zone per unit width of every year since construction, based on LiDAR and echo sounder measurements. Positive values correspond to landward and negative values to seaward sediment transport.

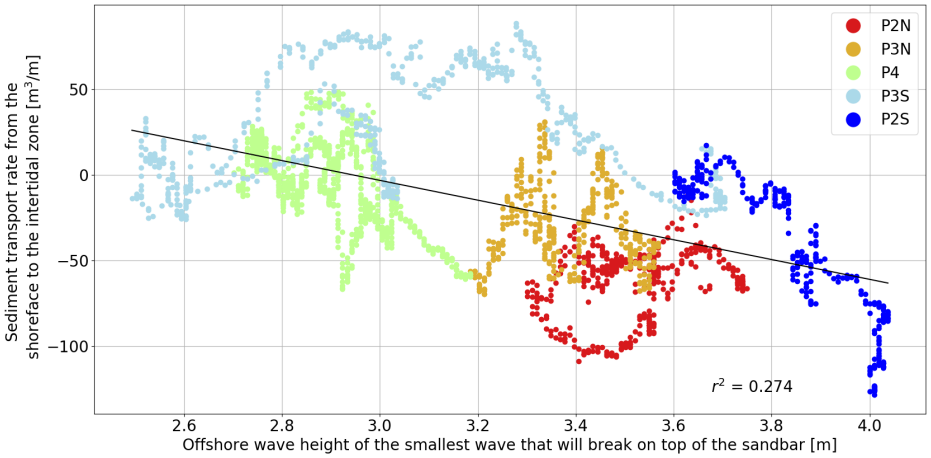

(a) Year 1

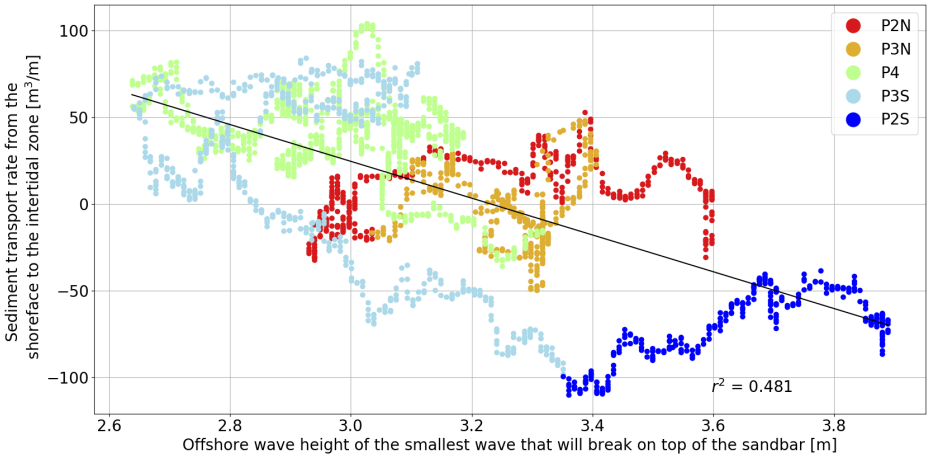

(b) Year 2

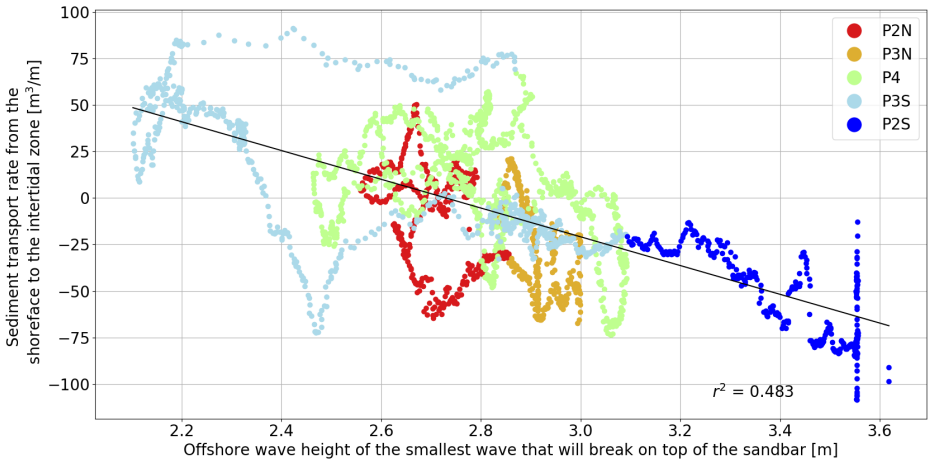

(c) Year 3

Figure B.9: Sediment transport rate from the shoreface to the intertidal zone of the first three years since construction of every longshore meter depending on the offshore wave height of the smallest wave that will break on top of the sandbar

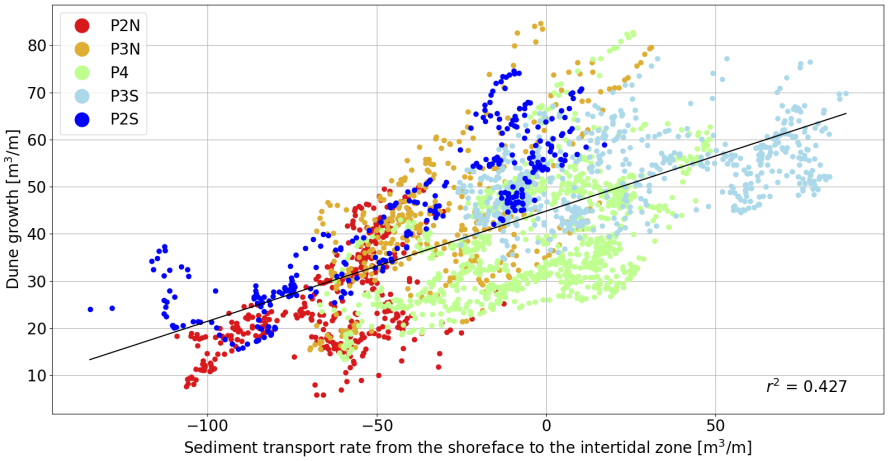

(a) Year 1

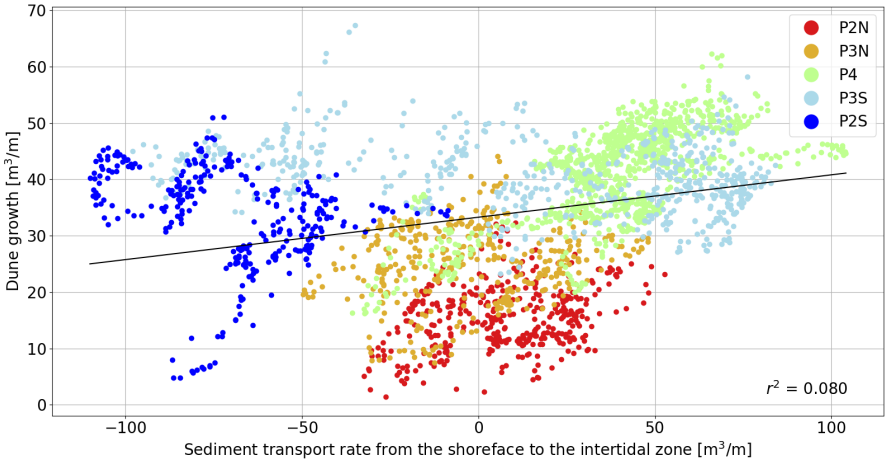

(b) Year 2

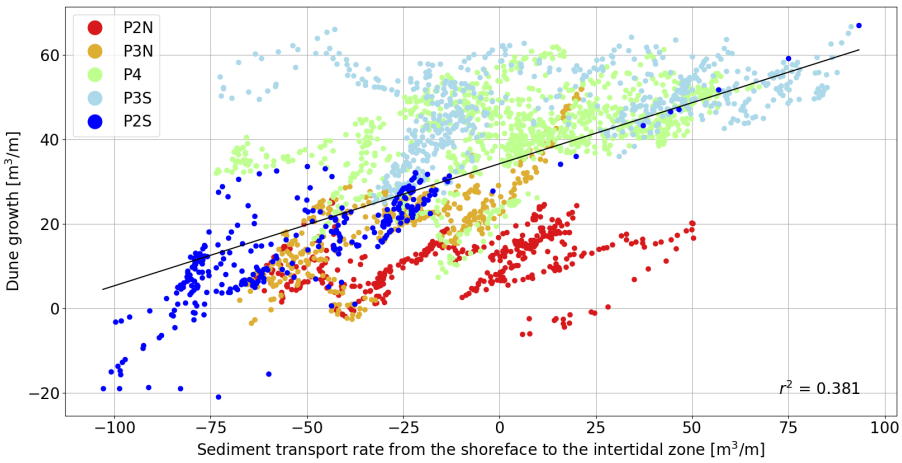

(c) Year 3

Figure B.10: Dune growth of the first three years since construction of every longshore meter depending on the sediment transport rate from the shoreface to the intertidal zone

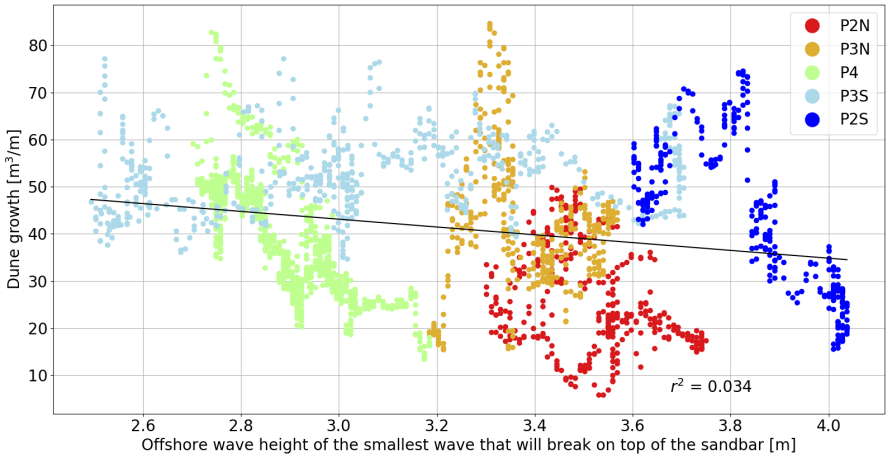

(a) Year 1

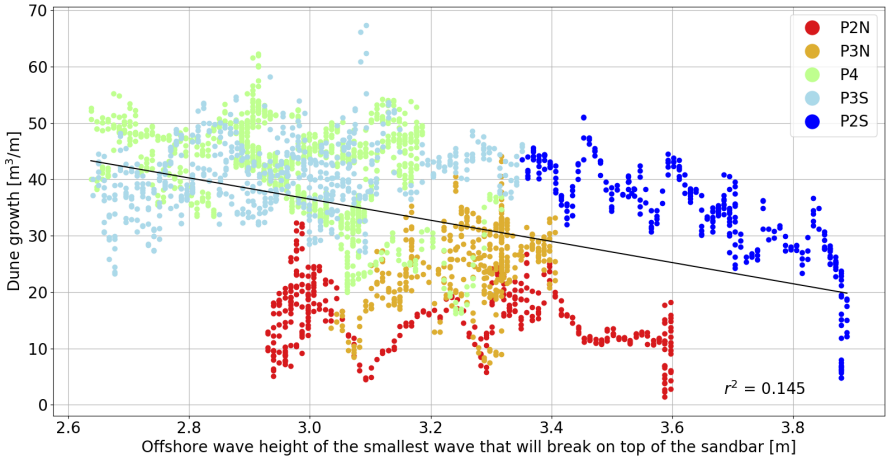

(b) Year 2

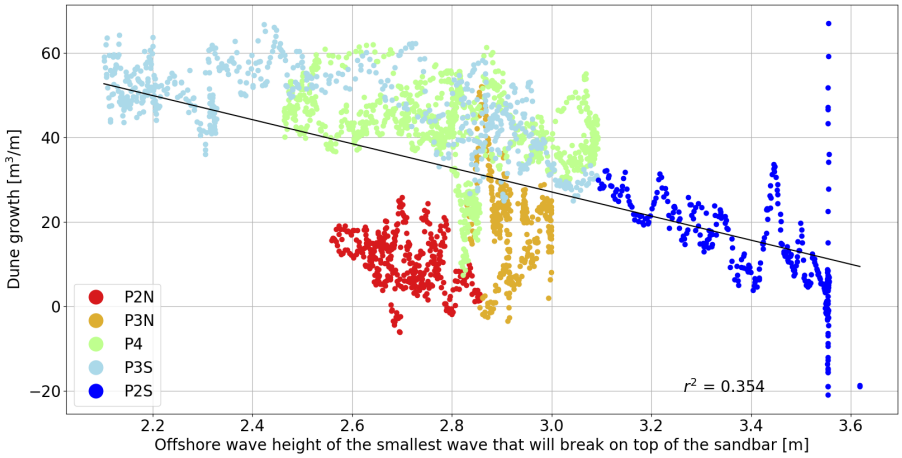

(c) Year 3

Figure B.11: Dune growth of the first three years since construction of every longshore meter depending on the offshore wave height of the smallest wave that will break on top of the sandbar

B.4. Longshore sediment transport rate per year

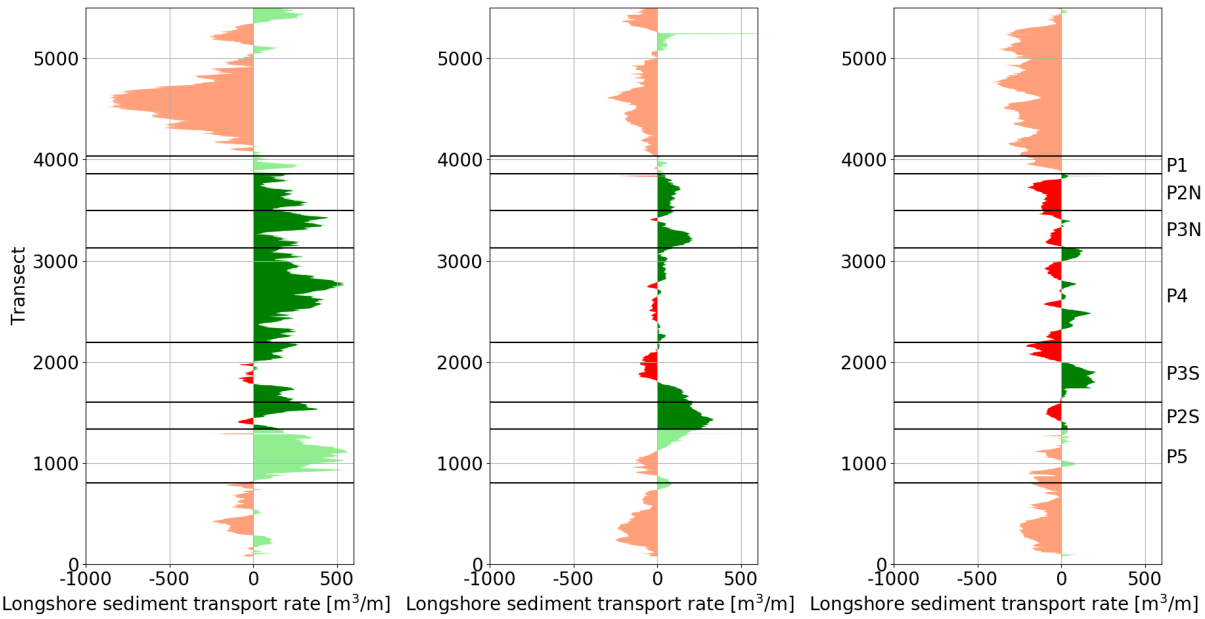

(a) Year 1 (b) Year 2 (c) Year 3

Figure B.12: Longshore sediment transport rate per unit width of every year since construction, based on LiDAR and echo sounder measurements. Positive values correspond to northward and negative values to southward sediment transport.

B.5. Sediment balance per year

This section gives the sediment balances for the first, second and third year since construction of the HD. These balances contain the volume changes of the dunes, beach, intertidal zone, shoreface and offshore zone, as well as net longshore and cross-shore sediment transport rates. The volume changes of the beach and dunes are based on LiDAR measurements. Volume changes of the offshore zone, shoreface and intertidal zone are based on echo sounder measurements.

Year 1

Table B.1: Volume changes of every domain for each profile type between May 2015 and April 2016

	Change in sediment volume (10^3 m^3)				
Profile	Offshore zone	Shoreface	Intertidal zone	Beach	Dunes
P2N	-14	-101	-32	-34	20
P3N	-10	-165	-32	-26	34
P4	-24	-530	-71	6	77
P3S	-31	-163	-15	-18	63
P2S	-19	-78	-27	-27	26
HD	-97	-1,037	-177	-100	220

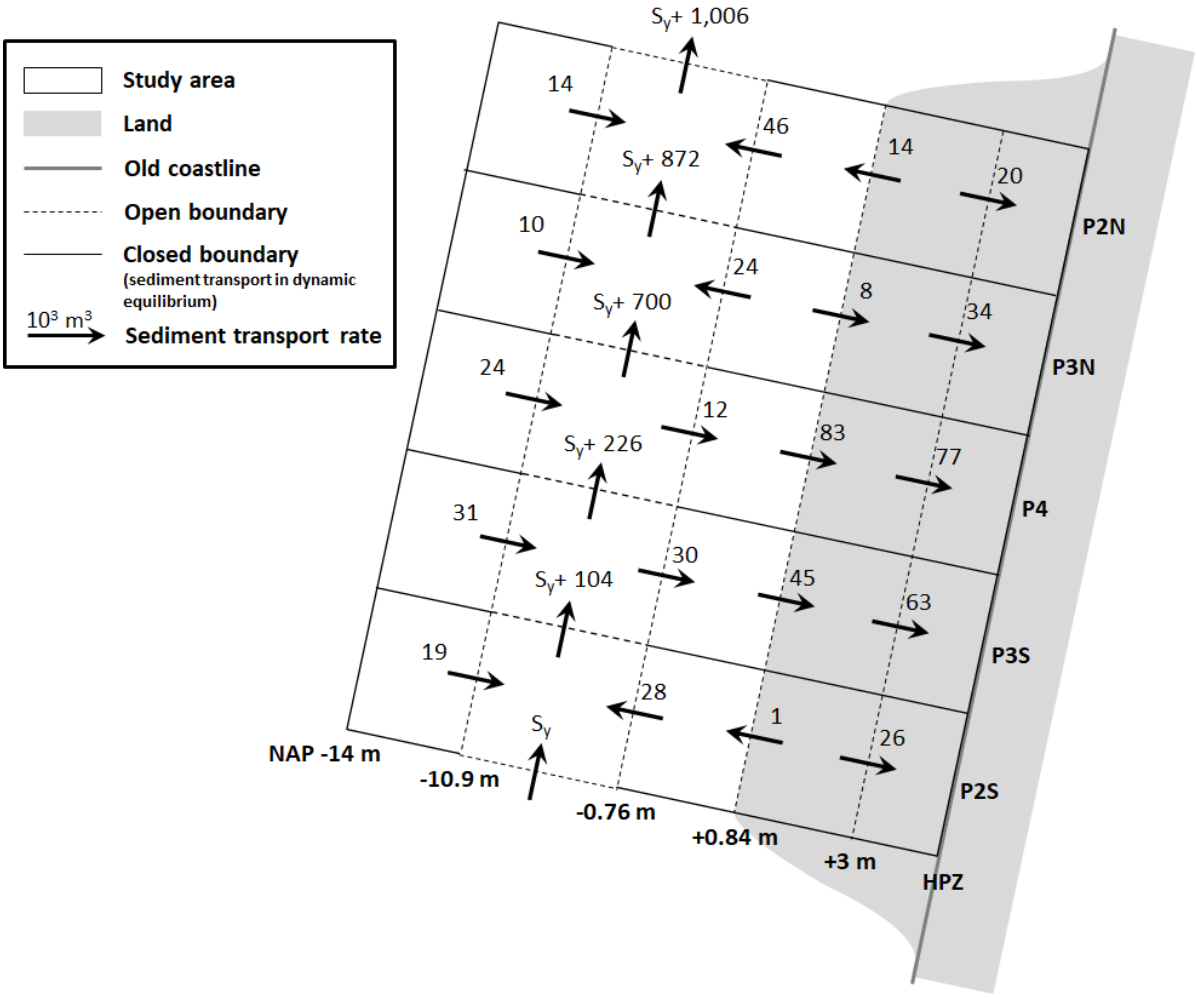

Figure B.13: Net sediment transport rates between May 2015 and April 2016. The black numbers correspond to 1000 m^3 of sediment.

Year 2

Table B.2: Volume changes of every domain for each profile type between April 2016 and April 2017

Profile	Change in sediment volume (10^3 m^3)				
	Offshore zone	Shoreface	Intertidal zone	Beach	Dunes
P2N	-4	-68	-1	-6	12
P3N	9	-78	0	-24	20
P4	45	-152	8	-2	81
P3S	28	-57	-48	11	49
P2S	14	-134	-37	-19	20
HD	91	-489	-78	-40	181

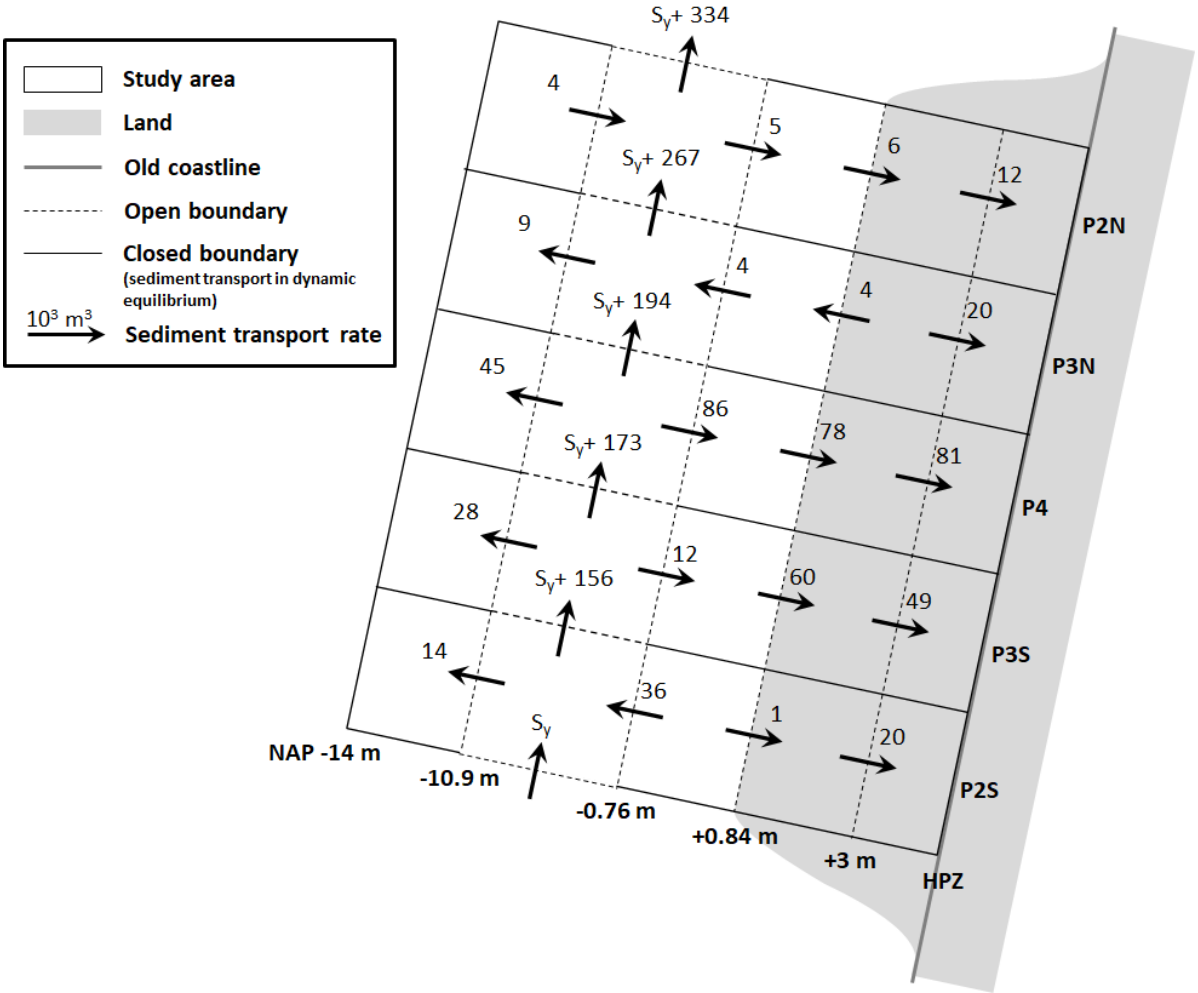

Figure B.14: Net sediment transport rates between April 2016 and April 2017. The black numbers correspond to 1000 m^3 of sediment.

Year 3

The nourishment constructed in March 2018 has affected the volume changes in P2S, because the latest echo sounder measurement was executed after construction of this nourishment. The sediment transport rates in the volume balance are therefore supplemented with a sediment transport rate S_n. For simplicity, this value is only added to the intertidal zone of P2N. The transport rate includes the nourished volume within the intertidal zone and shoreface of the study area, as well as the volume losses between the construction date and the measurement date.

The nourished volume within the intertidal zone and shoreface of the study area is roughly 210,000 m^3. The losses after construction are estimated at 40,000 m^3, based on the volume losses between April 13, 2018 and May 14, 2018 (M.O. Enschedé, personal communication, November 22, 2018). The additional sediment transport S_n is 250,000 m^3. The sediment loss through longshore transport is approximately 78,000 m^3.

Table B.3: Volume changes of every domain for each profile type between April 2017 and April 2018

	Change in sediment volume (10^3 m^3)				
Profile	Offshore zone	Shoreface	Intertidal zone	Beach	Dunes
P2N	25	56	-20	-7	9
P3N	47	17	-21	-11	16
P4	66	-85	-32	-33	81
P3S	34	-118	-25	-6	57
P2S	26	60	70-S_n	-27	9
HD	198	-69	-28-S_n	-84	172

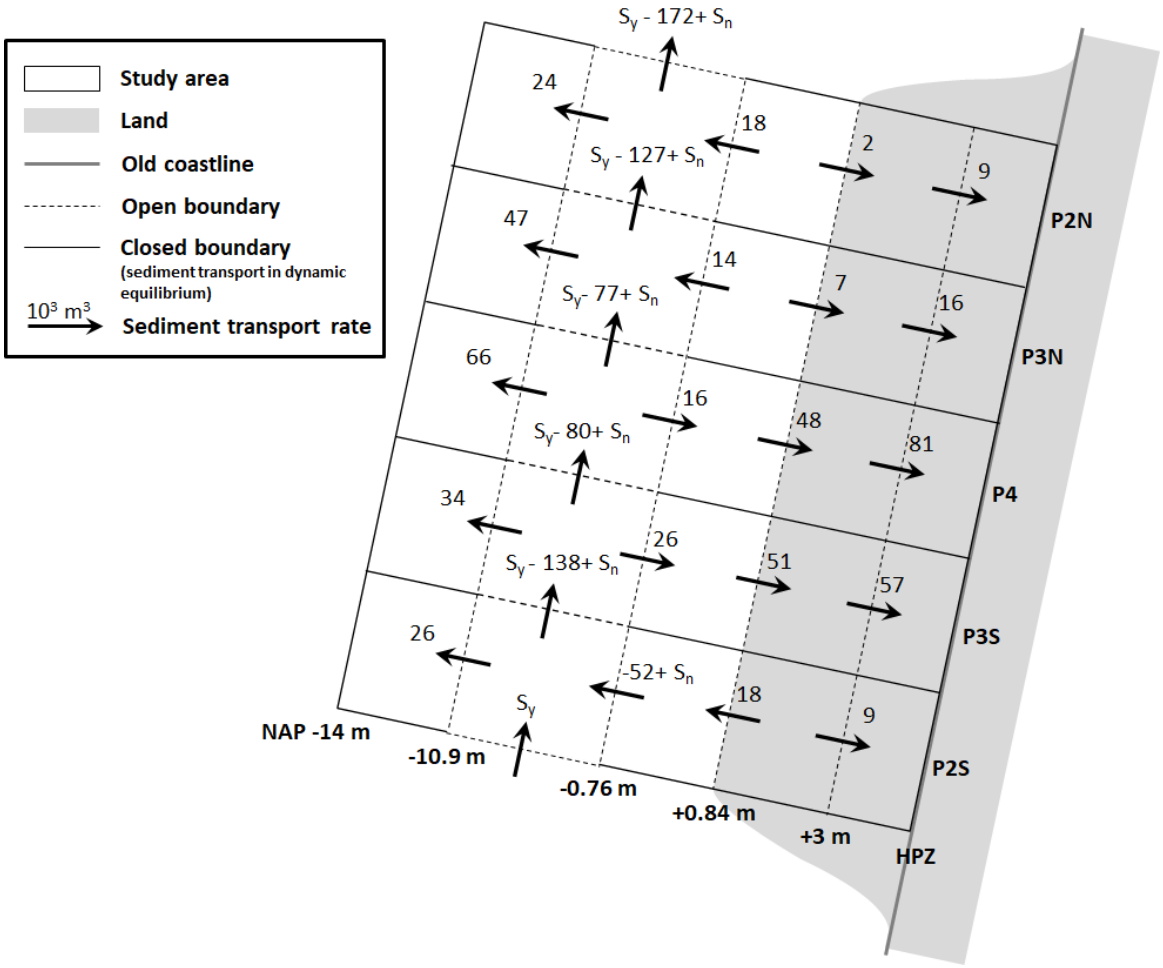

Figure B.15: Net sediment transport rates between April 2017 and April 2018. The black numbers correspond to 1000 m^3 of sediment.

C

Maps of bed level differences

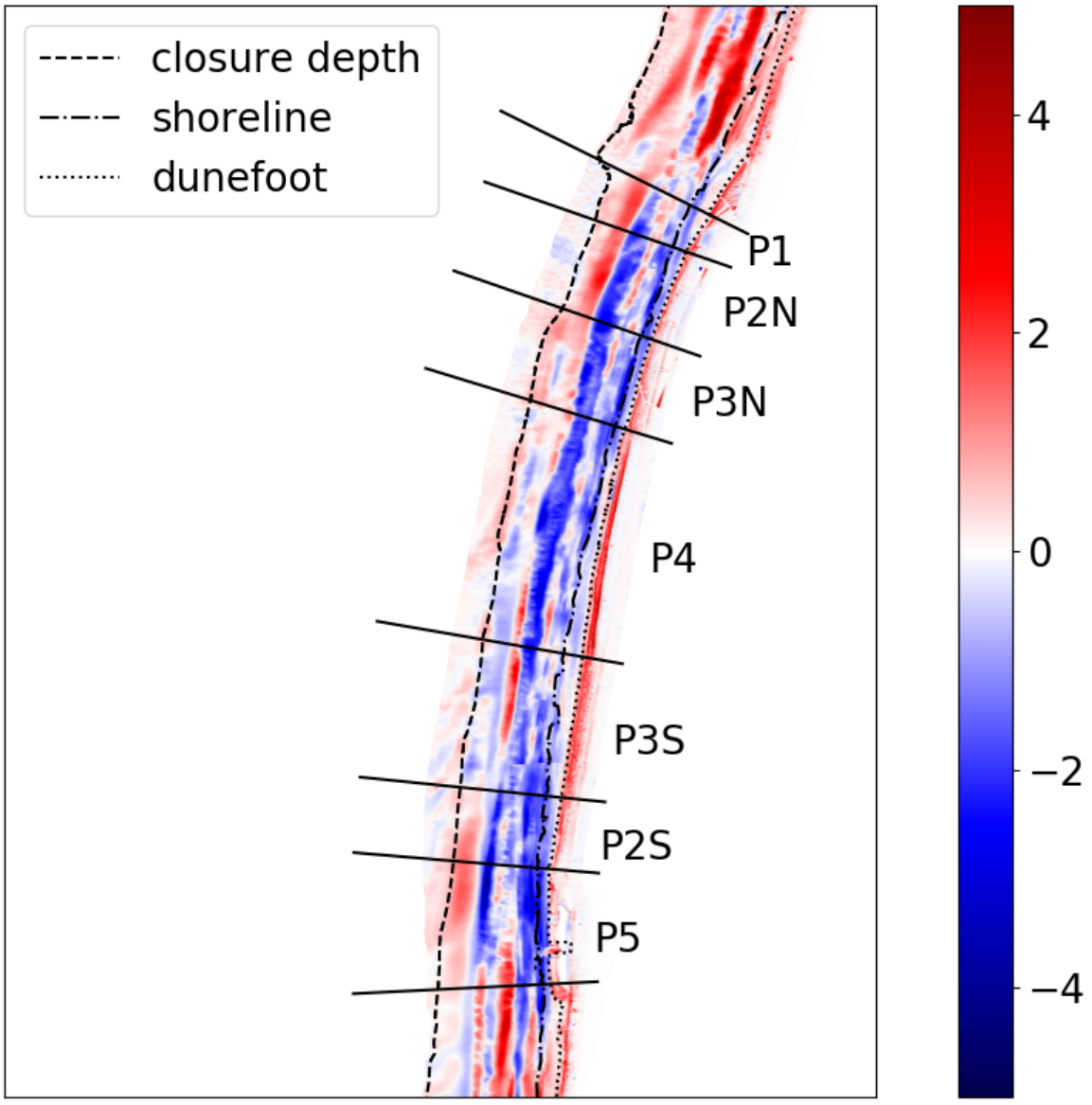

Figure C.1: Bed level difference of the HD between May 2015 and April 2018, based on LiDAR and echo sounder measurements.

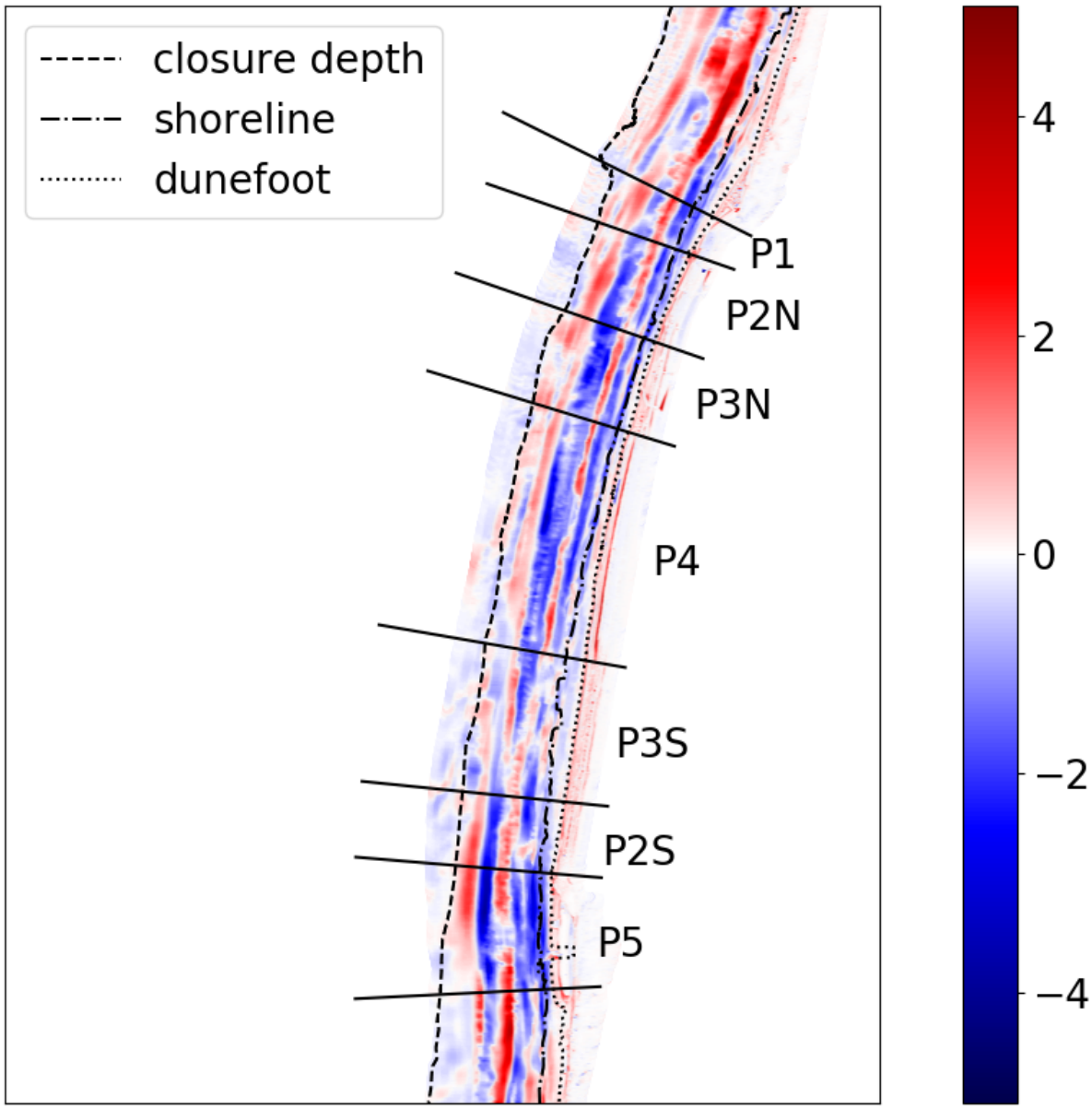

Figure C.2: Bed level difference of the HD between May 2015 and April 2016, based on LiDAR and echo sounder measurements.

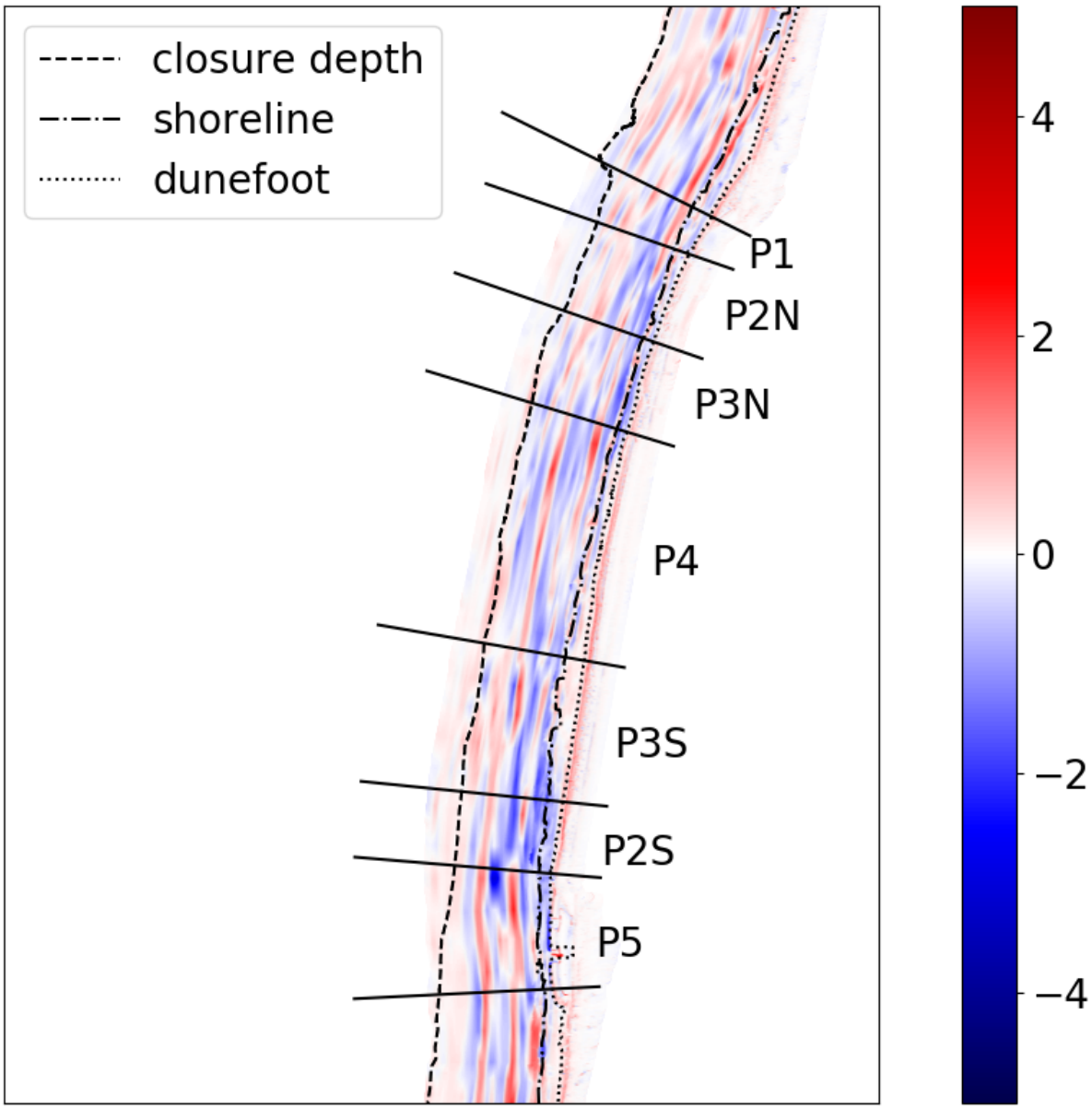

Figure C.3: Bed level difference of the HD between April 2016 and April 2017, based on LiDAR and echo sounder measurements.

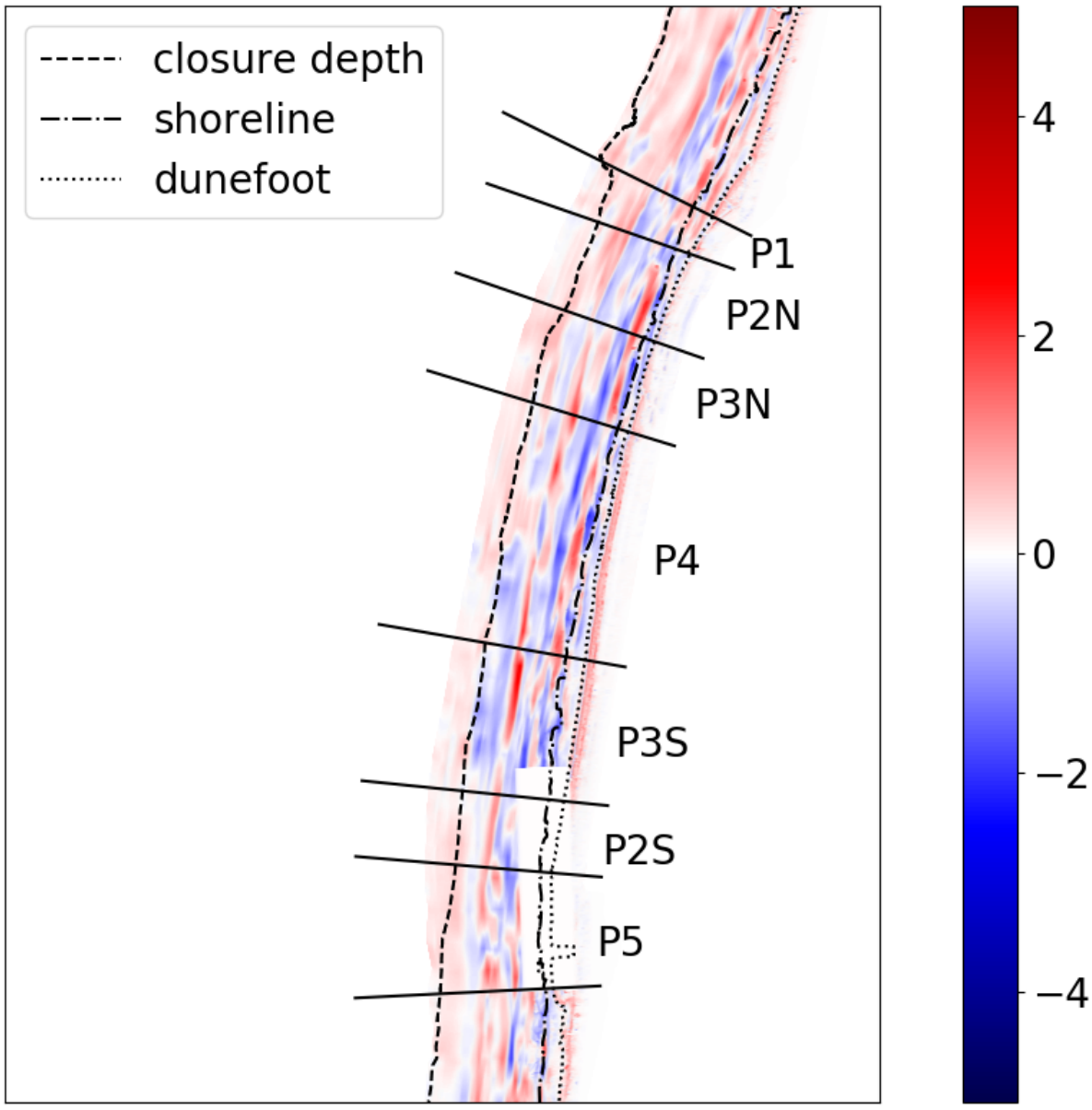

Figure C.4: Bed level difference of the HD between April 2017 and April 2018, based on LiDAR and echo sounder measurements.

D

Additional nourishment 2018

The total nourished volume was 920,000 m^3. Sediment losses during construction were approximately zero as a result of calm weather conditions (P.G.F. Brandenburg, personal communication, November 22, 2018).

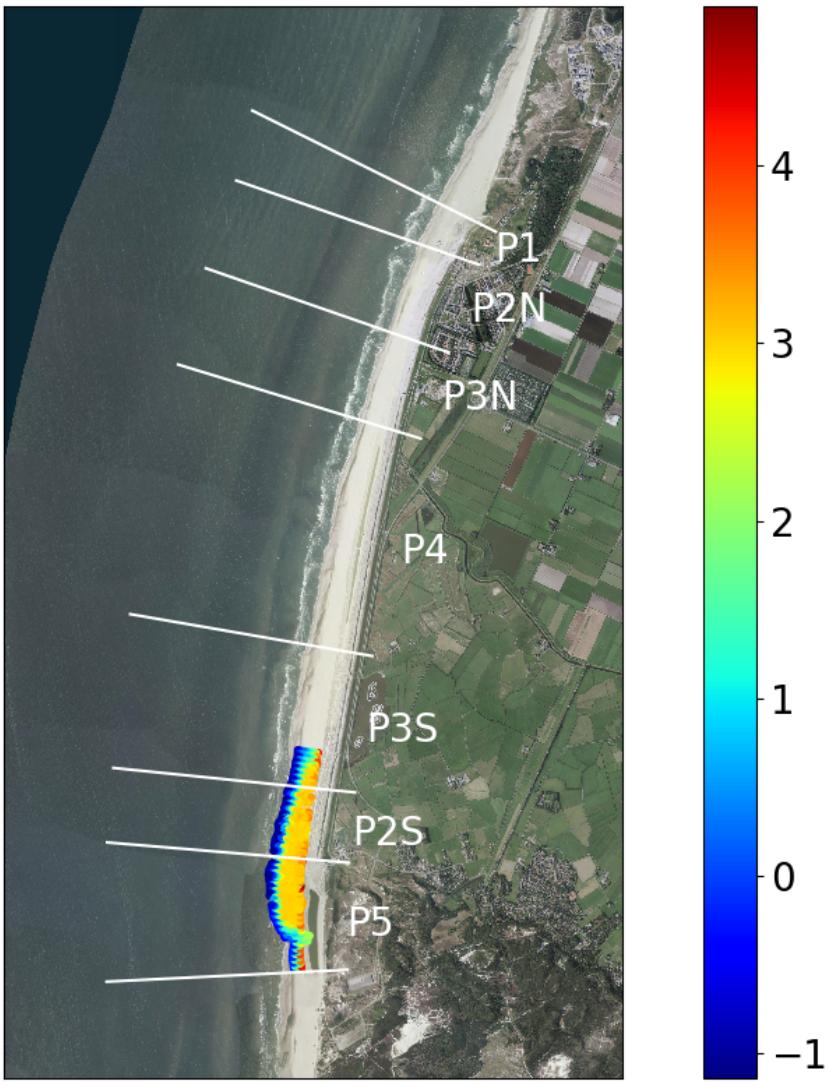

Figure D.1: Location and topography of the additional nourishment constructed in March 2018

E

AeoLiS model description

(This chapter is based on Hoonhout (2018))

The modelling study is done with AeoLiS: a process-based numerical model that simulates aeolian sediment transport. This appendix gives a descriptions of the numerical implementations in this model.

AeoLiS focusses on aeolian sediment transport under supply-limiting factors, like in coastal environments. These supply-limiting factors are soil moisture contents, sediment sorting and armouring, bed slope effects, air humidity and roughness elements.

The model computes spatiotemporal varying sediment availability. For this purpose, the domain is divided into horizontal grid cells and vertical layers (2DV). Moreover, the grain size distribution is divided into fractions, which allows for a horizontal and vertical distribution of grain sizes. A bed composition module is used to compute the sediment availability for each sediment fraction individually. AeoLiS uses existing model concepts, like the shear velocity threshold (equation 2.7) and critical fetch.

E.1. Transport equation

AeoLiS solves a 1DH advection equation for the instantaneous sediment mass per unit area c (in kg/m^2), see the equation below:

$$\frac{\partial c}{\partial t} + u_z \frac{\partial c}{\partial x} = E - D \tag{E.1}$$

where:

E	Erosion terms
D	Deposition terms

While denoted as a sediment concentration c, AeoLiS actually computes the sediment mass per unit area $z_a \cdot c$, where z_a is the height where aeolian sediment is transported. For conciseness, the sediment mass per unit area is still referred to as c. The net entrainment is based on the balance between the equilibrium sediment concentration c_{eq} and the instantaneous sediment concentration c. This balance is limited by the available sediment in the bed m_a:

$$E - D = \min\left(\frac{\partial m_a}{\partial t} \;;\; \frac{c_{eq} - c}{T_a}\right) \tag{E.2}$$

where:

m_a	Available sediment in the bed
T_a	Adaptation time scale

The adaptation time scale is assumed equal for erosion and deposition ($T \approx 1$ s for aeolian transport). The saturated or equilibrium sediment concentration c_{eq} is obtained by dividing the equilibrium sand flow S_{eq} (from equation 2.8) by u_z. The sediment concentration is by definition non-negative, see equation E.3. The factor $\sqrt{d_n/D_n}$ is excluded in this equation, because sediment sorting is already accounted for through the weighting factors (as described below).

$$c_{eq} = \max\left(0 \;;\; \alpha C \frac{\rho_a}{g} \frac{(u_z - u_c)^3}{u_z}\right) \tag{E.3}$$

E.2. Multiple sediment fractions

For multiple sediment fractions, the net entrainment is calculated for every sediment fraction, which is denoted by the sediment fraction index k. The equilibrium sediment concentration for every fraction is modified by a weighting factor $\hat{w}$, as explained in section 2.2.2:

$$E_k - D_k = \min\left(\frac{\partial m_{a,k}}{\partial t} \;;\; \frac{\hat{w}_k \cdot c_{eq,k} - c_k}{T_a}\right) \tag{E.4}$$

where:

$\hat{w}$	Weighting factor
$()_k$	For sediment fraction k

It is common to use the grain size distribution of the bed as a weighting factor for the equilibrium sediment concentration. This approach assumes, in case of erosion, that all sediment at the bed surface is equally exposed to the wind. In case of deposition, the weighting factor for the equilibrium sediment concentration depends on both the grain size distribution in the air and at the bed surface, due to the nature of saltation in which continuous action between grains takes place. A bed interaction parameter ζ denotes the ratio between these grain size distributions. The weighting of erosion and deposition of individual fractions is computed according to:

$$\hat{w}_k = \frac{w_k}{\sum_{k=1}^{n_k} w_k} \tag{E.5}$$

and:

$$w_k = (1-\zeta)\, w_k^{air} + (1-\hat{S}_k)\, w_k^{bed} \tag{E.6}$$

where:

w	Unnormalised weighting factor
n_k	Number of sediment fractions
ζ	Bed interaction parameter
w^{air}	Weighting factor based on the grain size distribution in the air
w^{bed}	Weighting factor based on the grain size distribution on the bed
$\hat{S}$	Effective sediment saturation of the air

The weighting factors based on the grain size distribution in the air and on the bed are computed using mass ratios:

$$w_k^{air} = \frac{c_k}{c_{eq,k}} \quad ; \quad w_k^{bed} = \frac{m_{a,k}}{\sum_{k=1}^{n_k} m_{a,k}} \tag{E.7}$$

The sum of the ratio w_k^{air} over the fractions denotes the degree of saturation of the air column for fraction k, which determines if erosion of a fraction may occur. Also, in saturated situations, erosion of a sediment fraction can occur due to an exchange of momentum between sediment fractions, which is represented by ζ. The effective degree of sediment saturation is therefore also influenced by the bed interaction parameter and defined as:

$$\hat{S}_k = \min\left(1 \;;\; (1-\zeta) \cdot \sum_{k=1}^{n_k} w_k^{air}\right) \tag{E.8}$$

When the effective saturation is greater than or equal to one, the air is (over)saturated and no erosion occurs. Consequently, the grain size distribution in the bed is less relevant. In case the effective saturation is less than one, erosion may occur and the grain size distribution of the bed also contributes to the weighting over the sediment fractions. The weighting factors for erosion are then composed of both the grain size distribution in the air and the grain size distribution at the bed surface.

For example, if bed interaction is disabled ($\zeta = 0$) and the air is 70% saturated, then the grain size distribution in the air contributes 70% to the weighting factors for erosion, while the grain size distribution in the bed contributes the other 30%, see the upper left panel of Figure E.1. A bed interaction value of $\zeta = 0.2$ represents the situation in which the grain size distribution at the bed surface contributes 20% to the weighting of the saturated sediment concentration over the fractions. In the example situation where the air is 70% saturated such value for the bed interaction parameter would lead to weighting factors that are constituted for 70% · (100% - 20%) = 56% based on the grain size distribution in the air and for the other 44% based on the grain size distribution at the bed surface, see the upper right panel of Figure E.1.

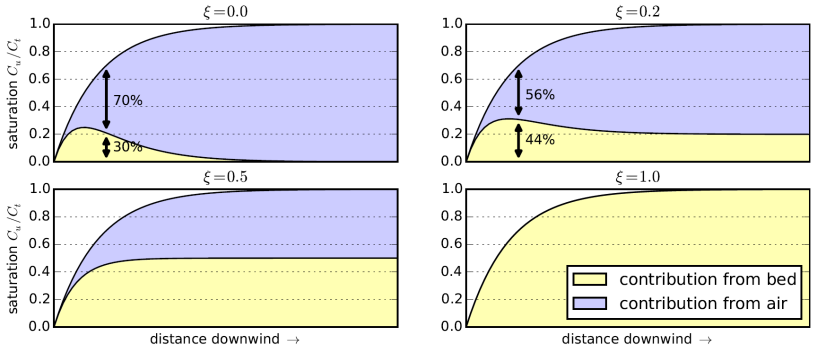

Figure E.1: Contributions of the grain size distribution in the air and on the bed to the weighting factor $\hat{w}_k$ for different values of the bed interaction parameter (Hoonhout, 2018)

E.3. Bed composition

Because the instantaneous sediment concentration c_k is computed for each sediment fraction individually, grain size distributions may vary over the model domain and in time, as explained in section 2.2.2. In order to allow the model to simulate the processes of sediment sorting and beach armouring, the bed is discretised in horizontal grid cells and vertical bed layers (2DV), see Figure E.2. This figure also presents a schematic overview of the bed composition discretisation.

Each grid cell consists of a minimum of three layers with a constant thickness. The top layer is the bed surface layer. It is the only layer that interacts with the wind and, therefore, sediment can only enter or leave the grid cell through this layer. It is also the only layer that determines to the spatiotemporal variety in sediment availability and the contribution of the grain size distribution on the bed to the weighting of the equilibrium sediment concentration. Underneath the bed surface layer, one or more bed composition layers are located. The bottom layer is the base layer and contains an infinite amount of erodible sediment according to the initial grain size distribution. The base layer cannot be eroded but can supply sediment to the other layers. Figure E.2 gives a schematic overview of these layers.

The detail in Figure E.2 shows the discretisation of the grain size distribution to a predefined number of sizes. Since the velocity threshold depends, among others, on the grain size, erosion from the bed surface layer tends to erode fines more easily than coarse sediment, see the top left panel of the detail in Figure E.2. If sediment is eroded from the bed surface layer, it is repleted with sediment from the bed composition layers. This repleted sediment has the same grain size distribution as that of the bed composition layer, see the bottom left panel of the detail in Figure E.2. If relatively more fines are eroded from the bed surface layer, this results in coarsening of that layer.

In case of deposition, the process is similar. Sediment is deposited in the bed surface layer, which then passes its excess sediment to the lower bed layers, see the upper and lower right panel of the detail in Figure E.2.

If more fines are deposited than passed to the lower bed composition layers, the bed surface layer becomes finer.

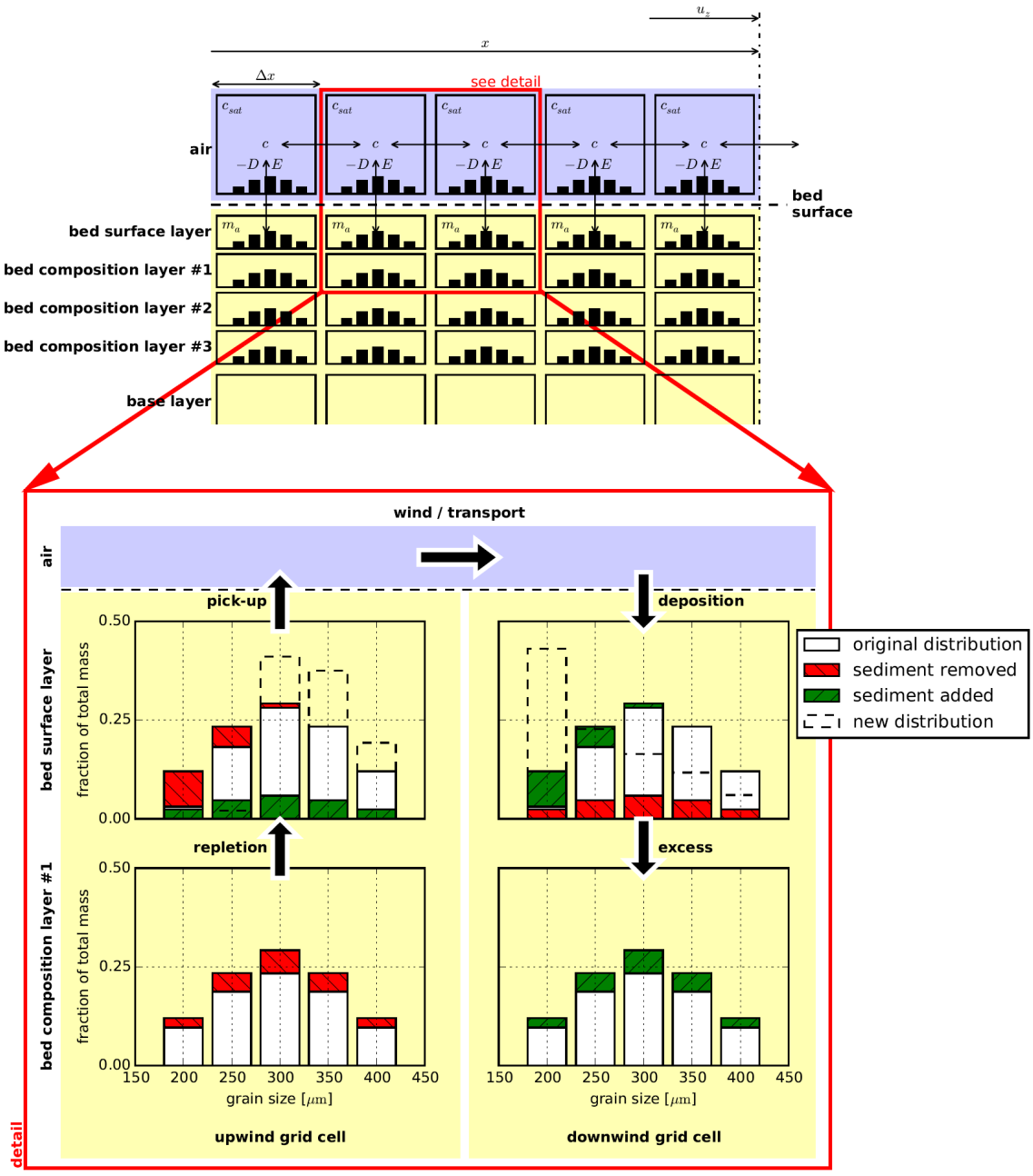

Figure E.2: Schematic overview of bed composition discretisation, and interaction between different layers and grid cells (Hoonhout, 2018)

As discussed in subsection 2.2.2, sediment sorting may lead to the emergence of non-erodible elements (coarse grains) on the bed, which may shelter the erodible sediments from wind erosion. The adapted velocity threshold of equation E.9 is implemented in AeoLiS to account for a reduced sediment availability due to sediment sorting.

$$u_{*c,R} = u_{*c} \cdot \sqrt{\left(1 - m \sum_{k=k_0}^{n_k} w_k^{bed}\right)\left(1 - \frac{m\beta}{\sigma} \sum_{k=k_0}^{n_k} w_k^{bed}\right)} \tag{E.9}$$

where:

m	Factor to account for the difference between the mean and maximum shear stress
k_0	Index of the smallest non-erodible sediment fraction in current conditions
β	Ratio between the drag coefficients of the roughness elements and the bed without roughness elements
σ	Ratio between the frontal area and the basal area of the roughness elements

The velocity threshold u_{*c} is obtained from equation 2.7 in case of sediment sorting only. When the soil moisture content is relevant as well, equation 2.19 must be used.

E.4. Hydraulic mixing

To ensure a good balance between processes that limit or enhance the sediment availability, both sediment sorting and hydraulic mixing must be sufficiently represented in the model.

In coastal areas, the upwind boundary is generally defined by the water line, as it is a zero-transport boundary for aeolian sediment transport. Hydraulic processes mix the sediment, as described in section 2.2.2. In AeoLiS, the mixing of sediment is simulated by averaging the sediment distribution over the depth of disturbance Δz_d. An empirical factor $f_{\Delta z_d}$ relates the depth of disturbance directly to the local breaker height according to:

$$\Delta z_d = f_{\Delta z_d} \cdot \min(H_0 \ ; \ \gamma \cdot h) \tag{E.10}$$

where:

Δz_d	Depth of disturbance
$f_{\Delta z_d}$	Empirical factor

Typical values for $f_{\Delta z_d}$ are 0.05 to 0.4, and 0.5 for γ.

E.5. Soil moisture content

AeoLiS includes the soil moisture content in the critical shear velocity using the formulation of Belly (1962) or Hotta et al. (1985). The drying of the beach is modelled using simplified equations for infiltration and evaporation. Infiltration is simulated by an exponential decay function with a drying time scale T_{dry}. Evaporation is represented by an adapted Penman-Monteith equation that uses meteorological time series of solar radiation, temperature and humidity. The volumetric moisture content at the new time step p_V^{n+1} is given as a function of the moisture content at the new time step p_V^n by:

$$p_V^{n+1} = \begin{cases} p & ; \text{ if } \eta > z_b \\ p_V^n \cdot e^{\left(\frac{\log(0.5)}{T_{dry}} \Delta t_n\right)} - E_v \cdot \frac{\Delta t_n}{\Delta z} & ; \text{ if } \eta \le z_b \end{cases} \tag{E.11}$$

where:

η	Instantaneous water level
T_{dry}	Drying time scale
Δt	Time step
E_v	Evaporation rate
Δz	Bed composition layer thickness

The evaporation rate E_v is implemented with the following equation:

$$E_v = \frac{m_v \cdot R_n + 6.43 \cdot \gamma_v \cdot (1 + 0.536 \cdot u_2)\delta_e}{\lambda_v \cdot (m_v + \gamma_v)} \cdot 9 \cdot 10^7 \tag{E.12}$$

where:

m_v	Slope of the saturation vapour pressure curve
R_n	Net radiance
γ_v	Psychrometric constant
u_2	Wind velocity at 2 m above the bed
δ_e	Vapour pressure deficit
λ_v	Latent heat vaporisation

E.6. Morphological feedback

AeoLiS calculates the total mass that should be exchanged between two grid cells for every sediment fraction k. The mass transfer between every adjacent grid cells is transformed to a bed level change for every grid cell. This exchange accounts for sediment sorting through the weighting factor $\hat{w}$, see equation E.13 The notation very similar to equation E.4.

$$\Delta z_k = \frac{\hat{w}_k \cdot c_{eq,k} - c_k}{T_a} \cdot \frac{\Delta t}{\rho_s (1-p)} \tag{E.13}$$